Tall Wind Profiles in Heterogeneous Terrain

Dissertation

Zur Erlangung des Doktorgrades der Naturwissenschaften
im Fachbereich Geowissenschaften
der Universität Hamburg

vorgelegt von

Heike Marei Konow
aus Henstedt-Ulzburg

Hamburg, 2015

Als Dissertation angenommen vom Fachbereich der Geowissenschaften der Universität Hamburg

aufgrund der Gutachten   von   Prof. Dr. Felix Ament
                           und   Prof. Dr. Burghard Brümmer

Hamburg, den 09. Dezember 2014

Prof. Dr. Christian Betzler
Leiter des Fachbereichs Geowissenschaften

Abstract

Electrical power generation by means of wind energy becomes more and more important. To increase efficiency, wind turbine heights grow to orders of 100 m or more. The surroundings of deployed wind turbines are seldom "ideal" in the sense of surface layer theory, which makes yield projections challenging with conventional methods. The scope of this thesis is the wind profile between 10 m and 250 m at a more realistic location. Observations used for these investigations were obtained from October 2000 until March 2012 at the Wettermast Hamburg site. It is located in the easterly outskirts of Hamburg, Germany. Its position and height allows for wind profile analysis in heterogeneous terrain and up to heights above the surface layer.

The roughness length is determined for the surroundings of the Wettermast Hamburg for 30°-wide wind direction sectors. If roughness length is to be determined from tall wind profiles at heterogeneous terrain, it proves to be beneficial to expand the logarithmic wind profile to include a linear term. This term accounts for a stronger increase of the wind speed at upper levels. The influence of surface roughness is largest in 10 m. However, even in this level close to the ground, influence of varying stratification is dominant. Atmospheric stratification is determined by Obukhov length and gradients of potential temperature. It is not always uniform throughout the entire measurement height. These deviations of stability result in deviations of wind speed as well. If only lower layer stability is used for wind profile estimations and the influence of deviating upper layer stability is neglected, wind speed is found to be overestimated. In this case, the wind speed can be mostly around 30% and up to 41% less than expected. In all heights, the effect of variation of atmospheric stratification is considerably larger than that of changing surface roughness. Stratification in upper layers influences the wind profile in all heights. It should be taken into account for wind speed estimations, especially at higher levels. Two mixing length models (Gryning et al., 2007; Peña et al., 2010) are evaluated with observations. No considerable improvement of the Peña et al. (2010) model over the Gryning et al. (2007) model can be found. For model wind speed estimations with those models at levels close to ground, a correct representation of surface roughness is most important. Correct stability classifications become more important at higher levels of wind speed prediction.

Zusammenfassung

Die Nutzung von Windenergie zur Stromerzeugung gewinnt immer mehr an Bedeutung. Zur Steigerung der Effizienz werden Windenergieanlagen immer größer und erreichen Höhen von 100 m oder mehr. Diese Anlagen werden allerdings selten in "idealen" Umgebungen im Sinne der traditionellen Ähnlichkeitstheorie aufgestellt. Dies erschwert Ertragsprognosen mit konventionellen Methoden. Diese Arbeit behandelt das Windprofil zwischen 10 m und 250 m in einer realistischeren Umgebung anhand von Messungen am Wettermast Hamburg zwischen Oktober 2000 und März 2012. Durch die Lage am Ostrand der Stadt Hamburg und die Messungen bis zu 250 m Höhe ist es möglich das Windprofil in einer heterogenen Umgebung und in Höhen oberhalb der Prandtl-Schicht zu untersuchen.

In dieser Arbeit wird die Rauhigkeitslänge für 30°-breite Windrichtungssektoren aus Messungen des Windprofils bestimmt. Es hat sich als sinnvoll erwiesen das logarithmische Windprofil hierfür um einen linearen Term zu erweitern, wenn Windprofile genutzt werden, die in größeren Höhen und in heterogenem Terrain gemessen wurden. Dieser lineare Term berücksichtigt die stärkere Zunahme der Windgeschwindigkeit in größeren Höhen. In 10 m Höhe ist der Einfluss der Oberflächenrauhigkeit auf das Windprofil ist am größten. Allerdings ist schon in dieser Höhe die Auswirkung verschiedener Schichtungen deutlich größer. Die Stabilität wird in dieser Arbeit sowohl durch die Obukhov-Länge L als auch durch Gradienten potentieller Temperatur klassifiziert. Die Stabilität ist dabei nicht immer einheitlich in der gesamten untersuchten Grenzschicht. Unterschiedliche Stabilitäten in der unteren und oberen Hälfte wirken sich auf das gesamte Windprofil aus. Wird nur die Stabilität in der unteren Schicht für die Abschätzung des Windprofils genutzt und weicht die wahre Stabilität in der oberen Schicht davon ab, resultiert dies in allen Höhen meist in einer Überschätzung der Windgeschwindigkeit. Dies bedeutet, dass die Windgeschwindigkeit meistens etwa 30% und bis zu 41% kleiner als erwartet ist. Auch die Stabilität in der oberen Schicht sollte daher bei der Abschätzung von Windprofilen, insbesondere in größeren Höhen, nicht vernachlässigt werden. Die Auswirkung von verschiedenen Stabilitäten auf das Windprofil ist in allen Höhen größer als der Einfluss verschiedener Oberflächenrauhigkeiten. Zwei Modellansätze nach dem Mischungswegprinzip (Gryning et al., 2007;

Peña et al., 2010) werden mit Messungen verglichen. Es kann keine substantielle Verbesserung des Peña-Modells gegenüber dem Gryning-Modell gefunden werden. Für die Windgeschwindigkeitsabschätzung mithilfe der Modelle in 10 m Höhe ist die korrekte Abschätzung der Oberflächenrauhigkeit am wichtigsten. In darüberliegenden Höhen wird die korrekte Klassifizierung der atmosphärischen Stabilität wichtiger.

Contents

List of Figures

List of Tables

1

Introduction

Wind is one of the more tangible meteorological quantities. People experience it during their day-to-day lives. It shapes landscapes and its energy has been utilized by men for hundreds of years. Wind energy has been used for travel by sailboats or by windmills to mill grain and pump water.

In recent years electrical power generation by means of wind energy became more and more important. Efforts have been made to cover a greater fraction of human's energy demands by renewable energy sources. In 2011, a Tsunami that hit Japan's east coast and caused a nuclear disaster at the Fukushima Daiichi power plant. As a reaction, the German federal government decided to replace nuclear power plants and fossil fuels as main energy sources with renewable energy resources until the year 2022 (Bundesregierung, 2012).

One way to meet the growing demands of wind energy power generation is to increase its efficiency. Power production from wind turbines depends on the swept area of the rotor. To maximize efficiency, wind turbine heights and rotor spans grew in recent years. Wind turbine hub heights for inland wind turbines are currently at $80-100\,\text{m}$ and rotor diameters are around $100\,\text{m}$ and up to $150\,\text{m}$. It is expected that hub heights will increase to exceed $100\,\text{m}$ in future (Pedersen, 2013; Hau, 2013). Since power is proportional to the cube of wind speed, even small errors in wind speed estimations result in larger errors in yield projections. Therefore, it is essential to find methods that describe wind profiles as precisely as possible. To assess potential locations for wind turbines or wind parks and the expected yield, the prevailing wind profile has to be estimated at this location. This is commonly done by extrapolating $10\,\text{m}$ wind speed measurements using the logarithmic wind profile (Schwartz and Elliott, 2005). However, this approach is not sufficient to estimate the wind speed at current hub heights as the logarithmic wind profile is not valid above the surface layer (SL) (van den Berg, 2008; Drechsel et al., 2012; Hau, 2013). Additionally, Hau (2013) points out that the wind energy assessment performed by methods proposed in the European Wind Atlas (Troen and Petersen, 1989) has another disadvantage as it neglects the orography at the potential site.

Furthermore, as a result of increasing size of wind turbines, rotors of wind turbines are exposed to stronger wind speed gradients between the upper and lower end of the area. Therefore, wind speed estimations are not only important at the hub height itself but also over the entire rotor height as this impacts power generation and load on the rotor (Wagner et al., 2009; Sathe et al., 2013; Draxl et al., 2014). Atmospheric stratification is of great interest in this context, because it impacts the wind profile. Additionally, it also influences other related effects such as the magnitude of wake effects behind wind turbines and wind farms (Christiansen and Hasager, 2005) and noise emissions from wind turbines (van den Berg, 2008). In addition to stratification of the atmosphere, surface roughness is an important quantity as well. Gusts generated by surface roughness elements impact the load as well as the expected yield at wind turbines (Suomi et al., 2013)

The wind profile within the boundary layer has been investigated by a great number of studies. Monin Obukhov similarity theory (MOST) has been developed in an attempt to describe turbulent behavior of boundary layer flow. From field experiments, in particular the Kansas field experiment in 1968 (Kaimal and Wyngaard, 1990), universal functions were developed (Businger et al., 1971; Dyer, 1974). These empirical functions are widely used (Foken, 2006b) and have been reevaluated throughout the years (Högström, 1988, 1996). Nevertheless, they are still subject to research (Liang et al., 2014; Hicks et al., 2014).

Several studies have been performed to assess the quality of wind speed estimation at current hub heights from numerical weather prediction (NWP) models outputs. Drechsel et al. (2012) analyze NWP model output in comparison with data from eight meteorological towers in Europe to determine the best output variable and interpolation method to estimated yields. They recommend the use of a logarithmically interpolated wind speed at 100 m from neighboring model levels. Devis et al. (2013) investigate prediction of wind speed at common hub heights by downscaling large scale global circulation model outputs. Draxl et al. (2014) compare WRF model wind speed predictions with varying planetary boundary layer (PBL) schemes, but find that no scheme is superior during stable stratification. All these studies emphasize the importance of an adequate description of boundary layer wind profiles for optimal results.

With increasing importance of power generation by wind energy it becomes more important to understand processes at "non-idealized" locations, both with respect to surface characteristics and observation height. Efforts have been made to transfer boundary layer theory from idealized conditions to more heterogeneous locations (van Ulden and Wieringa, 1996). In recent years the focus of boundary layer wind profile research has shifted more towards the description of stable stratification both in modelling (Mauritsen et al., 2007; Buzzi et al., 2011) and analysis of observations (van de Wiel et al., 2012; Ferreres et al., 2013). Furthermore, several studies (e.g. van Ulden and Wieringa, 1996; Pelliccioni et al., 2012) state that wind profile description from similarity theory for heights up to 200 m is not sufficient and recommend an extension by means of geostrophic similarity theory. Therefore,

attempts have been made to extend the well known surface layer wind profile to heights beyond the SL (Zilitinkevich and Esau, 2005; Gryning et al., 2007; Emeis et al., 2007; Peña et al., 2010). As Holtslag et al. (2013) point out, future tasks in boundary layer research include the investigation of the role of heterogeneous surfaces on boundary layer processes, study of processes at extremely stable stratification, and the need for a climatology of relevant parameters such as stratification, PBL depth and surface fluxes.

Observations used in this thesis are taken at the Wettermast Hamburg. It is located at the easterly outskirts of Hamburg. Here, measurements are taken up to 250 m height. This allows for systematical analyses of the boundary layer in the transition area between urban and rural terrain at higher levels. Since the beginning of operation of the Wettermast Hamburg site in 1963 some studies have been published using observations from this site. During the early stages of observation, Link (1966) investigated the influence of the mast structure on wind measurements. Wamser (1976) investigated the structure of turbulence at varying surface roughnesses in the years 1971 to 1973. Lange (2001) gives an extensive overview of the boundary layer climatology at the Wettermast Hamburg site for the years 1995 until 2000. In the study of Brümmer et al. (2012), this overview is extended to the larger number of available observations.

This thesis aims to broaden the understanding of boundary layer wind profiles at less than "ideal" conditions. To sufficiently interpret observations taken at the Wettermast Hamburg, it is essential to characterize the site, its surroundings and the present climatology. Therefore, one question that will be investigated is: **What are important characteristics of the Wettermast Hamburg site and its observations?**

As mentioned above, two important influences on the wind profile at levels close to the ground are surface roughness and atmospheric stability. Several approaches exist to characterize surface roughness. This will be summarized by answering the question: **How can the roughness length z_0 be derived from observations at tall masts in heterogeneous terrain?**

In general, atmospheric stratification is determined from surface layer measurements. In this thesis, the wind profile not only in the surface layer but also above is studied. This raises the question: **Is it sufficient to determine atmospheric stability for wind profile estimates by means of stratification close to the surface?**

Furthermore, it is interesting to assess which influence is stronger on boundary layer wind profiles: surface roughness or atmospheric stratification. Therefore, the question **How do varying surface roughness and atmospheric stratification influence the boundary layer wind profile?** is approached.

As previously mentioned, several attempts have been made to extend the formulation of the logarithmic wind profile beyond the surface layer. These will be investigated by examining the question:

How well are mixing length models able to describe the wind profile in heterogeneous terrain in the surface layer and above?

The increasing importance of power generation by means of wind energy demands for validation of current wind profile descriptions, especially at less than ideal locations. By utilizing observations from the Wettermast Hamburg site it is possible to investigate the following question: **How large are uncertainties of wind speed estimations at levels in the order of current and future wind turbine hub heights?**

These research questions are investigated in the course of this thesis. It is structured as follows: In **Chapter 2** the characteristics of the boundary layer wind profiles are discussed. Two wind profile model formulations (Gryning et al., 2007; Peña et al., 2010) are introduced that aim to extend the traditional logarithmic wind profile description beyond the surface layer.

For adequate interpretation of observations it is essential to assess the measurement setup and other influencing factors. **Chapter 3** gives an overview of the Wettermast Hamburg site. In particular, it highlights the following points:

- The layout of the Wettermast Hamburg site itself and the different elements that compose this site are described. The instrumentation and its features are discussed as well. Observations at the Wettermast Hamburg do not necessarily represent the state of the boundary layer at the site itself but is more a representation of the upstream conditions. It is therefore essential to assess the surrounding area around the measurement site and its probable impact on measurements.

- Measurements that are taken at a meteorological tower are subject to disturbances of the mast structure. It is aimed to assess the magnitude of these disturbances on observations and to determine the operational range of wind directions.

- The observational basis used in this thesis is the time between October 2000 and March 2012. A description of the wind climatology in Hamburg in this period is given.

One influencing factor on the wind profile is the underlying surface roughness. Its characteristics and the influences on wind profiles are covered in **Chapter 4**:

- Roughness length z_0 as a measure of surface roughness is derived from wind profile observations. A method to determine z_0 from measurements at tall masts is introduced. Also, wind speed dependency of the results is investigated.

- The impact of varying surface roughness on wind speed is analyzed by means of measurements and mixing length wind profile models. The model results are validated with observations from the Wettermast Hamburg.

The second large influence on the wind profile is the atmospheric stratification. This is investigated in **Chapter 5** in detail.

- A climatology of atmospheric stratification at varying wind speeds and wind directions is presented. Additionally, the stratification of the boundary layer is analyzed separately for two layers: 10 m to 110 m and 110 m to 250 m.

- The observed wind profile at different stratification conditions is investigated. In particular, the impact of varying stability in upper layers is analyzed.

- Wind profile models are validated with wind speed observations at different stability categories.

This thesis is summarized with conclusions and outlook in **Chapter 6**.

2

Boundary Layer Wind Profiles

The boundary layer is the domain of a flow where the influence of a surface is present. In the atmosphere this layer is called atmospheric boundary layer (ABL) or planetary boundary layer. The basic characteristics of ABL and boundary layer flow are described in this chapter. explanations in this chapter are mainly based on the textbooks by Stull (1988), Arya (2001) and Foken (2006b).

In Section 2.1 the structure of the ABL is discussed. Formulations for the wind profile in the surface layer are presented in Section 2.2. To assess the wind profile in heights of current and future wind turbines, the formulations have to be extended into layers above the surface layer. Methods for this extension are presented in Section 2.3.

2.1 Boundary Layer Structure

The ABL is the domain of the atmosphere which is influenced by the underlying surface and its characteristics (shape, roughness, albedo, moisture content, heat emissivity and heat capacity) (Emeis, 2013). Its vertical extent is highly variable and it often has a distinct diurnal cycle (Stull, 1988). One can identify three main types of boundary layers over land which are mainly classified by the radiation's influence or the lack thereof. The convective boundary layer (CBL) develops due to heat input from below and is dominated by intense vertical mixing resulting in small vertical gradients. The stable boundary layer (SBL) occurs often during nighttime where the ground cools due to emission of long-wave radiation and thus also cools the lowest air layers. This results in low turbulence and large vertical gradients. When clouds, wind and precipitation override the radiation's influence, a neutral boundary layer (NBL) forms near the ground which has almost no diurnal variation (Emeis, 2013).

Generally, the influence of the surface on the atmospheric flow is strongest near the ground and decreases with height until it is considered to be negligible in the free atmosphere. Corresponding to

this decrease, the atmospheric boundary layer is sub-divided into several layers. Closest to the ground or the roughness elements is the laminar sublayer. It extents up until the order of a few millimeters. Above follow the surface layer and the Ekman layer.

The surface layer is the layer where most humans spend the majority of their life. In this layer the turbulent fluxes vary by less than 10% with height. It is therefore also called constant-flux layer. The Coriolis force in this height is small and can usually be neglected. Therefore, the wind direction is almost constant with height in this layer.

The Ekman layer follows above the surface layer up to the top of the boundary layer. In contrast to the surface layer, the turbulent fluxes in the Ekman layer are not constant but decrease with height until they vanish at the top of the ABL. Additionally, the Coriolis force is no longer negligible and causes a change of the wind direction with height.

Wind turbines from previous generations rarely extend above the surface layer. In the last years however, the hub height of wind turbines has grown considerably and now often reaches into the Ekman layer. To be able to estimate the wind speed in those larger heights but also to asses the load of wind shear on the rotor, it is necessary to extend the well-known equations beyond the surface layer height.

2.2 The Wind Profile in the Surface Layer

Atmospheric flow in the surface layer is influenced by surface friction. Mainly two approaches exist to describe the wind profile in the surface layer: the logarithmic wind profile and the power law.

2.2.1 The Logarithmic Wind Profile

To describe the wind profile in the surface layer it is assumed that the mean flow is stationary and horizontally homogeneous, that the momentum flux is vertically constant and that the Coriolis force is small. Originating from gradient transport theory and with the assumption that the vertical momentum exchange coefficient is proportional to the mixing length l, an equation for the vertical wind speed gradient can be derived (see textbooks, e.g. Etling, 2008):

$$\frac{\partial \overline{u}}{\partial z} = \frac{u_*}{l} \quad . \tag{2.1}$$

Here, $\partial \overline{u}/\partial z$ is the vertical gradient of the average wind speed and u_* is the friction velocity. The mixing length is often thought of as a measure for the maximum eddy size. In neutral conditions this size mainly depends on distance from the surface. Therefore, l is proportional to height: $l = \kappa z$. κ is the dimensionless Kármán constant κ.

In diabatic conditions, eddy size and accordingly mixing length depend on stratification. Therefore mixing length formulation is extended by the stability dependent profile function $\phi_m(z/L)$: $l = \kappa z \, \phi_m^{-1}$. In agreement with Monin Obukhov similarity theory (MOST), the dimensionless wind shear now only is a function of the stability parameter (z/L) (Foken, 2006a):

$$\frac{\kappa z}{u_*} \frac{\partial \overline{u}}{\partial z} = \phi_m\left(\frac{z}{L}\right) \quad . \tag{2.2}$$

Here, L is the Obukhov length:

$$L = -\frac{\overline{\theta}}{\kappa g} \frac{u_*^3}{\overline{w'\theta'}} \quad . \tag{2.3}$$

In this formulation, $\overline{\theta}$ is the mean potential temperature, g is acceleration due to gravity, and $\overline{w'\theta'}$ is the turbulent vertical transport of sensible heat which is proportional to the turbulent sensible heat flux $(H = \rho c_p \overline{w'\theta'}$; ρ is the density of air, c_p is specific heat at constant pressure)[1].

Several attempts have been made to determine the form of the stability dependent profile functions $\phi_m(z/L)$. Following the Kansas field experiment in 1968, Businger et al. (1971) determined the form $\phi_m = 1 + bz/L$ for stable and $\phi_m = (1 - az/L)^p$ for unstable stratification. Values of the constants a, b, and p were determined empirically from this and following experiments (Businger et al., 1971; Dyer, 1974). In addition, the value of the Kármán constant κ was a subject of discussion for quite some time. Högström (1988) modified the previously found values for a, b, and p to allow for the now widely agreed-upon Kármán constant κ=0.4 (Stull, 1988; Arya, 2001). Here, the universal functions derived by Businger et al. (1971) and modified by Högström (1988) are given exemplarily:

$$\phi_m\left(\frac{z}{L}\right) = \begin{cases} 1 + 6\dfrac{z}{L} & \text{stable} \\[2mm] 1 & \text{neutral} \\[2mm] \left(1 - 19.3\dfrac{z}{L}\right)^{-1/4} & \text{unstable} \end{cases} \tag{2.4}$$

Integrating Equation (2.2) from z_0 to the height z leads to the formulation for the wind profile, the so-called logarithmic wind profile:

$$u = \frac{u_*}{\kappa}\left(\ln\left(\frac{z}{z_0}\right) - \psi_m\left(\frac{z}{L}\right)\right) \quad . \tag{2.5}$$

The roughness length z_0 is an integration constant and is taken as the height, at which wind speed reaches zero, ψ_m is the integral of the universal function.

---

[1]The above notation follows the principle of Reynold's decomposition. A measured quantity $x = \overline{x} + x'$ comprises the mean value $\overline{x}$ and the turbulent deviations from that mean x'. In the course of this thesis, the overline that denotes averages will be omitted and turbulent deviations will be indicated by a dash at the variable (Foken, 2006b).

In case of neutral stratification Equation (2.5) has the well-known form:

$$u(z) = \frac{u_*}{\kappa} \ln \left(\frac{z}{z_0} \right) \quad .$$

(2.6)

2.2.2 The Power Law

Aside from the logarithmic profile, a widely used formulation for the wind profile is the power law (Blackadar, 1997). This empirical formulation allows for the estimation of the wind profile from only one measurement at the height z_a:

$$u(z) = u_{z_a} \left(\frac{z}{z_a} \right)^p \quad .$$

(2.7)

With the measuring height z_a and the Hellman exponent p, which ranges between 0 and 1 and depends on surface roughness and stability. Sedefian (1980) showed that the Hellman exponent can be expressed as a function of roughness length z_0 and stability parameter $\zeta = z/L$:

$$p = \frac{\phi_m \left(\frac{z}{L} \right)}{\ln \left(\frac{z}{z_0} \right) - \psi_m \left(\frac{z}{L} \right)} \quad .$$

(2.8)

ϕ_m and ψ_m are the universal functions from Section 2.2.1.

When surface roughness increases, p increases due to the enhanced turbulent mixing. Unstable stratification results in a reduction of the Hellman exponent, whereas in stable conditions p increases (Blackadar, 1997).

Emeis (2013) mentions that in conditions favorable for wind energy conversion (i.e. strong wind speed which is often associated with neutral stratification and smooth terrain) the power law acts as a good estimate for the surface layer wind profile.

2.3 Extending the Wind Profile Above the Surface Layer

The formulations mentioned in Section 2.2 are developed to describe the conditions in the surface layer. As the wind power generation evolves and wind turbines reach larger heights, an estimate for the conditions well above the surface layer is necessary. Gryning et al. (2007) (Sect. 2.3.1) and Peña et al. (2010) (Sect. 2.3.2) attempt to extend the surface layer formulation into the Ekman layer by expanding the mixing length definition. Another approach to expanding the wind profile is to develop a two layer model with separate equations for surface layer and Ekman layer (Emeis et al., 2007; Etling, 2008).

2.3.1 Gryning et al. (2007)

The approach of Gryning et al. (2007) is based on the mixing length hypothesis. They devise an extended formulation for the modified mixing length to include additional formulations for the middle of the boundary layer L_{MBL} and the upper boundary layer L_{UBL}. The different length scales are joined by inverse summation:

$$\frac{1}{l} = \frac{1}{L_{\mathrm{SL}}} + \frac{1}{L_{\mathrm{MBL}}} + \frac{1}{L_{\mathrm{UBL}}} \quad . \tag{2.9}$$

For neutral stratification the surface layer length scale is proportional to the height: $L_{\mathrm{SL,n}} = l = \kappa z$. The upper boundary layer length scale is proportional to the distance to the boundary layer top z_i, leading to: $L_{\mathrm{UBL,n}} = z_i - z$. A parametrization for $L_{\mathrm{MBL,n}}$ has been devised by taking advantage of Rossby similarity theory and by empirically fitting the theoretical profiles to measurements at Høvsøre and Hamburg:

$$L_{\mathrm{MBL,n}} = \frac{u_{*0}}{f\left(-2\ln\left(\frac{u_{*0}}{f z_0}\right) + 55\right)} \quad . \tag{2.10}$$

Here, u_{*0} is the friction velocity at the lowest measuring level (which is considered to be constant throughout the surface layer) and f is the Coriolis parameter.

Accordingly, an empirical parametrization for the middle boundary layer length scale for non-neutral stratification L_{MBL} has been devised:

$$L_{\mathrm{MBL}} = \frac{u_{*0}}{f\left(-2\ln\left(\frac{u_{*0}}{f z_0}\right) + 55\right)} \cdot \exp\left(\frac{\left(\frac{u_{*0}}{fL}\right)^2}{400}\right) \quad . \tag{2.11}$$

By using the above parameterizations for the length scale in the different parts of the boundary layer Gryning et al. (2007) derived equations to describe the wind profile based on stability:

$$\frac{u(z)}{u_{*0}} = \frac{1}{\kappa}\left[\ln\left(\frac{z}{z_0}\right) + \frac{z}{L_{\mathrm{MBL,n}}} - \frac{z}{z_i}\left(\frac{z}{2L_{\mathrm{MBL,n}}}\right)\right] \qquad \text{neutral} \tag{2.12}$$

$$\frac{u(z)}{u_{*0}} = \frac{1}{\kappa}\left[\ln\left(\frac{z}{z_0}\right) + b\frac{z}{L}\left(1 - \frac{z}{2z_i}\right) + \frac{z}{L_{\mathrm{MBL}}} - \frac{z}{z_i}\left(\frac{z}{2L_{\mathrm{MBL}}}\right)\right] \qquad \text{stable} \tag{2.13}$$

$$\frac{u(z)}{u_{*0}} = \frac{1}{\kappa}\left[\ln\left(\frac{z}{z_0}\right) - \psi\left(\frac{z}{L}\right) + \frac{z}{L_{\mathrm{MBL}}} - \frac{z}{z_i}\left(\frac{z}{2L_{\mathrm{MBL}}}\right)\right] \qquad \text{unstable} \tag{2.14}$$

In the same way as Equation (2.5), the non-neutral formulations (2.13) and (2.14) include a stability correction term. b is a dimensionless constant resulting from the stability correction for which different values are commonly used. Dyer (1974) proposes $b = 5$, Businger et al. (1971) suggest $b = 4.7$ and Högström (1988) gives $b = 6$. In this thesis a medium value of $b = 5$ is used. $\psi\left(\frac{z}{L}\right)$ is the stability

correction term for unstable cases. Derived from the universal function $\phi_m = (1 - 12z/L)^{-1/3}$, it is

$$\psi\left(\tfrac{z}{L}\right) = \frac{3}{2}\ln\left(\frac{1+x+x^2}{3}\right) - \sqrt{3}\arctan\left(\frac{1+2x}{\sqrt{3}}\right) + \frac{\pi}{\sqrt{3}} \tag{2.15}$$

and $x = (1 - 12z/L)^{1/3}$.

Necessary input parameter for wind profile calculations at height z by Equations (2.12) – (2.14) are the surface layer friction velocity u_{*0}, roughness length z_0, and the Obukhov length L. Since no measurements of the boundary layer height z_i are available, this height has to be parameterized using the Rossby-Montgomery formula (Zilitinkevich and Baklanov, 2002):

$$z_i = 0.1\frac{u_{*0}}{f} \quad . \tag{2.16}$$

From the Wettermast Hamburg measurements a time period of one year (2007) has been used to derive the empirical constants in (2.10) and (2.11). Compared to the number of observations used in this study it is justifiable to test this parametrization again with the larger sample size, even if the measurements used for the derivation are part of the sample.

2.3.2 Peña et al. (2010)

Peña et al. (2010) use a similar approach as Gryning et al. (2007), to extend the mixing length formulation from surface layer length scale l by inverse summation. However, in Peña et al.'s approach the formulation of the mixing length is adjusted to:

$$\frac{1}{l} = \frac{1}{\kappa z} + \frac{(\kappa z)^{d-1}}{\eta^d} \quad . \tag{2.17}$$

Here, the increase of l with height is limited to η. This is the maximum value that the length scale l reaches asymptotically in the free atmosphere. d is the parameter that controls the rate of this growth.

Table 2.1: Empirical values of Equation (2.21) for varying stratification. Values taken from Peña et al. (2010). Stability categories will be further defined in Table 5.1.

Stability class	very unstable	unstable	near unstable	neutral	near stable	stable	very stable
A	2.4	2.1	1.9	1.7	1.6	1.5	1.5
B	4.3	4.6	4.8	5	5.1	5.2	5.2

Using this definition for length scale leads to a description of the wind profile at diabatic conditions:

$$u(z) = \frac{u_{*0}}{\kappa} \left[\ln\left(\frac{z}{z_0}\right) + \frac{1}{d}\left(\frac{\kappa z}{\eta}\right)^d - \left(\frac{1}{1+d}\right)\frac{z}{z_i}\left(\frac{\kappa z}{\eta}\right)^d - \frac{z}{z_i} \right] \qquad \text{neutral} \quad (2.18)$$

$$u(z) = \frac{u_{*0}}{\kappa} \left[\ln\left(\frac{z}{z_0}\right) + b\frac{z}{L}\left(1 - \frac{z}{2z_i}\right) + \frac{1}{d}\left(\frac{\kappa z}{\eta}\right)^d - \left(\frac{1}{1+d}\right)\frac{z}{z_i}\left(\frac{\kappa z}{\eta}\right)^d - \frac{z}{z_i} \right] \qquad \text{stable} \quad (2.19)$$

$$u(z) = \frac{u_{*0}}{\kappa} \left[\ln\left(\frac{z}{z_0}\right) - \psi_m + \frac{1}{d}\left(\frac{\kappa z}{\eta}\right)^d - \left(\frac{1}{1+d}\right)\frac{z}{z_i}\left(\frac{\kappa z}{\eta}\right)^d - \frac{z}{z_i} \right] \qquad \text{unstable}$$

$$(2.20)$$

The parameter d has been estimated with different values: Blackadar (1962) proposed $d = 1$, whereas Lettau (1962) suggested $d = 5/4$. Peña et al. (2010) used both values side by side and only found $d = 5/4$ to fit the observations slightly better for near-neutral conditions in the lowest tens of meters. In this thesis $d = 1$ is used since Peña et al. found no large advantage of one value over the other.

Based on the analysis of measurements at Høvsøre (Denmark) during July 2008 to October 2008, the maximum length scale η has been parameterized to be:

$$\eta = \frac{\kappa z_i}{\left[d\left(1+d\right)^{1/d}\right]} \left[\left(\left[\ln\left(\frac{u_{*0}}{f_c z_0}\right) - A\right]^2 + B^2 \right)^{1/2} + \ln\left(\frac{z_i}{z_0}\right) \right]^{-1/d} . \qquad (2.21)$$

The values of A and B are empirically estimated and are listed in Table 2.1.

2.3.3 Two Layer Model

Emeis et al. (2007) and Etling (2008) propose a two layer model to extend the wind profile description beyond the surface layer. In their approach, the wind profile formulations of the surface layer and the Ekman layer are combined to ensure a smooth transition between the two. Depending on height, three formulations are given for heights in the surface layer ($z < z_{SL}$) at the top of the surface layer ($z = z_{SL}$), and in the Ekman layer ($z > z_{SL}$). For $z < z_{SL}$ the logarithmic wind profile (2.5) is used. In the Ekman layer ($z > z_{SL}$) the wind profile is described by the Ekman layer wind profile equation. In this case, the height variable is the height above the top of the surface layer. The wind profile at the top of the surface layer is the transition between both layers. Here, the wind profile is described by Ekman layer wind profile equations for $z = z_{SL}$.

Necessary input variables for this model are surface roughness length z_0, geostrophic wind speed u_g, height of the surface layer z_{SL}, surface layer friction velocity u_{*0}, and angle between geostrophic and surface wind α. Only z_0 and u_{*0} can directly be determined from Wettermast Hamburg observations. This approach is not quite feasible for analyses with the current data set and is therefore not used.

3

Wettermast Hamburg

All analyses in this study to answer the scientific questions introduced in Chapter 1 are based on observations at the Wettermast Hamburg site. The Wettermast Hamburg is located at the border between the city of Hamburg and its easterly rural surrounding area. Therefore, measurements taken at this site allow for analyses not only at different atmospheric stratifications but also for distinctly different surface roughnesses depending on the wind direction.

Careful interpretation of observational data requires detailed information about the experimental setup. Therefore, an overview on the Wettermast Hamburg site and its instrumentation will be given in the first section of this chapter. Measurements at tall towers are likely affected by the tower itself. This influence will be discussed in Section 3.2. Besides these disturbances, measurements at specific heights are strongly determined by the environment of the site which is, in case of the Wettermast Hamburg, rather heterogeneous with an urban area in the west and rural terrain towards the east. More details will be presented in Section 3.3. An overview on the observational basis of this study and a description of the wind climatology at the Wettermast Hamburg site will be given in Section 3.4.

3.1 The Wettermast Hamburg Site - Layout and Instrumentation

The measuring site "Wettermast Hamburg" is located at the easterly outskirts of Hamburg (53.519°N, 10.103°E). It consists of a 305 m tall tower, a 12 m mast and several other instruments in the vicinity (Brümmer and Lange, 2004; Brümmer et al., 2012). Measurements at 50 m and above are conducted at the tall main mast. Below 50 m height however, the main mast is surrounded by operational buildings and trees (Fig. 3.1). Therefore, surface measurements and measurements at 2 m and 10 m height are taken at a secondary mast, located on a meadow approximately 170 m to the north-east of the main mast.
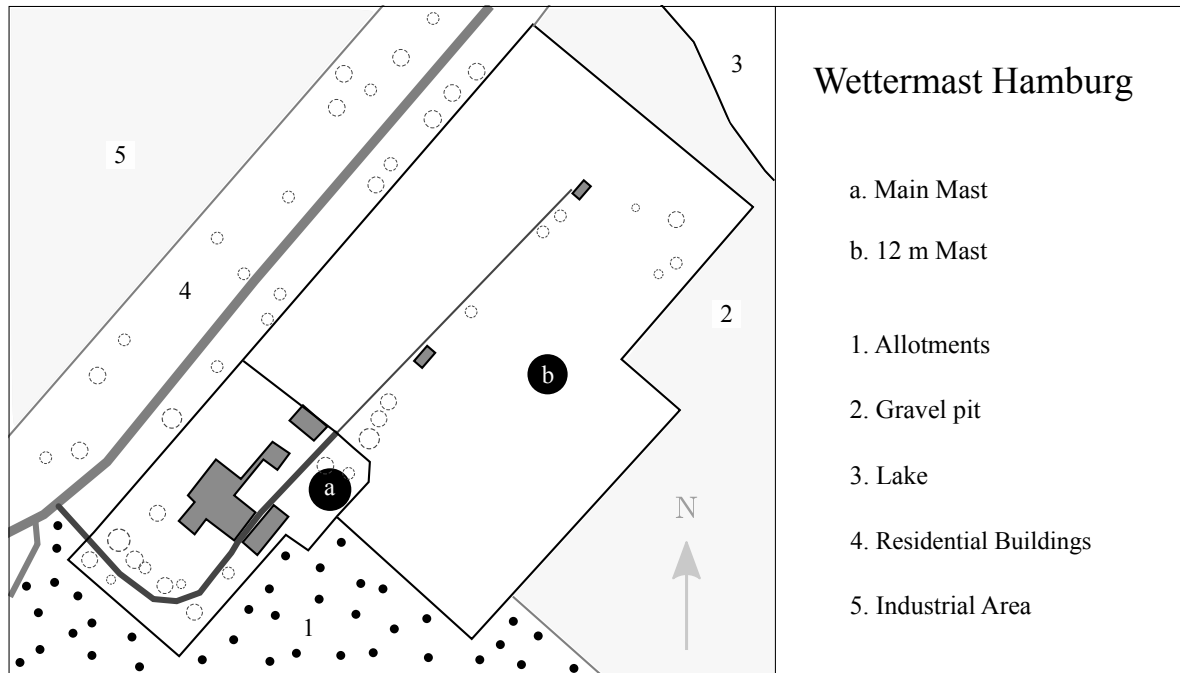
Figure 3.1: Sketch of the Wettermast Hamburg site and immediate surroundings. Position of main mast is marked with a, position of the secondary mast with b. Buildings and trees in proximity of main mast are approximately 10 m high.
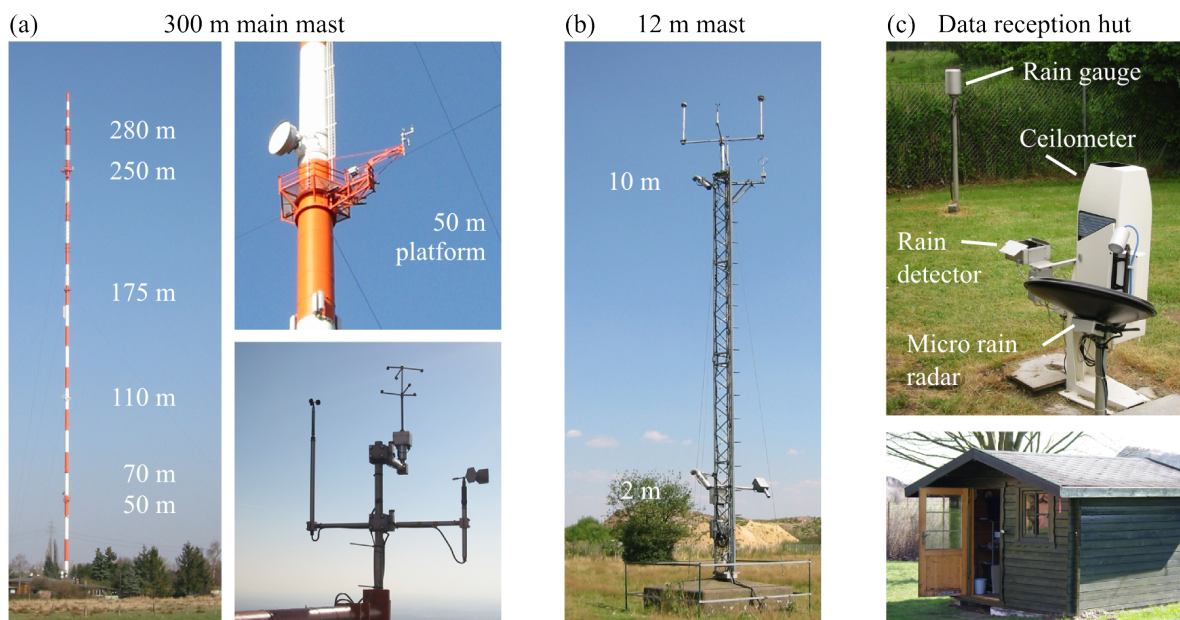
Figure 3.2: Instrumentation at the Wettermast Hamburg site: (a) the main mast with platform heights with exemplary instrumentation, (b) the 12 m high secondary mast, (c) supplemental instrumentation. Pictures courtesy of I. Lange.

Table 3.1: Excerpt of instrument distribution in different measuring heights at the Wettermast Hamburg site. Data from instruments marked with (x) are not used in this thesis.

Measuring height (m)	2	10	50	70	110	175	250	280
Wind		x	x		x	x	x	(x)
Temperature	(x)	x	x		x	x	x	(x)
Humidity	(x)	(x)	(x)		(x)	(x)	(x)	(x)
Irradiance		(x)						
Surface Temperature	(x)							

The main mast is a 305 m high radio tower (Fig. 3.2 (a)) operated by Norddeutscher Rundfunk (NDR) and equipped with meteorological instruments at several heights. It is a solid cylindrical mast of 2 m diameter. The measurement heights are 50, 70, 110, 175, 250, and 280 m. At 50, 110, 175, 250, and 280 m, hexagonal platforms are installed. At the edge, pointing in the direction of 190°, a boom is mounted, equipped with several instruments. In 70 m the boom that carries the instruments is attached directly to the mast.

The platforms at 50, 110, 175, and 250 m are equipped, amongst others, with three-dimensional ultrasonic anemometers (METEK USA-1) and a platinum resistance thermometer (Pt-100). At 280 m only an ultrasonic anemometer (METEK USA-1) is installed. At 70 m height, temperature but no wind measurements are conducted. The METEK USA-1 ultrasonic anemometers sample data with a frequency of 20 Hz. The measurements have a resolution of $0.01 \, \mathrm{m \, s^{-1}}$ and an accuracy of $0.1 \mathrm{m \, s^{-1}}$. The Pt-100 thermometers sample data with 1 Hz frequency, 0.01 K resolution, and 0.1 K accuracy (Brümmer et al., 2012).

The secondary mast is a 12 m high lattice mast (Fig. 3.2 (b)). It is located on a meadow about 170 m to the north-east of the main mast. The measuring heights on this mast are 2 m and 10 m. The instrumentation in 10 m is equal to the instrumentation on the main mast with an ultrasonic anemometer and a platinum resistance thermometer. In 2 m height temperature but not wind is measured.

Measurements from the instrumentation described above will be used throughout this study. In addition, a varying number of instruments are present at the measurement site. Capacitive humidity sensors are installed in all heights, except for 70 m, instruments for irradiance measurements (pyranometer and pyrgeometer) are mounted on top of the 12 m mast, and an infrared thermometer measures the surface temperature from 2 m height. Rain sensors, a ceilometer and a micro rain radar are permanently operated and located near the main mast (Fig. 3.2 (c)). Other instruments, i.e. Sodar, Wind Lidar, or Radiometer, were only present temporarily during measurement campaigns.
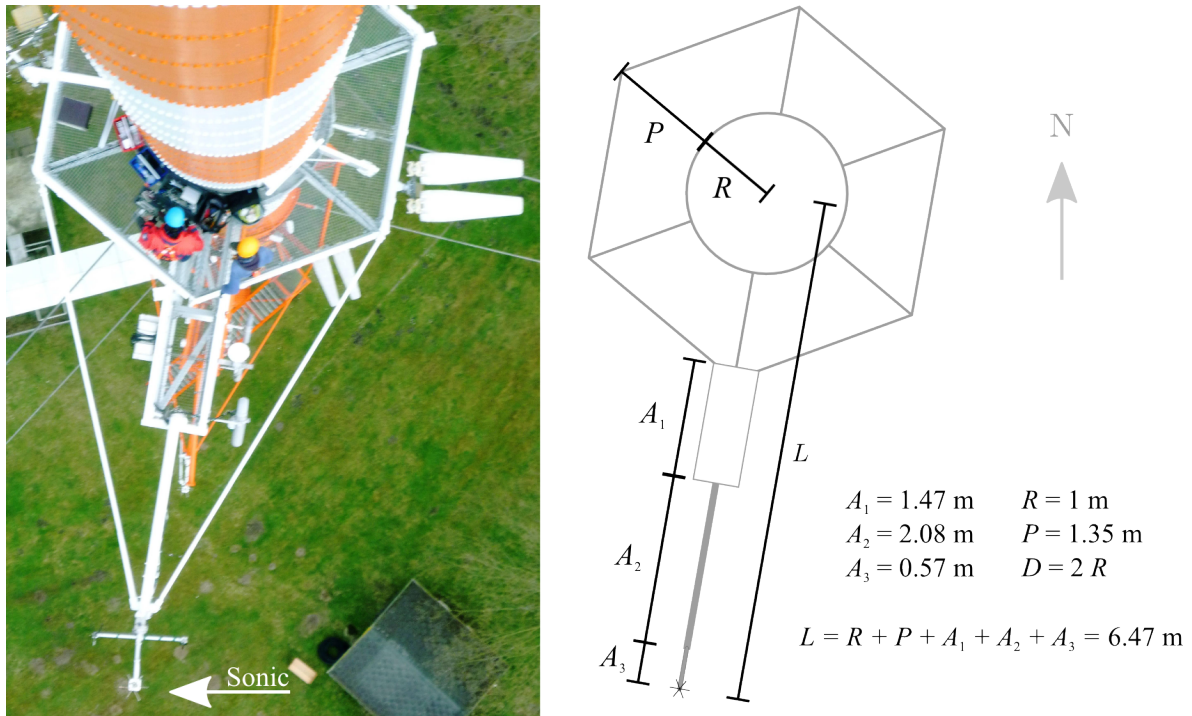
Figure 3.3: Platform layout at Wettermast Hamburg in 50, 110 and 175 m. Left: picture of the 110 m platform, photograph by courtesy of M. Jacob. Right: Sketch of platforms. Mast's radius R, platform width P, length of boom segments A_{1-3}, anemometers distance from mast center L. The boom extends towards the direction 190°. Sonic anemometer location is marked with $*$.

3.2 Influence of the Wettermast Hamburg on Wind Measurements at the Mast

When instruments are mounted on a meteorological mast, they not only register the environmental state of the boundary layer. Instead, every measured quantity is taken from a flow which is disturbed by the mounting structure itself. Therefore, the impact of these disturbances has to be estimated and appropriate correction methods have to be applied when possible. In general, there are two types of mast structures in use: open lattice or solid cylindrical masts, like the Wettermast Hamburg.

The platforms of the Wettermast Hamburg are approximately 1 m wide. At the edge of the platforms booms are mounted. And at the end of those booms the anemometers are installed at a distance of 6.47 m from the mast's center (Fig. 3.3).

Several studies have been published on the disturbances of the air flow by mounting structures, considering both solid cylindrical towers and open lattice masts. Authors investigating the influence of open lattice type masts found different values for the width of the wake region, depending on the mast geometry. For an open lattice type mast Barthlott and Fiedler (2003) observe a wake region of 40°,

Dabberdt (1968) observes 60° and Cermak and Horn (1968) state that the flow in a leeward sector of 30° is disturbed by the mast. All these studied masts vary slightly in their geometries, which explains why the determined width of the wake region width varies between 30° to 60°.

Gill et al. (1967) conducted wind tunnel measurements of quarter scale models of open lattice-type structures as well, but also on solid cylindrical towers. They found that the lattice-type structures generally influence the air flow only moderately, whereas solid towers and stacks generate stronger turbulence. In their experiment they observed that the flow behind a solid stack was disturbed in a 180° wide sector. If a wind speed measurement accuracy of $\pm 10\%$ within an angle of 180° is desired, Gill et al. recommend the following ratio between the mast diameter D and the distance from the mast's center L:

$$L = 3D \quad . \tag{3.1}$$

At the Wettermast Hamburg the ultrasonic anemometers are installed on booms with $L = 3.24D$ (see Fig. 3.3) which satisfies the requirement. In a direction range of $100° \leq dd \leq 280°$ ($\pm 90°$ from boom direction) a wind speed accuracy of $\pm 10\%$ is therefore expected.

Although the flow at the Wettermast Hamburg is almost always turbulent (Jacob, 2013), the velocity reduction $\frac{u}{u_\infty}$ in a laminar flow can be used as a first estimate to assess the wind speed measurement accuracy in the near field of the mast. According to Borovenko et al. (1965), it can be estimated by:

$$\frac{u}{u_\infty} = f(r, \varphi) = \sqrt{1 - \frac{a^2 \left[2r^2(2\cos^2 \varphi - 1) - a^2\right]}{r^4}} \quad , \tag{3.2}$$

with measured wind speed u, speed of the undisturbed flow u_∞, the mast's radius a and polar coordinates (r, φ). With this ideal concept, the measurement accuracy at the Wettermast Hamburg would be $\pm 2.4\%$ ($a = 2$ m, $r = 6.47$ m). Here, the wind speed in front and behind the mast are reduced and accelerated at angles perpendicular to the flow direction. These theoretical estimations have been reviewed at the Wettermast Hamburg as well: from September 1963 to November 1964 – during the early stages of measurements at the Wettermast Hamburg facility – Link (1966) investigated the mast's influence on the wind measurements for this specific setting. To this end, two additional booms were mounted in 110 m height, pointing towards the directions of 70° and 310°. In this study Link found that wind speed was underestimated in windward directions by at most 4.5% and on average 2.7%. Perpendicular to the flow, measured wind speed was overestimated by at most 10.5% and on average 6.6%. Additionally, the author recommended the operative sector for wind measurements to be $40° \leq dd \leq 340°$, because the influence of the mast on the flow was too strong in the leeward directions.

Summarizing the literature overview, Link (1966)'s findings at the Wettermast Hamburg correspond well with wind tunnel results from Gill et al. (1967). Also, the ideal approach of the velocity reduction from the potential flow theory (3.2) shows similar results to the measurements. The acceleration around the mast perpendicular to the flow, however, appears to be higher in measurements than the
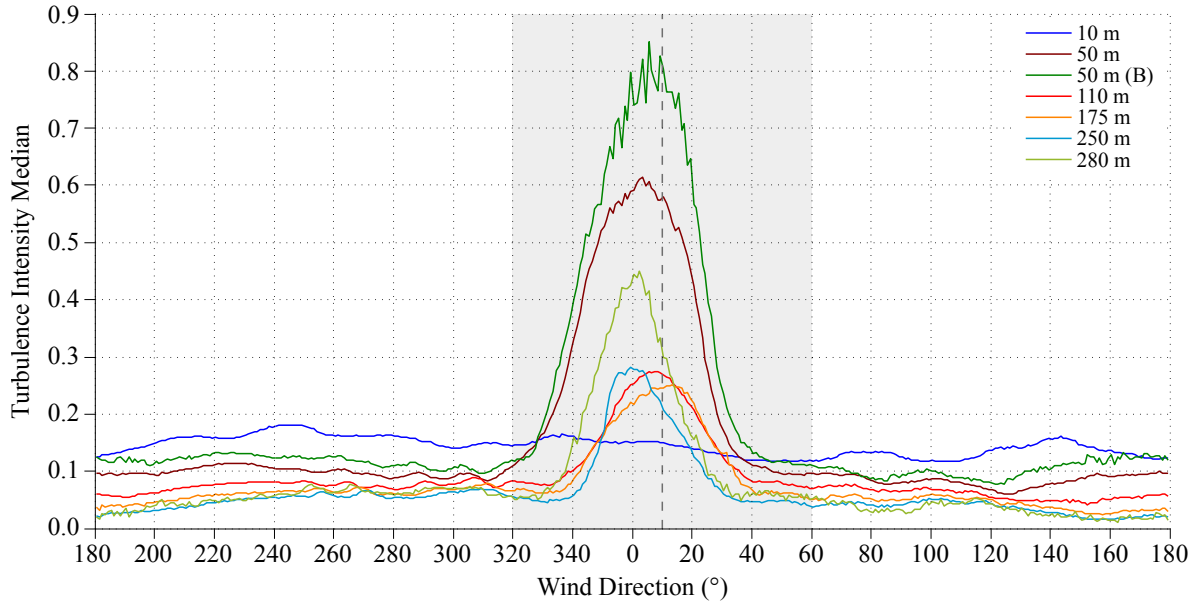
Figure 3.4: Turbulence intensity I_u medians from 10-minute intervals for $1°$ wind direction intervals. The dashed line represents the position of the mast with regards to the anemometers. Measurements at 10 m height are taken at a separate mast located roughly 170 m northeast of the main mast. Additional measurement data at 50 m height – labeled "50 m (B)" – stems from a second ultrasonic anemometer that is also installed at 50 m height but below the regular one at that height. The gray area marks the sector that is determined to be disturbed by the flow around the mast.

theory suggests.

Beginning in October 2000, ultrasonic anemometers have been installed at the Wettermast Hamburg. This now allows for verification of the previous findings by using turbulence measurements. With this data turbulence intensity can be used to determine the magnitude of flow disturbance caused by the mast. Turbulence intensity of the wind component in direction of mean wind u is the dimensionless ratio of standard deviation σ_u and wind speed (Stull, 1988):

$$I_u = \frac{\sigma_u}{\overline{u}} \quad . \tag{3.3}$$

When measurements are conducted at a meteorological tower, not only the environmental turbulence – caused by the surrounding surface roughness – is observed, but also turbulence induced by the flow around the mast's structure is registered. Thus, turbulence intensity measured by ultrasonic anemometers at the Wettermast Hamburg is a superposition of turbulence induced by surrounding surface roughness and mast-induced turbulence. Turbulence intensity can therefore provide information about the flow area disturbed by the mast itself. Figure 3.4 shows the medians of turbulence intensity for $1°$-wide wind direction intervals at different heights. Turbulence intensity is generally higher at lower measuring heights because of the stronger turbulence caused by the closer surface. At 10 m, the turbulence

intensity median fluctuates around 0.15 without any wind direction dependency. This measurement is taken on top of a separate mast (see Section 3.1) and therefore, the turbulence intensity median is not influenced by any supporting structures. The measurements at the other heights show that the turbulence intensity median is distinctly increased at wind directions close to the mast's direction compared to the supposedly undisturbed directions. From this analysis at different heights it is concluded that the wind direction range between 60° and 320° is undisturbed by the mast's structure.

These initial considerations have been further investigated by Jacob (2013). Here, measurements at the Wettermast Hamburg and Sodar observations during a time period from April 2010 to July 2012 at the site are compared. Jacob states as well that wind measurements are influenced by mast circulation. Additionally, it is mentioned that the width of the disturbed sector varies with height. In general, Jacob's findings support the above stated range of disturbed wind directions. The variations of the range with height are ascribed to varying geometry of the platforms at different measurement heights. In addition Jacob mentions that the width of the sector that has to be considered as disturbed not only varies between measurement heights but also with the averaging interval used. The magnitude of variations due to measuring height, however, predominates the magnitude of variations due to the averaging interval.

Additionally, Jacob (2013) quantifies the deviations between wind speed measured at the Wettermast Hamburg and wind speed measured by Sodar. Here, for wind directions just outside the disturbed sector and up to perpendicular to the boom direction, wind speed are up to 20% higher than the comparison measurements from the Sodar. However, the exact value of this deviation is uncertain. Hein (2012), Heitmann (2012), and Sudmeyer (2012) compare measurements at the Wettermast Hamburg with Sodar and Wind Lidar measurements. All authors mention systematic deviations – both over- and underestimation – between wind speed measurements at mast and Sodar. The potential overestimation of wind speed at wind directions perpendicular to the boom direction that Link (1966) mentions is confirmed by Jacob (2013). However, since the exact amount of this effect is unclear, no correction is applied in this thesis.

Based on the above analysis and the recommendations given by Jacob (2013), only wind directions dd between

$$60° \leq dd \leq 320° \tag{3.4}$$

are included in all following analyses, to avoid measurements from obviously disturbed wind directions. The exclusion range (3.4) results in a wake region of 100° width. This is wider than the wake region stated by Link (1966) but narrower than the wake region mentioned by Gill et al. (1967). Any time step where the wind direction in at least one height is outside this range will be omitted. It has to be considered, however, that wind direction measurements in the wake region are influenced by these disturbances themselves and no undisturbed wind direction measurements over the whole time period are available. Even when comparing measurements from ultrasonic anemometers with Sodar

Table 3.2: Description of the site's surrounding characteristics. The wind direction range between $320°$ and $60°$ is excluded in this study due to disturbances of the mast structure on the measurements from those directions (see s. 3.2). The estimated roughness length z_0 is assessed based on the surrounding characteristics and values given by Stull (1988) and Arya (2001).

direction	distance from site			z_0 from idealized estimations
	< 200 m	< 500 m	< 1000 m	
$60°–90°$	meadow	lake	scattered buildings	0.007 m – 0.2 m
$90°–120°$	meadow	gravel pit	meadow	0.007 m – 1 m
$120°–150°$	meadow	gravel pit	meadow	0.007 m – 1 m
$150°–180°$	meadow, buildings	allotment	meadow, railway sidings	0.015 m – 0.15 m
$180°–210°$	meadow, buildings	allotment	railway sidings	0.015 m – 0.15 m
$210°–240°$	meadow, buildings	allotment	railway sidings	0.015 m – 0.15 m
$240°–270°$	meadow, buildings	industrial area	industrial area	0.015 m – 0.5 m
$270°–300°$	meadow, buildings	industrial area	industrial area	0.015 m – 0.5 m
$300°–320°$	meadow, buildings	industrial area	industrial area	0.015 m – 0.5 m

and Wind Lidar data, a deviation range of $\pm 10°$ is found (Heitmann, 2012; Sudmeyer, 2012). Nevertheless, the error made by taking the wind direction measured by ultrasonic anemometers mounted on the mast is assumed to be reasonably small and will therefore not be corrected. Likewise, the supposed wind speed deviations have not been corrected in this thesis since it has not been possible to distinguish the amount of deviation due to mast circulation from a systematic over- or underestimation of wind speed measurements of other instruments.

3.3 Surroundings of the Wettermast Hamburg

The Wettermast Hamburg site is situated at the easterly outskirts of the city of Hamburg. The immediate surroundings of the site are therefore not homogenous but are dominated by different roughness elements, depending on distance from the mast and wind direction (Fig. 3.5).

The 12 m mast is located on a meadow and the immediate surrounding is relatively smooth and undisturbed. The tall mast is surrounded by operational buildings and trees of approximately 10 m height. But as measurements at this mast are only conducted at 50 m or above, these obstacles are not expected to influence the measurements considerably. The site is surrounded by allotment gardens (south), a gravel pit (east and north) and industrial buildings (west). The more distant area around the measurement site towards the west is characterized by industrial buildings and the city of Hamburg. East of the site the terrain is mainly rural. Detailed descriptions of roughness characteristics of the surroundings and roughness length estimated from studies in idealized conditions are given in Table 3.2.
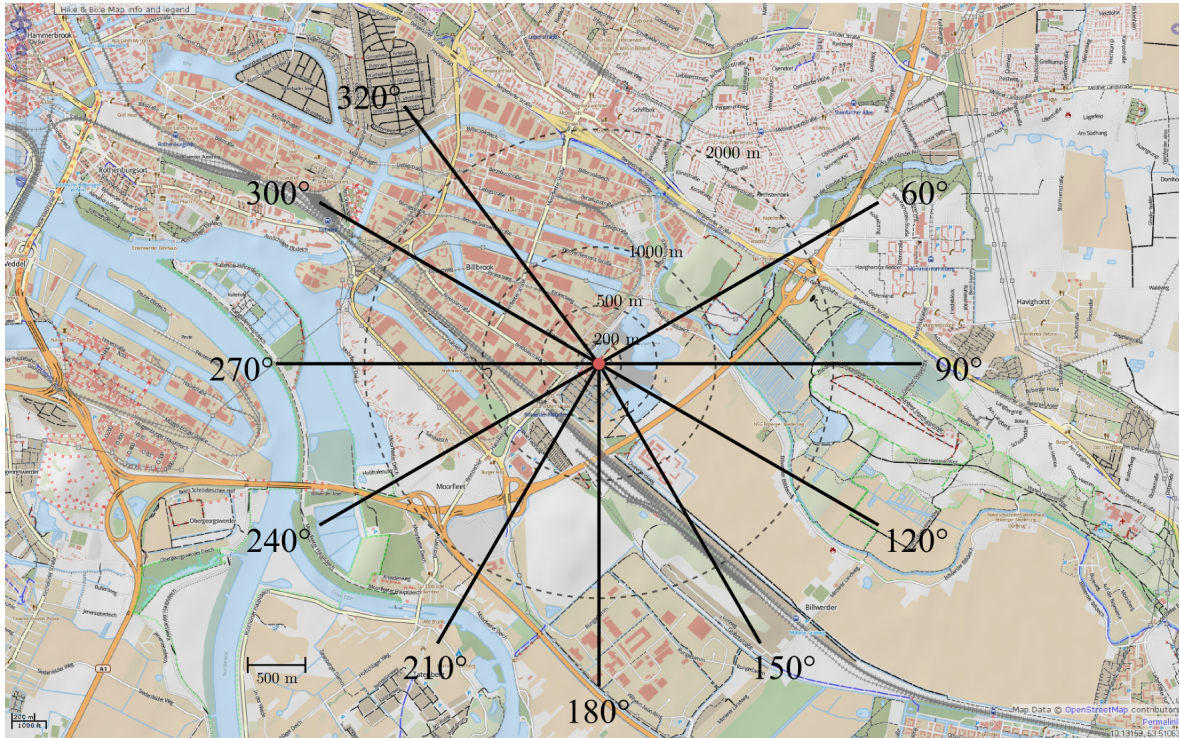
Figure 3.5: Map of the location and surroundings of the Wettermast Hamburg. The wind direction range between 320° and 60° is excluded in the analysis due to the disturbances of the mast structure on the measurements from those directions (Sect. 3.2). Map source: OpenStreetMap (http://www.openstreetmap.org).

The surroundings of the Wettermast Hamburg site are far from homogenous. It can therefore be expected that changes in surface characteristics result in formation of an internal boundary layer (IBL) which could influence the wind profile. Arya (2001) mentioned that the height of the IBL h_i that develops behind a step change in surface roughness can be estimated in neutral stratification by:

$$h_i = z_{0,2} \cdot c \left(\frac{x}{z_{0,2}} \right)^{0.8} \quad . \tag{3.5}$$

$z_{0,2}$ is the new surface roughness behind the step change. c is an empirical constant, which is dependent on the definition of IBL height and which Arya recommends to be 0.38. The distance from the step change in surface roughness is x. The height of an IBL grows with increasing distance from the step and is also larger with larger roughness lengths. According to Arya (2001), little is known about the shape of Equation (3.5) for stable or unstable stratification. It can however be assumed, that the IBL top is higher at unstable and lower at stable stratification.

Equation (3.5) can be used to roughly estimate the vertical extent of the influence of changes in surface roughness at the surroundings of the Wettermast Hamburg. For example, the meadow around the 12 m mast extends to approximately 200 m distance. With an assumed surface roughness of

$z_{0,\text{meadow}} = 0.007\,$m the vertical extent of the layer which is influenced by the smoother surface of the meadow is 9.7 m. This corresponds with the lowest measuring height of wind speed used in this study. Therefore, measurements in 10 m might represent another layer than those at larger heights in some cases. The roughness length of the allotment gardens (distance approximately 500 m) south of the site is estimated as $z_{0,\text{allotment}} = 0.15\,$m. Accordingly, the vertical extent of the layer, influenced by the allotments is 37.5 m.

The two examples above show that the surroundings of the Wettermast Hamburg are not homogeneous and that effects due to changes in surface characteristics propagate to layers of varying heights. However, data used in this study are averaged over a relatively large sample and the vertical extent of possible IBLs are sure to vary over time due to changing stratification. Therefore, the effect is considered to be small.

3.4 Data Availability and Wind Climatology

The Wettermast Hamburg facility is operated since 1963. The primary instrumentation was substituted in the early 1990s and since 1995 continuous digital measurements are available. Beginning in 1995, the instrumentation was constantly expanded and improved (Link, 1966; Brümmer et al., 2012).

For this study data from October 2000 until March 2012 are available. Unless indicated otherwise, 10-minute averages of all quantities are used. Since the instruments in 280 m height were installed only in July 2010, this height is disregarded. This results in a total of 601 632 possible measurement intervals. The number of available measurements in each height is shown in Figure 3.6. Since the number of possible measurements fluctuates depending on the number of days in each month, the number of available measurements is normalized with the maximum number of 10-minute intervals in each month.

As can be seen in Figure 3.6, top, the number of available observations varies at each measurement level. Some reasons for data gaps are maintenance at the measurement infrastructure, replacement of instruments, maintenance on the radio tower itself, or stroke of lightning which causes power outage at the tower. Since not all of these reasons occur at all measurement levels at the same time, this results in a different number of available observations. Only complete profile measurements without missing values are used. This results in a total of 523 531 (87%) wind profiles (Fig. 3.6, bottom). Furthermore, any time step where the wind direction in one or more heights was in the disturbed wind direction range $320° \leq dd \leq 60°$ is discarded as well, leaving 407 666 (68%) profiles. To ensure a minimum of turbulent mixing in the ABL, only wind speeds $\geq 1\,\text{m s}^{-1}$ are considered. 374 766 (62%) profiles comply with this prerequisites and are available for this study.
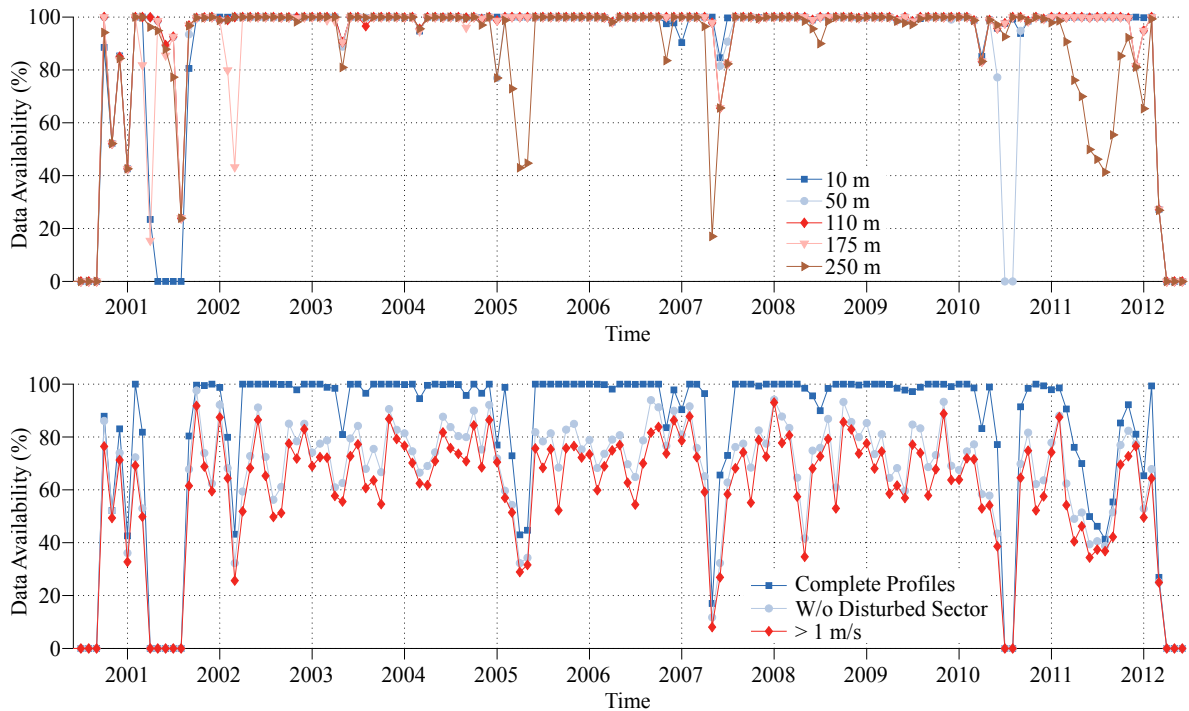
Figure 3.6: Data availability within observation period. Top: data availability at each height during the time period used for this study. Bottom: data availability of profile measurements for increasingly strict requirements: complete profiles; additionally, wind direction not within the disturbed sector; additionally, wind speed larger than $1 \, \mathrm{m \, s^{-1}}$. Since the number of possible measurements fluctuates depending on the number of days in each month, the number of available measurements is normalized with the maximum number of measurements.

As illustrated in Figure 3.7, the frequency of occurrence of wind direction and wind speed varies at different heights. West and southeast are the two prevailing wind directions in all heights. Most frequent wind directions are around west which is typical for a location in the mid-latitudes. The second most frequent direction is southeast. The frequency of occurrence of those easterly winds decreases with height, but even in 250 m winds from southeast are more frequent than those from east or south. One possible explanation for the frequent occurrence of southeasterly winds would be local effects like canalization within the valley of the river Elbe (Brümmer et al., 2012). However, the cause of these southeasterly winds is still subject to ongoing research.

Overall, wind speeds increase with height due to the reduction of surface friction. In 10 m the wind speed is mainly smaller than $5 \, \mathrm{m \, s^{-1}}$ and some wind speeds are between 5 and $10 \, \mathrm{m \, s^{-1}}$. Wind speeds smaller than $5 \, \mathrm{m \, s^{-1}}$ are considerably less frequent in larger heights. Small wind speeds ($< 5 \, \mathrm{m \, s^{-1}}$) show, except for 10 m height, almost no direction dependency. Therefore, in contrast to high wind speeds which predominantly occur at westerly directions, low wind speeds occur at all wind directions with the same frequency. Larger wind speeds ($> 10 \, \mathrm{m \, s^{-1}}$) are more frequent at 110 m and above. Even
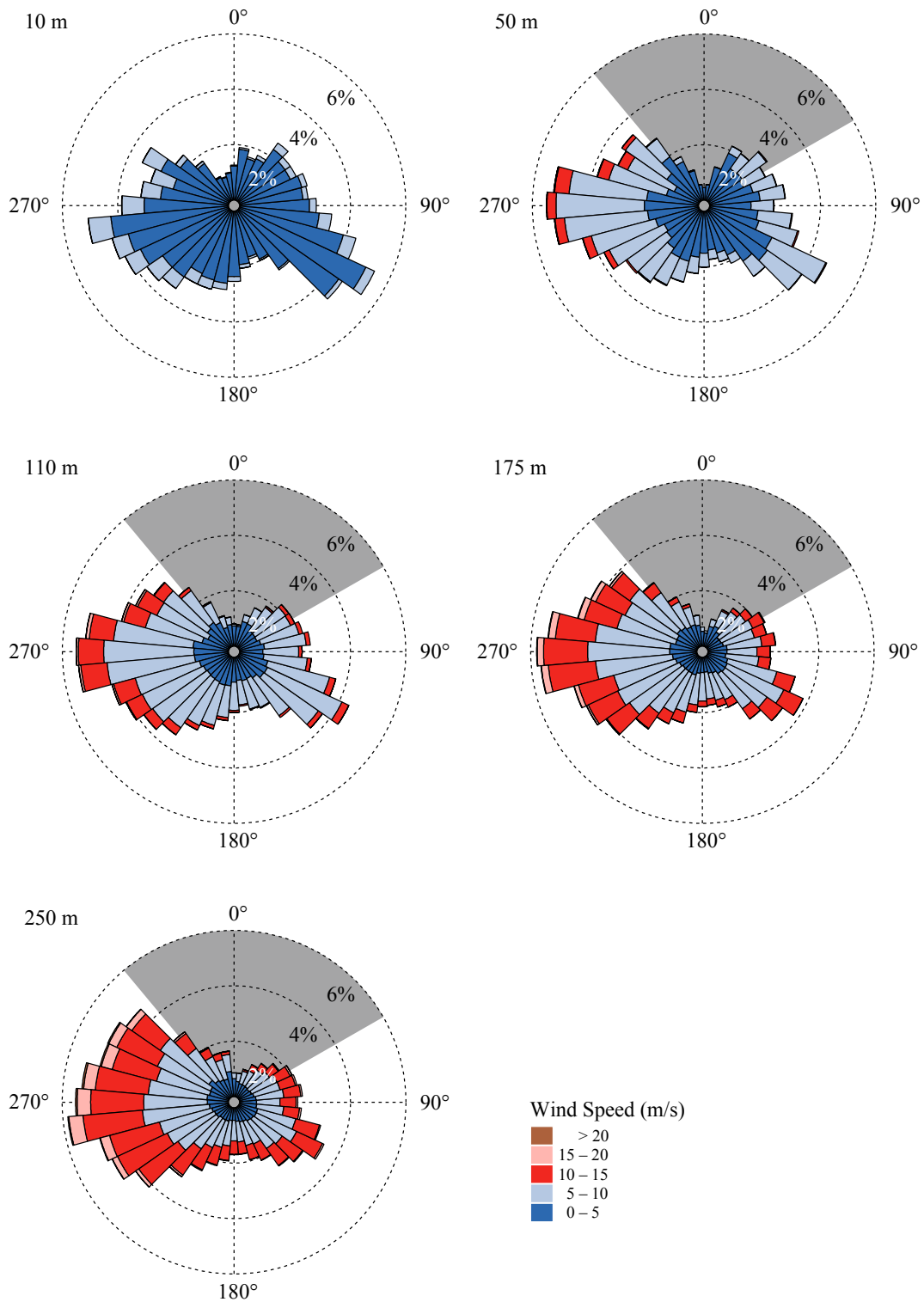
Figure 3.7: Frequency distribution of wind speed classes (colors) per 10°-wide wind direction sector for the measuring heights 10 to 250 m. The gray area (heights 50 to 250 m) marks the sector which is considered to be disturbed due to the main mast itself (Eq. (3.4)).
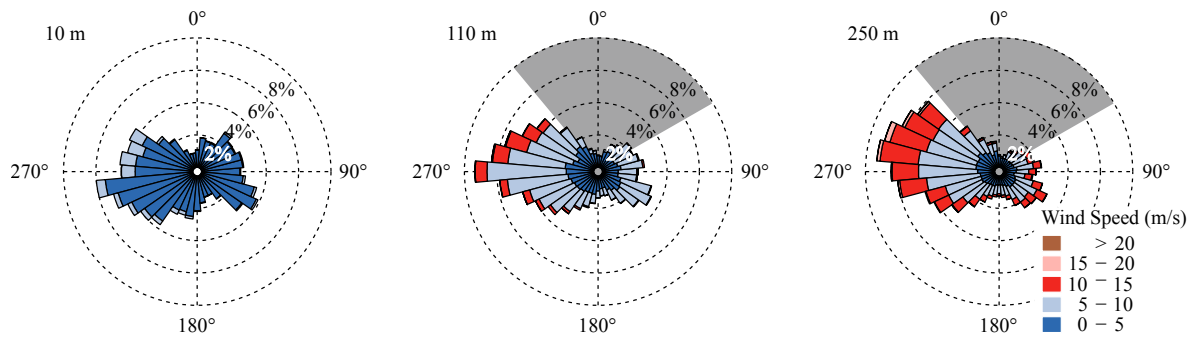
Figure 3.8: Relative frequency distribution of wind speeds per wind direction during summer months (JJA) exemplary for the heights 10, 110, and 250 m. Frequency of occurrence is normalized with overall number of profiles from summer months. The gray area (heights 110 and 250 m) marks the sector which is considered to be disturbed due to the main mast itself.
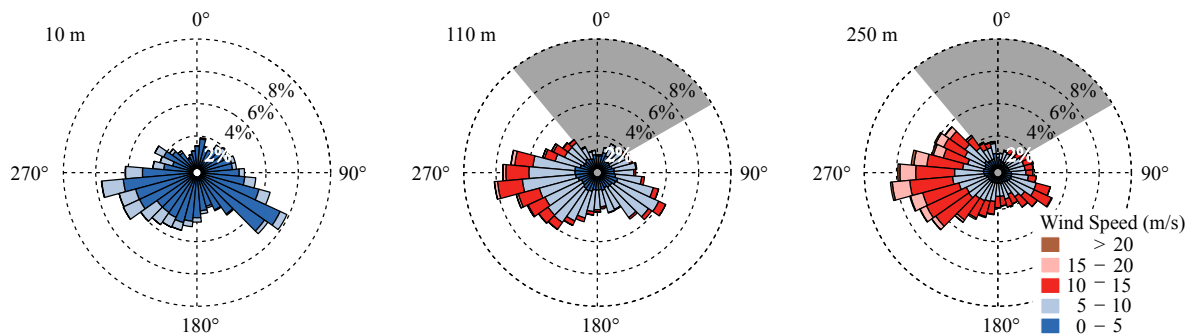
Figure 3.9: Same as 3.8, but for winter months (DJF). Frequency of occurrence is normalized with overall number of profiles from winter months.

larger wind speeds ($> 15\,\mathrm{m\,s^{-1}}$) also almost exclusively occur at westerly directions.

The increase of wind speed with height is also dominant when distinguishing between summer (June, July, August, Fig. 3.8) and winter (December, January, February, Fig. 3.9) months. During summer months westerly directions are more dominant (up to 7% per class), while wind from southeast is less frequent with up to 4% in 10 m and even less in larger heights. High wind speeds are less frequent in all heights than in the overall distribution (Fig. 3.7). Wind speeds $> 15\,\mathrm{m\,s^{-1}}$ are only present at westerly directions and no wind speeds above $20\,\mathrm{m\,s^{-1}}$ occur.

During winter months easterly directions are more frequent than during summer. For smaller wind speeds, i.e. $\leq 5\,\mathrm{m\,s^{-1}}$ in 10 m, this is even the most frequent wind direction. In 110 m the most frequent wind direction is again west (more than 8% of the data) with the highest wind speeds. Easterly directions (approx. 6% per class) are second most frequent here. In 250 m west is the dominant wind direction. The highest wind speeds ($> 20\,\mathrm{m\,s^{-1}}$) only occur from westerly directions. High wind speeds occur more often during winter than during summer months.

Lange (2001) and Brümmer et al. (2012) give an extended description of the climatology at the Wettermast Hamburg site covering the main climate variables (pressure, temperature, humidity, wind, radiation, clouds, and precipitation). In this study it is stated that wind speed follows an annual cycle where highest monthly wind speeds occur in January and lowest in August. This corresponds with the observations above.

In this chapter, the measurement site Wettermast Hamburg is described and information to aid the interpretation of measurement data are collected.

- The Wettermast Hamburg site is located at the easterly outskirts of Hamburg and consists of a 305 m high main mast and a 12 m high secondary mast. In this study wind and temperature observation from five measurement levels between 10 m and 250 m are used.

- The mast's layout poses a challenge regarding the disturbance of the flow due to mast circulation. The disturbed wind direction sector is identified by means of turbulence intensity. To avoid the disturbances of observations by the mast's structure, only the wind direction range $60°$ to $320°$ is used for further investigations.

- The location of the Wettermast Hamburg site at the easterly outskirts of Hamburg allows for the analysis of the wind profile at different surface roughnesses depending on the wind direction. Overall, the terrain to the west of the site is mostly urban. To the east it is mainly rural. However, since the surroundings are far from homogeneous, attention must be paid to those inhomogeneities when interpreting results.

- Measurements at the Wettermast Hamburg during a time period from October 2000 until March 2012 are available for this study. Only measurements are used that comprise complete profiles throughout the entire mast height. Additionally, the wind direction in all heights has to be outside the disturbed sector and the wind speed larger than $1\,\mathrm{m\,s^{-1}}$. 62% of the maximum possible measurements comply with those prerequisites.

- The prevailing wind directions at the Wettermast Hamburg site are westerly directions with overall higher wind speeds than from other directions. Southeasterly wind directions are second most frequent. From this directions, however, mostly low wind speeds are present. Higher wind speeds occur during winter than during summer. Also, most cases with southeasterly wind direction occur during winter.

4

Surface Roughness

The boundary layer wind profile is influenced by the surface roughness. Due to the drag of the air flow over a rough surface turbulence is induced. This causes downward impulse flux which extracts momentum from higher levels and thus influences the shape of the wind profile.

The Wettermast Hamburg is located in the transition area of the city of Hamburg and its rural surroundings. This presents the unique opportunity to transfer the common methods of determining the surface roughness from meteorological measurements at rather ideal locations to a site, where the surface features are less homogeneous.

An overview of the common methodology for quantifying the surface roughness is given in Section 4.1. The friction velocity u_* is a measure of impulse flux which is sensitive to surface friction. It is derived from flux variance similarity in Section 4.2. To quantify the surface roughness, the roughness length z_0 is calculated from wind profile measurements in Section 4.3 and the sensitivity on wind speed of this results is assessed in Section 4.4. Eventually, modeled wind speeds from the approaches of Gryning et al. (2007) and Peña et al. (2010) are compared to measurements at different surface roughnesses in Section 4.5.

4.1 Methodology

In principle there are two main approaches to quantify the surface roughness around a measuring site: the *geometric method* of determining the surface roughness by assessing the geometrical characteristics of the roughness elements or *micrometeorological method* of calculating roughness parameters by meteorological observations of wind or turbulence (Foken, 2006b; Grimmond and Oke, 1999). The geometric approach incorporates the estimation of values for the surface roughness by using general data determined from wind tunnel measurements in idealized flows over simplified areas with rough-

ness elements (Bechtel et al., 2011). The advantage of this approach is that no towers or environmental measurements are needed to quantify the surface roughness. In case of the Wettermast Hamburg site however, the surrounding surfaces are far from ideal or even homogeneous. Therefore, such methods would only give a rough estimate and a micrometeorological method will be used. In micrometeorological methods, measurements of quantities in the lower boundary layer are used to quantify surface roughness. An advantage of this approach is that the surface roughness can comprise a mix of different roughness elements and no prior categorization is necessary. For this purpose, the roughness length z_0 is used. It is defined as the height at which the wind speed vanishes (Eq. 2.6).

Several approaches for the determination of the roughness length from micrometeorological measurements have been proposed in literature. In general, mainly three methods are used to obtain the roughness length from measurements: analysis of gustiness, use of drag coefficient, and profile method (Wieringa, 1993; Verkaik and Holtslag, 2007).

Friction caused by surface roughness elements generates turbulence and the resulting gustiness of the flow can be used to determine surface roughness. The gustiness is quantified by the standard deviation of horizontal wind speed σ_u. The turbulence intensity $I_u = \sigma_u/\overline{u}$ is the standard deviation of wind speed, homogenized with average wind speed $\overline{u}$ to account for the fact that at higher wind speeds larger variability of wind speed occurs. It can be related to roughness length z_0 by the approximation (Lumley and Panofsky, 1964):

$$I_u = \frac{\sigma_u}{\overline{u}} \approx \frac{1}{\ln(z/z_0)} \quad . \tag{4.1}$$

Here, σ_u and $\overline{u}$ are taken at height z. Wieringa (1993) states that for roughness length calculation at 10 m the fetch extends several kilometers in upwind direction. Therefore, roughness lengths derived by this method represent more an spacial average than a local value.

From the logarithmic wind profile, the ratio of friction velocity and average wind speed can be used to determine the roughness length. This ratio is the drag coefficient $C_D = (u_*/\overline{u})^2$. It relates to the surface roughness as (Wieringa, 1992):

$$C_D = \left(\frac{\kappa}{\ln(z/z_0)}\right)^2 \quad . \tag{4.2}$$

Here, κ is the dimensionless Kármán constant (commonly agreed upon to be 0.4, (Stull, 1988; Arya, 2001; Etling, 2008)). Since z_0 from this method is height dependent, Wieringa (1992) states that the drag coefficient is useful for estimating the surface roughness in numerical models at fixed levels, but not as suitable for surface layer wind analysis.

Most often, the roughness length is determined from wind profile measurements (Foken, 2006b). Arya

(2001) and Wieringa (1993), for example, suggest to calculate z_0 from wind profiles according to:

$$\overline{u}(z) = \frac{u_*}{\kappa} \ln\left(\frac{z}{z_0}\right) \quad . \tag{4.3}$$

Strictly speaking, Equation (4.3) is only valid in the surface layer. Fiedler and Panofsky (1972) therefore proposed an *effective roughness length* $z_{0,e}$. This is a measure of surface roughness in heterogeneous terrain for large scale characterization that can be calculated from profiles that extend above the surface layer. They define the effective roughness length as the roughness length homogeneous terrain would have to reproduce the correct momentum flux near ground. To derive $z_{0,e}$ from profile measurements, they introduce an additional length scale that accounts for larger eddy size in higher levels. The extended logarithmic wind profile in neutral stratification is then of the form:

$$u = \frac{u_*}{\kappa} \ln\left(\frac{z}{z_{0,e}}\right) + \beta z \quad . \tag{4.4}$$

The additional constant in the second term is proposed as $\beta = 144f$ (f being the Coriolis parameter) but Fiedler and Panofsky found evidence that it could also be smaller. The derived effective roughness length is often used in large scale modeling to represent the inhomogeneity of surface roughness in grid cells (Hasager et al., 2003; Leclerc and Foken, 2014).

For neutral stratification vertical flux of horizontal momentum is not enhanced or diminished by buoyancy effects (Wieringa, 1993). It is therefore convenient to estimate the surface roughness from measurements taken in a neutrally stratified surface layer where no additional stability correction is necessary. Although several studies determined z_0 from profile measurements at diabatic conditions (Blatt, 2010; Graf et al., 2014), in this thesis only profiles at neutral stratification are considered.

Dense placement of roughness elements often causes elevation of the wind field (Foken, 2006b; Graf et al., 2014). In this case, it might be necessary to calculate a displacement height d. However, since the surroundings of the Wettermast Hamburg are far from homogeneous and the individual roughness elements are relatively scattered, this has been omitted in this thesis.

Several studies have been published that state typical roughness length values for varying surface characteristics. Wieringa (1993) listed an extensive collection of the roughness lengths calculated at different experiments and the methods used in these studies. The investigated surfaces range from very smooth (flat snow field with z_0 between 0.0001 and 0.0007 m) to very rough conditions (regularly built town with z_0 between 0.7 and 1.5 m). Grimmond (1998) and Grimmond and Oke (1999) further expanded the knowledge about the values of z_0 for different surfaces by analyzing inhomogeneous terrain in large cities. They found z_0 to vary between 0.3 m for residential areas and > 2 m for high-rising urban core areas with multistory buildings.

Verkaik and Holtslag (2007) calculated the roughness length z_0 at the meteorological tower in Cabauw, Netherlands, with the three methods mentioned above (gustiness analysis, wind profile, and drag coefficient). All those methods produced different values. For some directions, the values varied between 10^{-3} and 10^{-1} m. The authors stated that the roughness length derived from gustiness analysis represents a superposition of local and distant surface roughnesses. The values of z_0 are often largest when determined with this method. If the roughness length is determined from the drag coefficient, it is found to represent more local characteristics than those from gustiness analysis. For the determination of z_0 from wind profiles Verkaik and Holtslag found that the results depended on the used height interval. Therefore, the roughness lengths estimated from different methods can not necessarily be compared directly. Grimmond (1998), Frank et al. (1999) and Hasager et al. (2003) also found seasonal variability of the roughness length due to changing vegetation during summer and winter months. It can therefore not be assumed that the value of z_0 is constant over time.

Surface conditions around the Wettermast Hamburg vary depending on the wind direction (Sect. 3.3). To the east of the site the landscape is quite flat dominated by rural surroundings. In the west mainly industrial buildings are present (see Figure 3.5). Therefore the roughness length has been calculated for different wind directions.

4.2 Friction Velocity

As will be shown in Section 5.1, the quality of eddy covariance measurements at the Wettermast Hamburg site is somewhat uncertain. Therefore, the friction velocity u_*, along with the Obukhov length L (Eq. (2.3)) later on, is recalculated to avoid these eddy covariance measurements. Even if the uncertainty of the eddy covariance measurements is not as obvious as for the Obukhov length, u_* should be recalculated to gain a coherent data set.

According to flux variance similarity, friction velocity and variance of wind speed are related. If the variance of vertical wind speed σ_w is scaled with the friction velocity u_* it is only a function of stability parameter (z/L) in unstable stratification and constant in stable stratification (Arya, 2001; Blackadar, 1997). Several studies have been carried out to determine the exact relation between variability of wind components and friction velocity. For unstable stratification the relation found is mainly of the form $\sigma_w/u_* = a_1 (a_2 - a_3 (z/L))^{1/3}$, where the constants a_{1-3} are empirically determined in these studies. For stable conditions, the ratio of variance and friction velocity is deemed to be constant $\sigma_w/u_* = b$. The recommendations of those studies (Tab. 4.1) and the resulting friction velocities vary only slightly. In the course of this thesis, the formulations by Hicks (1981) and Sorbjan (1987) are

Table 4.1: Flux variance relations for determining friction velocity u_* from wind speed variances proposed by different authors.

Study	σ_w/u_*, unstable	σ_w/u_*, stable
Panofsky and Dutton (1984)	$1.25\left(1-3\dfrac{z}{L}\right)^{1/3}$	
Panofsky et al. (1977)	$1.3\ \left(1-3\dfrac{z}{L}\right)^{1/3}$	
Blackadar (1997)		1.3
Hicks (1981)	$1.25\left(1-2\dfrac{z}{L}\right)^{1/3}$	
Sorbjan (1987)		1.5
Stull (1988)	$1.9\ \left(\dfrac{z}{L}\right)^{1/3}$	$\sqrt{2.5}$

used to recalculate u_* for further use, as described by the following equation:

$$\frac{\sigma_w}{u_*} = \begin{cases} 1.25\left(1-2\dfrac{z}{L}\right)^{1/3} & L < 0 \\ 1.5 & L > 0 \end{cases} \quad . \tag{4.5}$$

For this approach of calculating u_*, the standard deviation of the vertical wind component σ_w is needed. The native recording interval of σ_w at the Wettermast Hamburg is five minutes. To match the averaging interval of the other wind profile measurements that are used throughout this work, the measurements of σ_w have to be extended to the averaging interval of ten minutes. For this, instead of simply averaging two five minute intervals, the variances between the two consecutive intervals need to be accounted for as well. According to Lange (2010), this can be achieved by:

$$\sigma^2 = \frac{1}{n}\left[\sum_{i=1}^{n}\left(\sigma_i^2 + \mu_i^2\right) - \frac{1}{n}\left(\sum_{i=1}^{n}\mu_i\right)^2\right] \quad . \tag{4.6}$$

Here, σ^2 is the squared standard deviation of an arbitrary quantity, n is the number of consecutive intervals to combine (in case of σ_w it is $n = 2$, for two five minute intervals), σ_i is the standard deviation, and μ_i is the average of one shorter interval. After extending the five minute standard deviation values of the vertical wind component to ten minute averages using Equation (4.6), the friction velocity is calculated according to (4.5).

The quality of recalculated friction velocity can be determined by utilizing the definition of drag coefficient ($C_D = (u_*/\bar{u})^2$). In neutral stratification friction velocity is proportional to wind speed with
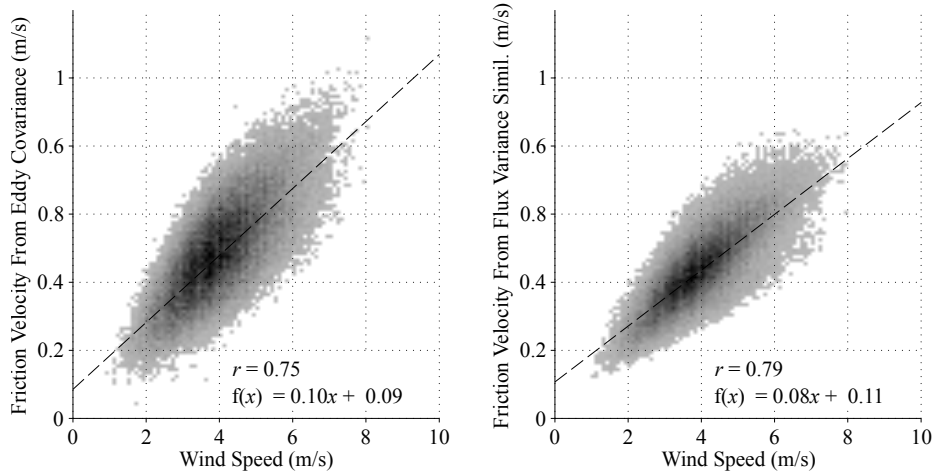
Figure 4.1: Comparison of friction velocity and wind speed in 10 m in neutral stratification. Shades denote data density. Left: friction velocity from eddy covariance measurements. Right: friction velocity, recalculated with flux variance similarity.

the drag coefficient C_D as proportionality constant: $u_* = \sqrt{C_D} \cdot u$ (e.g. Etling, 2008). The correlation coefficient r (see Appendix A.2) between friction velocity u_* and wind speed u is larger for better agreement between these two quantities (Fig. 4.1). Between wind speed and friction velocity from eddy covariance measurements is $r = 0.75$, while the correlation between wind speed and friction velocity from flux variance similarity is $r = 0.79$. While this slight increase might not seem like a big improvement, in combination with the improved calculation of the Obukhov length L (as will be discussed in Sect. 5.1) this leads to a more reliable data set of turbulent flux measurements.

4.3 Estimation of the Roughness Length from Average Profiles

To appraise the measurements at the Wettermast Hamburg site, the roughness characteristics of the surroundings are one essential quantity to consider. Therefore, as mentioned previously (Sect. 4.1), the roughness length is determined from wind profile measurements in this section. The roughness length z_0 is calculated from comparison of measured profiles with the logarithmic wind profile for neutral stratification. Additionally, an effective roughness length $z_{0,e}$ is derived from an extended, log-linear wind profile to account for the changing shape of the profile at higher levels.

4.3.1 Roughness Length from Linear Wind Profiles

As a first estimate, the roughness length will be calculated from profile measurements by applying the logarithmic wind profile. Only complete profiles (Sect. 3.4) in neutral stratification are considered

for this analysis. If the temperature gradient between all used heights is $|\Delta\theta/\Delta z| < 0.005$ K/m the stratification is deemed to be neutral. Additionally only profiles are selected with downward impulse flux ($u_* \geq 0.1\,\mathrm{m\,s^{-1}}$). Smaller values indicate an unusual state of the boundary layer with upward momentum transport. The wind speed has to be greater than $1\,\mathrm{m\,s^{-1}}$ to ensure a reasonably well mixed boundary layer.

For the roughness analysis all wind directions are sub-divided into $30°$-wide sectors between $60°$ and $320°$. The range between $320°$ and $60°$ is disregarded due to the disturbance of the flow by the mast's structure (Sect. 3.2). From 601 632 measurements conducted in the observation period, 69 726 (12%) profiles remain that meet all the above mentioned requirements.

These remaining profiles are homogenized with the wind speed at the reference height $u(z_{\mathrm{ref}} = 175\,\mathrm{m})$ to eliminate the effect of different overlying large-scale wind speeds on the profiles at different times. z_{ref}=175 m is chosen as a reasonable compromise between a measuring height that is high enough to ensure a relatively undisturbed flow and low enough to very likely still lie within the surface layer. Equation (4.3) then becomes:

$$\frac{u(z)}{u(z_{\mathrm{ref}})} = c \ln\left(\frac{z}{z_0}\right) \quad . \tag{4.7}$$

Here, c is a proportionality constant.

The shape of the resulting profiles varies depending on the wind direction (Fig. 4.2). In some directions the wind profile at higher levels deviates from the logarithmic form quite a bit, whereas in other directions the profile is almost perfectly logarithmic. A least squares fit of the form $f(x) = a_1 \ln(x/a_2)$ is performed to adapt Equation (4.7) to the average profiles. Additionally, to asses the impact of the deviation from the logarithmic profile at higher levels, this fit is performed three times, using the lowest three (10 to 110 m), lowest four (10 to 175 m), and all five (10 to 250 m) heights respectively.

As can be seen in the two exemplary wind direction sectors in Figure 4.2, the profile deviates considerably from the logarithmic law in south-easterly directions ($180° - 210°$, Fig. 4.2 (a)). This in turn leads to strong differences in the fitted profiles. In other directions, however, the average wind profile seems to be mostly logarithmic ($270° - 300°$, Fig. 4.2 (b)). These deviations from the logarithmic form for some wind direction sectors cause a sensibility of the calculated roughness lengths to the number of heights that are used.

The calculated roughness lengths from a least squares fit of the logarithmic profile (4.7) to average normalized wind profiles, considering three, four, and five heights, are listed in Table 4.2. The resulting roughness lengths are larger the more heights are considered. However, the impact of the varying number of considered heights varies for different wind direction sectors. For $180° - 210°$, roughness lengths range between 0.34 m for three heights and 0.82 m for all five heights. Hence, the difference of roughness lengths is $\Delta z_0 = 0.47$ m in this sector. The roughness length in the sector $270° - 300°$, on
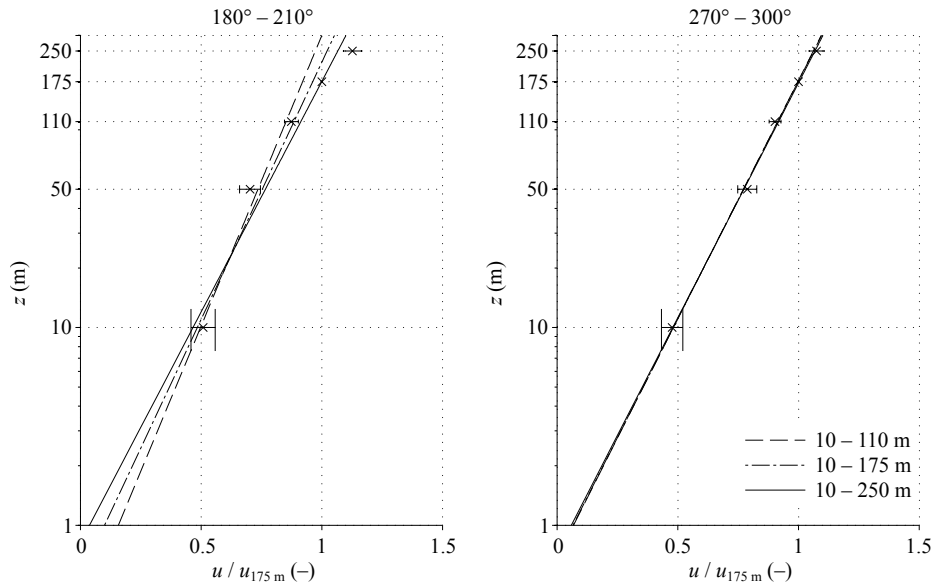
Figure 4.2: Averages of the normalized wind speed profiles (markers) for two exemplary 30°-wide wind direction classes. The horizontal error bars denote the standard deviation of the measurements. The lines represent the least squares fit of the logarithmic wind profile according to Equation (4.7) with different number of heights considered: the lowest three heights (dashed line), lowest four heights (dash-dotted line), and all five heights (solid line). Different height of error bar ends due to logarithmic display.

the other hand, varies only slightly between 0.69 m and 0.72 m for varying number of heights. This leads to a difference of roughness lengths of only $\Delta z_0 = 0.04$ m. It can therefore not be concluded that the inclusion of all five heights results in an increase of the roughness length in general. This behavior depends on the wind direction.

Another indicator for the impact of the deviation from the logarithmic profile form is the value of the RMSE for the three different fits. The RMSE is calculated for all levels, even those that are not considered for the least squares fit. Therefore, it indicates the goodness of the fit to the entire profile. If the measured wind profile is mostly logarithmic up to 250 m, the RMSE should be of the same order, regardless of the number of included heights and even a fit with only the lowest three levels considered should be a good estimator of the wind speed at higher levels. On the other hand, if the profile deviates from the logarithmic form at higher levels, the RMSE should decrease, indicating a poorer fit to the data if less levels are considered. For the direction sector $180° - 210°$, the RMSE decreases by almost half from 0.079 for the three-height fit to 0.047 for the fit including all heights. In wind directions $270° - 300°$, on the other hand, the RMSE is almost constant regardless of the number of levels included (0.011 for three levels and 0.010 for all five levels).

From the above analysis it becomes quite clear that the estimated z_0 strongly depends on the height of the topmost measurement considered for this analysis for some wind direction sectors. If only

Table 4.2: Roughness length z_0 and root mean square error (RMSE) between fitted function and normalized wind speed at different wind direction sectors between $60°$ and $320°$ for a least squares fit of the logarithmic wind profile (Eq. (4.7)). z_0 is calculated using the lowest three, four, and all five heights of the Wettermast Hamburg. The RMSE is calculated for all levels, regardless if they are considered for the least squares fit. Δz_0 is the difference of roughness lengths depending on how many heights are used to derivate z_0. N is the number of profiles that are included in the analysis. The wind directions between $320°$ and $60°$ are disregarded due to disturbances of the mast structure.

		$60° - 90°$	$90° - 120°$	$120° - 150°$	$150° - 180°$	$180° - 210°$
10 to 110 m	z_0 (m)	0.35	0.35	0.20	0.13	0.34
	RMSE	0.053	0.033	0.022	0.067	0.079
10 to 175 m	z_0 (m)	0.49	0.44	0.23	0.23	0.55
	RMSE	0.036	0.023	0.018	0.048	0.056
10 to 250 m	z_0 (m)	0.64	0.52	0.27	0.36	0.82
	RMSE	0.030	0.020	0.016	0.042	0.047
	Δz_0	0.29	0.17	0.07	0.22	0.47
	N	2295	4426	2290	2629	6543

		$210° - 240°$	$240° - 270°$	$270° - 300°$	$300° - 320°$
10 to 110 m	z_0 (m)	0.74	0.96	0.69	0.34
	RMSE	0.053	0.025	0.011	0.029
10 to 175 m	z_0 (m)	0.93	1.05	0.69	0.40
	RMSE	0.036	0.018	0.010	0.022
10 to 250 m	z_0 (m)	1.16	1.17	0.72	0.49
	RMSE	0.030	0.015	0.010	0.017
	Δz_0	0.42	0.21	0.04	0.15
	N	14699	19542	9931	2843

the lowest three heights are used for the fit of the logarithmic profile and calculation of z_0, those values are much lower than those where all heights are considered. Additionally, this dependence on the number of considered measuring heights in some cases even changes order of roughness values for wind direction sectors: For example, z_0 is 0.20 m if calculated from the lowest three heights for wind direction sector $120° - 150°$ and 0.27 m if five heights are used. The roughness length for the neighboring wind direction sector $150° - 180°$, on the other hand, is 0.13 m if calculated from the lowest three heights and 0.36 m if all five heights are considered. As a result, if only the three lowest heights are used, it would be deduced that in $150° - 180°$ the roughness is higher than in the other sector. Inversely, if all heights are considered, the higher surface roughness would be assigned to $120° - 150°$. This illustrates that the estimation of surface roughness by means of z_0 is not certain at all. Even if in most direction sectors the order of roughness is consistent, for some directions this is also dependent on the method of deriving z_0.

Verkaik and Holtslag (2007) compared different methods of estimating roughness length from measurements at the 200 m high mast in Cabauw, Netherlands. They found as well that the roughness length is larger if higher levels are considered. The roughness lengths range from 0.03 m to 0.15 m for the same wind direction sector if different heights are considered. They attribute these discrepancies to the formation of an IBL close to the mast. Hertwig (2013) analyzes the impact of various stability thresholds and the number of measurement levels on the resulting roughness lengths for a $60°$ wide wind direction sector at Wettermast Hamburg. However, the more measurement heights are considered for this analysis, the larger the calculated roughness length. This is attributed to different heights of the surface layer.

One could assume that the over logarithmic increase of wind speed is caused by the lack of homogeneity in some directions and thus the existence of internal boundary layers (IBLs). These develop behind step changes in surface roughness. According to Bradley (1968) this kind of increase would occur at rough to smooth transitions in the upstream surface characteristics. As described in Section 3.3, the only rough to smooth transition in the extremely influenced sector $180° - 210°$ occurs in the immediate vicinity of the mast which would not lead to the development of an IBL that reaches up to about 100 m at the mast.

Another possible explanation would be that the stratification is not purely neutral but slightly stable which would increase the wind speed compared to the wind profile at neutral stratification. However, this cannot be confirmed when analyzing the temperature gradients closer. Even the temperature gradients over the entire mast height and between intermediate heights are within the above defined bounds $|\Delta\theta/\Delta z| < 0.005$ K/m. Additionally, Hertwig (2013) states that different stability thresholds only marginally influence the results of the roughness length calculation at the Wettermast Hamburg.

Therefore, it cannot be concluded with certainty what causes the stronger than logarithmic increase with height in some wind direction sectors. One remaining possible explanation is that the surface

layer does not extend up to the highest measurement levels and those therefore lie above it. Without means to determine the height of the surface layer, this can neither be confirmed nor disproved.

When comparing those calculated roughness lengths to the values given in literature (Sect. 3.3), the deviation is quite large. In $240° - 270°$ the calculated roughness lengths range between 0.96 m and 1.17 m, while literature states roughness lengths between 0.015 m and 0.5 m. In other directions, for example $270° - 300°$, the values are in moderate agreement. Here, a roughness length up to approximately 0.5 m is expected from literature research and the calculated values range between 0.69 m and 0.72 m.

To conclude, the calculation of roughness length from wind profiles measurements using the logarithmic wind profile is highly sensitive to the number of levels used. The shape of the average wind profile deviates from the theoretical logarithmic form in some wind direction sectors, while it is almost perfectly logarithmic up to 250 m in other sectors.

4.3.2 Roughness Length from Log-Linear Wind Profiles

The above findings show that the calculation of z_0 from wind speed profiles has to be handled with great care. The choice of the number and height of measurements can influence the results tremendously, because in some cases it cannot be assumed that the wind profile is logarithmic throughout the entire height of the mast. This leads to the assumption that, even though the averaged profiles have been carefully selected with regards to neutral stratification, the strictly logarithmic form of the wind profile (4.7) has to be modified to derive z_0 from tall profiles. To account for the different shape of the wind profile, a second, linear term is introduced into Equation (4.7), as described in Section 4.1:

$$u(z) = \frac{u_*}{\kappa} \ln \left(\frac{z}{z_{0,e}} \right) + \beta z \quad . \tag{4.8}$$

Here, $z_{0,e}$ is the effective roughness length, which can be taken as an estimator of the roughness length z_0 for tall profiles. Fiedler and Panofsky (1972) proposed this approach of estimating the effective roughness length from wind profiles that extend to levels above the surface layer (Sect. 4.1) by expanding the length scale to account for larger eddies at higher levels.

Again, the profiles are homogenized with the wind speed in 175 m and a least squares fit of Equation (4.8) to the average measured profiles is performed for each wind direction sector:

$$\frac{u(z)}{u(z_{\text{ref}})} = c_1 \ln \left(\frac{z}{z_{0,e}} \right) + c_2 z \quad . \tag{4.9}$$

Here, c_1, $z_{0,e}$ and c_2 are parameters that are determined during the fit (Tab. 4.3). The resulting profiles (Fig. 4.3) match the average profiles better than before. The RMSE is one order of magnitude smaller
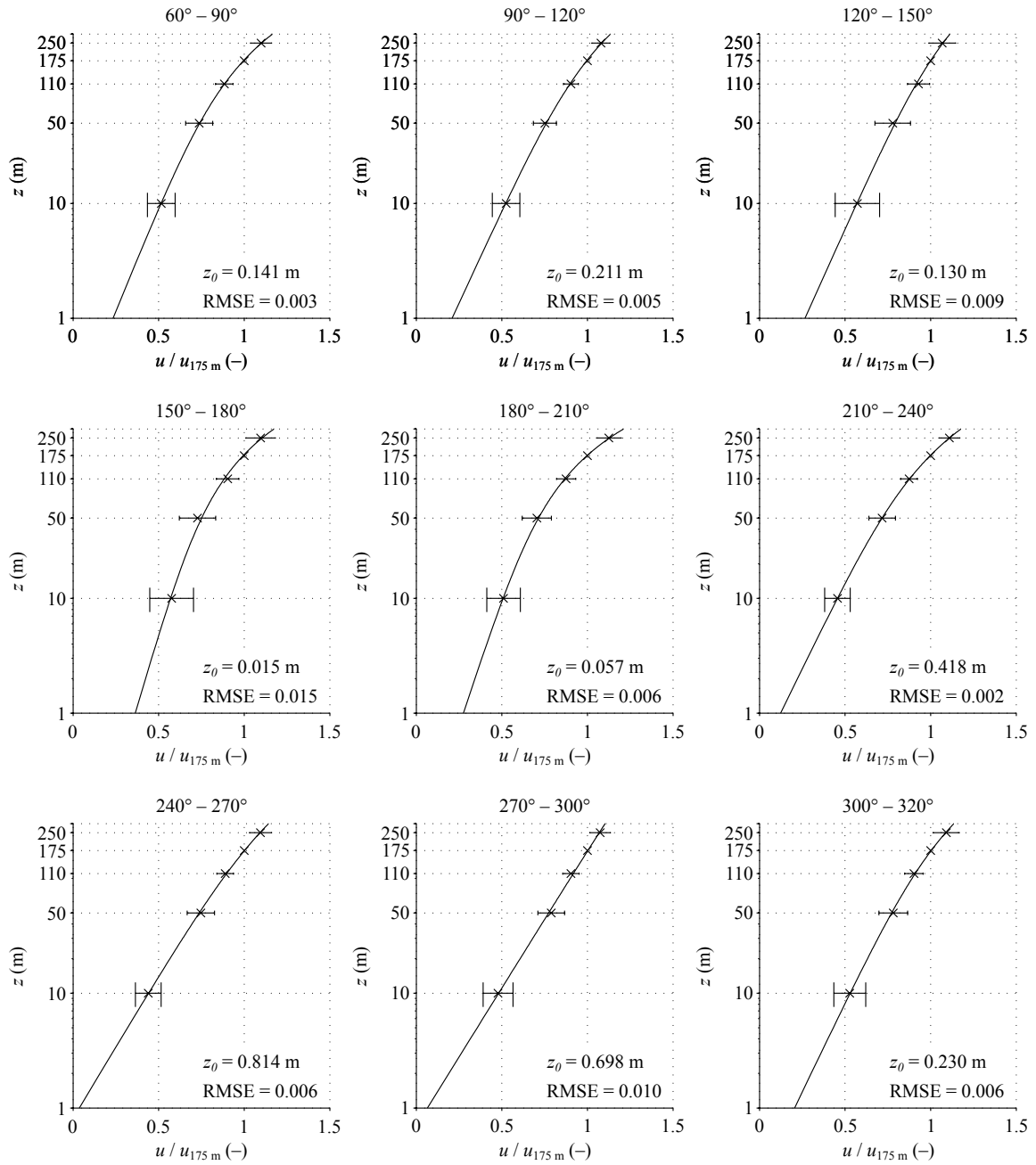
Figure 4.3: Averages of the normalized wind speed profiles (dashed lines) for 30°-wide wind direction classes. The solid line represents the least squares fit of the extended logarithmic wind profile according to equation (4.8). The error bars denote the standard deviation. Wind directions between 320° and 60° are excluded due to disturbances induced by the mast structure. The values of $z_{0,e}$ indicate the effective roughness length for each sector. Different height of error bar ends due to logarithmic display.

Table 4.3: Effective roughness length $z_{0,e}$ and root mean square error (RMSE) between fitted function and normalized wind speed at different wind direction sectors between $60°$ and $210°$ for a least squares fit of a log-linear wind profile (Eq. (4.8)). The fit parameters c_1 and c_2 from this fit are given as well. The wind directions between $320°$ and $60°$ are disregarded due to disturbances of the mast structure.

	$60° - 90°$	$90° - 120°$	$120° - 150°$	$150° - 180°$	$180° - 210°$
$z_{0,e}$ (m)	0.14	0.21	0.12	0.01	0.06
RMSE	0.003	0.005	0.009	0.015	0.006
c_1	0.12	0.13	0.13	0.09	0.10
c_2	0.0009	0.0005	0.0004	0.0011	0.0013

	$210° - 240°$	$240° - 270°$	$270° - 300°$	$300° - 320°$
$z_{0,e}$ (m)	0.41	0.81	0.70	0.23
RMSE	0.002	0.006	0.010	0.006
c_1	0.14	0.17	0.18	0.14
c_2	0.0008	0.0004	0.0000	0.0005

than with the fit of Equation (4.7) for almost all directions and its variation between the different wind directions is much smaller (Tab. 4.3).

The calculated effective roughness lengths are now up to one order of magnitude smaller than those in Section 4.3.1 and comply with the literature values much better. The highest values are found in the westerly sectors ($240° - 270°$: $z_{0,e} = 0.81$ m and $270° - 300°$: $z_{0,e} = 0.70$ m), where the terrain is dominated by the buildings of the industrial area. As stated in Table 3.2, roughness length values between 0.015 m and 0.5 m are estimated in those sectors. Grimmond (1998) estimated roughness lengths from wind profiles in particular for urban surroundings and they found values between 0.46 m and 1.32 m for residential areas.

In Figure 4.4 effective roughness length $z_{0,e}$, roughness length z_0 from fit of the logarithmic profile to all heights and the approximated maximum roughness from geometric estimations $z_{0,geom}$ are illustrated for all directions. The roughness lengths from wind profile measurements z_0 and $z_{0,e}$ show roughly the same characteristics with larger values in southwesterly to westerly directions. However, $z_{0,e}$ values are considerably smaller than z_0 values from traditional logarithmic wind profile estimations. In southeasterly to southerly directions the roughness lengths are smallest. The roughness length from geometric estimations $z_{0,geom}$ in easterly to southeasterly directions is higher than the calculated values. Towards southwest to west, on the other hand, $z_{0,geom}$ values are smaller than values from wind profile measurements. The deviation is assumed to originate from the fact that roughness lengths from geometric estimations are only a rough approximation of the surface roughnesses that impact the wind profile at the Wettermast Hamburg.
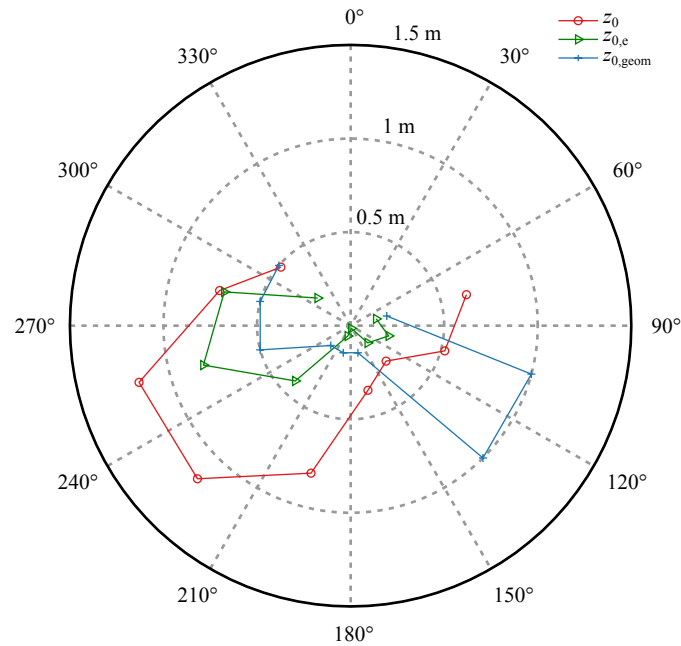
Figure 4.4: Comparison of roughness lengths at different sectors. z_0 is the roughness length calculated from logarithmic wind profile fit to all measurement heights (Tab. 4.2). $z_{0,e}$ is the effective roughness length (Tab. 4.3). $z_{0,geom}$ is the approximated maximum roughness from geometric estimations (Tab. 3.2).

The effective roughness lengths in easterly sectors ($150° - 180°$ and $180° - 210°$) are much lower than the roughness lengths derived from the purely logarithmic fit (now 0.01 m and 0.06 m compared to 0.36 m and 0.82 m from logarithmic fit, respectively). These values are the overall smallest ones, which might seem surprising since the terrain in those directions is dominated by allotments with bushes, trees, and even small houses. However, as stated by Verkaik and Holtslag (2007), the calculation of roughness length from profile measurements is more of an average over a larger fetch area. In neutral conditions the footprint extends to a distance of approximately ten times the measuring height from the site. In case of measurements at the Wettermast Hamburg this would mean that the surface characteristics up to 2.5 km apart from the mast influence the measured profile. Therefore, even if the immediate surroundings of the sectors $150° - 180°$ and $180° - 210°$ are seemingly rough, the surface characteristics farther away are again smoother (railway sidings), therefore these seemingly low roughness lengths are not completely unreasonable.

As mentioned in Section 4.1, $z_{0,e}$ is also subject so seasonal variations. Effective roughness length is larger in westerly directions during summer (June, July, August) than during winter (December, January, February). In summer months $z_{0,e}$ values for wind directions between 240° and 320° are 0.93 m, 0.80 m, and 0.24 m. This is slightly higher than the average over all seasons. During winter months $z_{0,e}$ values decrease to 0.67 m, 0.57 m, and 0.20 m. This can be explained by the fact that most plants have no foliage during this time. The annual variation of $z_{0,e}$ in southeasterly directions, however,

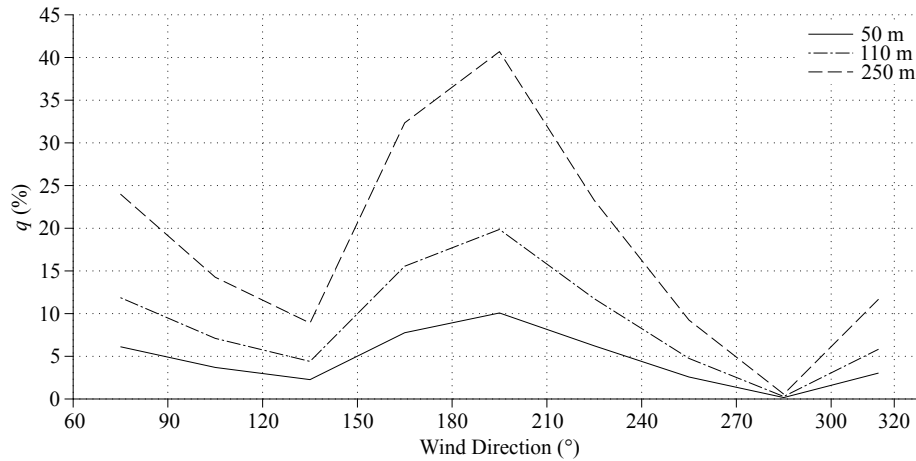**Figure 4.5:** Ratio of linear and logarithmic term q (Eq. (4.10)) for several evaluation heights and wind direction sectors. Values are depicted at the center of their respective wind direction interval.

is quite surprising. Values are smaller during summer than during winter time. For wind directions between $90°$ and $180°$, $z_{0,e}$ values are $0.13\,\text{m}$, $0.12\,\text{m}$, and $0.01\,\text{m}$ during summer and $0.21\,\text{m}$, $0.23\,\text{m}$, and $0.0.3\,\text{m}$, respectively. This reduction in surface roughness during summer cannot explained by surface characteristics in these directions. One explanation would be possible changes in land use that might have occurred in these wind direction sectors over the years. For example, the moderate hills on the gravel pit area are not stationary but change location every so often. To fathom this effect, the temporal evolution of effective roughness length should be evaluated. In this thesis, values of effective roughness length over all years and all seasons are used to characterize surface roughness.

As stated in Section 4.3.1, the measured wind profile deviates from the logarithmic wind profile only for some sectors. This can be quantified by evaluating Equation (4.9) at the height z_{eval} and calculating the ratio q between the linear and logarithmic term of this equation:

$$q = \frac{c_2 \cdot z_{\text{eval}}}{c_1 \ln(z_{\text{eval}}/z_{0,e})} \quad . \tag{4.10}$$

Generally, the ratio q is small if the profile is approximately logarithmic and the linear term therefore is close to zero. The more dominant the linear term becomes, the larger q gets (Fig. 4.5).

What has been concluded from the shortcomings of the previous, logarithmic fit can now be quantified: in sector $270° - 300°$ the linear term of (4.9) only is $q_{270° - 300°} = 0.4\%$ of the logarithmic term in $110\,\text{m}$. In the levels above and below, the linear term is relatively unimportant, as well. This indicates that the average wind profile from those directions is logarithmic throughout the entire height. The sectors $150° - 180°$ and $180° - 210°$ show the strongest influence of the linear term with $q_{150° - 180°} = 15.0\%$ and $q_{180° - 210°} = 18.7\%$ in $110\,\text{m}$. The linear term becomes even more important at higher levels ($q_{150° - 180°} = 34.1\%$ and $q_{180° - 210°} = 41.7\%$ in $250\,\text{m}$.). Even in $50\,\text{m}$ the linear term is still more dominant than in other directions. However, it is smaller than in the heights above. This indicates

that the wind profile in those directions deviates strongly from the logarithmic form. In the remaining sectors the profile is mostly logarithmic with a linear influence of 11% or less in 110 m and 25% or less in 250 m. The linear term becomes increasingly important at higher levels in all directions. Therefore, the linear portion of the profile should not be neglected in general when using profiles that extend above 110 m. However, if the measured profile is almost logarithmic, as in wind direction sector $270° - 300°$, the linear term of Equation (4.9) is small and does not induce large deviations from the ideal logarithmic profile.

Fiedler and Panofsky (1972) propose the coefficient β in Equation (4.8) to be $144 f$ ($= 0.0168$ in case of Wettermast Hamburg, f is the coriolis parameter), but mention that the values could be smaller as well. In comparison with the fit parameters above it is found that those are a little smaller than the values proposed by Fiedler and Panofsky (0.0107 for $180° - 210°$, less in other sectors). Therefore, the fit parameters found in this study are in good agreement with the findings of Fiedler and Panofsky (1972).

In summary, the roughness length can be determined from average wind profiles. Sometimes, the situation at a site or aim of the analysis requires measured wind profiles that extend above 110 m. In these cases, however, it is necessary to expand the logarithmic wind profile to include a linear term. This term then accounts for a stronger increase of the wind speed at upper levels. The effective roughness lengths that are derived from log-linear fits are in good agreement with the values found in literature.

4.4 Sensitivity of Roughness Length Derivation on Wind Speed

In the previous section the effective roughness length $z_{0,e}$ is derived from log-linear wind profiles. The footprint of $z_{0,e}$ generally depends on measuring height and stability. Therefore, the derived values of $z_{0,e}$ should not vary with wind speed. To verify this, the ratio q of linear and logarithmic term and the roughness length are analyzed in regard to wind speed.

4.4.1 Ratio of Linear and Logarithmic Term

The ratio q of linear and logarithmic term (Eq. (4.10)) can be utilized to estimate the effect of the wind speed on the wind profile shape. For this purpose, the wind profiles are further classified according to the wind speed in 10 m. Only categories are analyzed that consist of 30 or more profiles. In most directions, q and therefore the shape of the wind profile is more or less constant with increasing wind speed. In some directions, however, the ratio and thus the influence of the linear term decreases with increasing wind speed (Fig. 4.6, top for $z_{eval} = 110$ m).
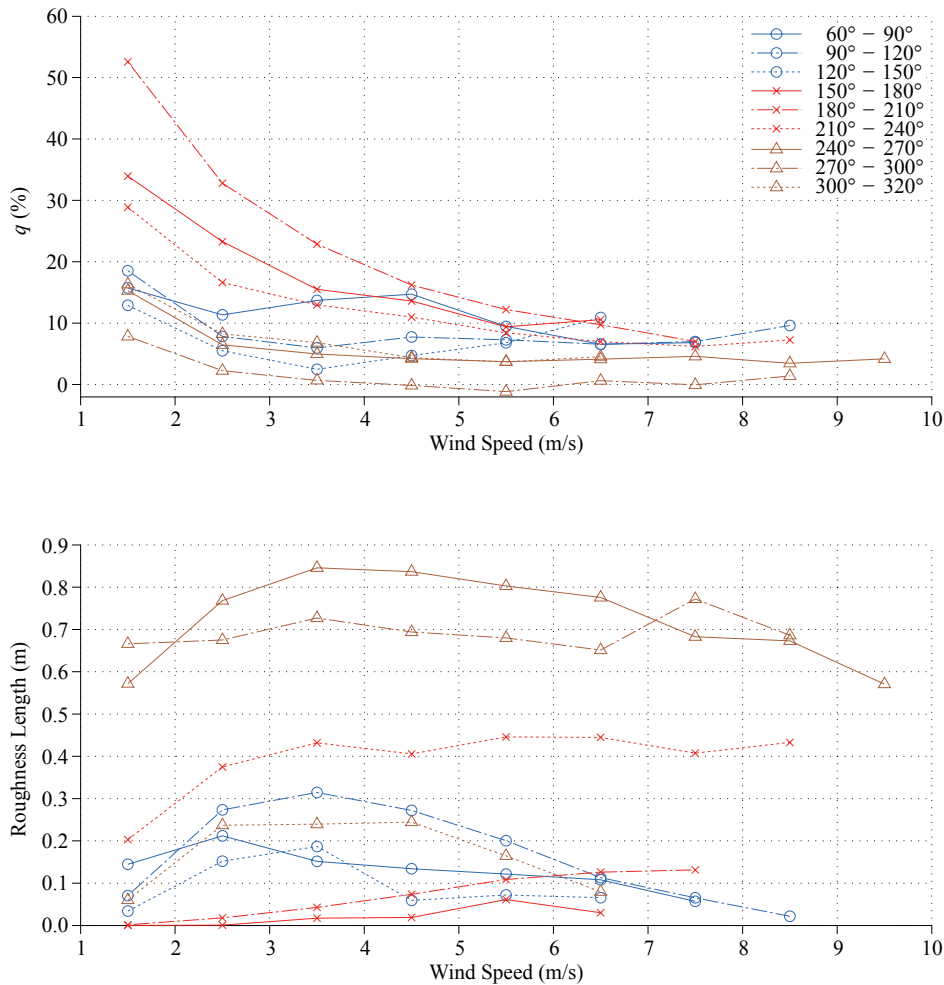
Figure 4.6: Sensitivity of roughness length derivation on minimum wind speed. Top: ratio q between linear and logarithmic term according to Equation (4.10) in 110 m. Bottom: resulting roughness lengths $z_{0,e}$ with regard to minimum wind speed. Values are depicted at the center of their respective wind direction interval. Only categories are analyzed that consist of 30 or more profiles.

The directions that stand out in this analysis are $150° - 180°$, $180° - 210°$, and $210° - 240°$. Here, the impact of the linear term is largest at small wind speeds and decreases with increasing wind speed. At lower wind speeds the linear term in sector $180° - 210°$ accounts for more than 50% of the profile. This value decreases rapidly with increasing wind speed, but only at higher speeds of 7–$8\,\mathrm{m\,s^{-1}}$ does this ratio reach about 10%. This indicates that at small wind speeds, the average wind profile is less logarithmic but approaches this shape more and more at higher wind speeds. In all other directions the shape of the wind profile is more or less constant with increasing wind speed. The least variance of q with wind speed occurs in sector $270° - 300°$. Here, even at 1–$2\,\mathrm{m\,s^{-1}}$ wind speed the linear term is less than 10% of the logarithmic term. This ratio decreases slightly until it becomes negative for wind speeds of 5–$6\,\mathrm{m\,s^{-1}}$ indicating that the linear term of Equation (4.9) actually reduces the wind speed compared to the logarithmic profile.

As already discussed in previous sections, the wind profile in sector $180° - 210°$ deviates the most from the logarithmic shape. Interestingly, if only wind profiles in this sector are considered with wind speeds larger than $4\,\mathrm{m\,s^{-1}}$, the deviation from the logarithmic shape is of the same order as for other wind direction sectors. At high wind speeds the turbulent mixing is stronger which can lead to a larger vertical extent of the surface layer. As suggested in the end of Section 4.3.1, the fact that the surface layer does not extend up to the higher measurement levels might cause the stronger deviation from the logarithmic profile. Inversely, the thicker surface layer at large wind speeds can therefore result in the better agreement of the measured wind profile with the logarithmic profile. The wind profile in sector $270° - 300°$, on the other hand, can be considered as mostly logarithmic throughout the entire height as shown in Sections 4.3.1 and 4.3.2. In this case, the shape of the profile does not change much regardless of the minimum wind speed. This indicates that the Wettermast Hamburg is completely submerged in the surface layer for these wind directions regardless of wind speed.

4.4.2 Roughness Length

One parameter that results from the least squares fit to the average wind profiles in Equation (4.9) is the effective roughness length $z_{0,\mathrm{e}}$. As before, the resulting effective roughness length can be analyzed for wind speed dependency in each wind direction sector (Fig. 4.6, bottom). Overall, the roughness length $z_{0,\mathrm{e}}$ is fairly constant with wind speed, as is ideally expected. A slight increase of $z_{0,\mathrm{e}}$ can be found between the wind speed categories 1–$2\,\mathrm{m\,s^{-1}}$ and 2–$3\,\mathrm{m\,s^{-1}}$ for several wind direction sectors. This indicates that the surface layer might not be sufficiently mixed at smaller wind speeds.

$z_{0,\mathrm{e}}$ decreases considerably in two wind direction sectors. For wind directions $90° - 120°$ and wind speeds larger than $3\,\mathrm{m\,s^{-1}}$ decreases $z_{0,\mathrm{e}}$ from values around 0.3 m to less than 0.1 m Similarly, in directions $300° - 320°$ the roughness length decreases slightly for higher wind speeds. Up to now, this effect can not be explained.

As shown in the previous section, the linear term is most dominant in the sectors $150° - 180°$ and $180° - 210°$ at small wind speeds and decreases considerably with increasing wind speed. Interestingly, the roughness length is almost constant or increases only slightly with wind speed in these sectors. This indicates that, although the shape of the wind profile changes with increasing wind speed, the roughness length calculated from those profiles is not influenced by varying wind speeds.

4.5 Modeling the Wind Profile at Different Surface Roughnesses

The model approaches by Gryning et al. (2007) and Peña et al. (2010) (Sect. 2.3) allow the estimation of the wind profile in the surface layer and above from measurements that are taken at or close to the

surface: roughness length z_0, friction velocity u_* from 10 m measurements, and the Obukhov length L evaluated at 50 m (cf. Sect. 2.3). These suggested models are evaluated with measurements from the Wettermast Hamburg with regard to varying surface roughness $z_{0,e}$ at neutral stratification. The input parameters u_*, L (see Sect. 5.1), and $z_{0,e}$ are determined at every available time step and a wind profile between 1 m and 300 m is calculated from both models.

The measurement profiles are sorted according to the roughness length that was determined in the previous section (see. Tab. 4.3). The surface roughness is categorized into four roughness classes: smooth surfaces with $z_0 \leq 0.2$ m, moderate roughness with 0.2 m $< z_0 \leq 0.4$ m, rough surfaces with 0.4 m $< z_0 \leq 0.6$ m, and extreme roughness with $z_0 > 0.6$ m. To eliminate possible effects of atmospheric stratification, only cases with neutral stratification are considered.

At the Wettermast Hamburg site the largest surface roughness can be found at westerly directions ($z_{0,240°-270°} = 0.81$ m and $z_{0,270°-300°} = 0.70$ m). Those wind direction sectors are also the ones with the overall highest wind speeds (Fig. 3.7). In this case, a direct comparison of wind profiles at different surface roughnesses is not appropriate. Therefore, the measured wind speed is normalized with wind speed in 250 m. In contrast to the homogenization of the wind speed in Section 4.3, here it is not desirable that the reference height is part of the surface layer but that the reference height is as undisturbed by the surface as possible. Therefore, the highest measurement level available has been used.

The observed wind speed ratio $u(z)/u_{250\,m}$ (Fig. 4.7, left) in 10 m is higher at low surface roughnesses ($z_{0,e} < 0.4$ m). With higher surface roughnesses ($z_{0,e} > 0.4$ m), on the other hand, the wind speed ratio is smaller. However, these distinct differences are also only partially present in 10 m measuring height. Already at 50 m the profiles no longer are sorted according to surface roughness.

The modeled wind profiles (Fig. 4.7, right) show the same basic shape as the measurements. However, the measured wind speed seems to increase stronger with height than the modeled one. The modeled wind speed is lowest for the category with the highest surface roughness ($z_0 > 0.6$ m). Between the two medium roughness categories (0.2 m $< z_0 \leq 0.4$ m and 0.4 m $< z_0 \leq 0.6$ m) there is not much difference in modeled wind speed in lower levels (≤ 50 m). Above 50 m the predicted wind speeds are higher for the rougher category 0.4 m $< z_0 \leq 0.6$ m than for the smoother category 0.2 m $< z_0 \leq 0.4$ m. The overall highest wind speeds are predicted for the smoothest category with $z_0 \leq 0.2$ m.

To quantify the deviations between the predicted wind profiles and the measurements, the RMSE and the average bias are calculated (Fig. 4.8). The bias is calculated by subtracting the measured wind speed from the estimated wind speed $u_{est} - u_{meas}$. Thus, negative bias values indicate that the predicted wind speed is smaller than the measured one, i.e. the model is underestimating the wind speed. To account for the effect that at higher average wind speeds also the errors can be larger, RMSE and bias are normalized with the average wind speed in each height.
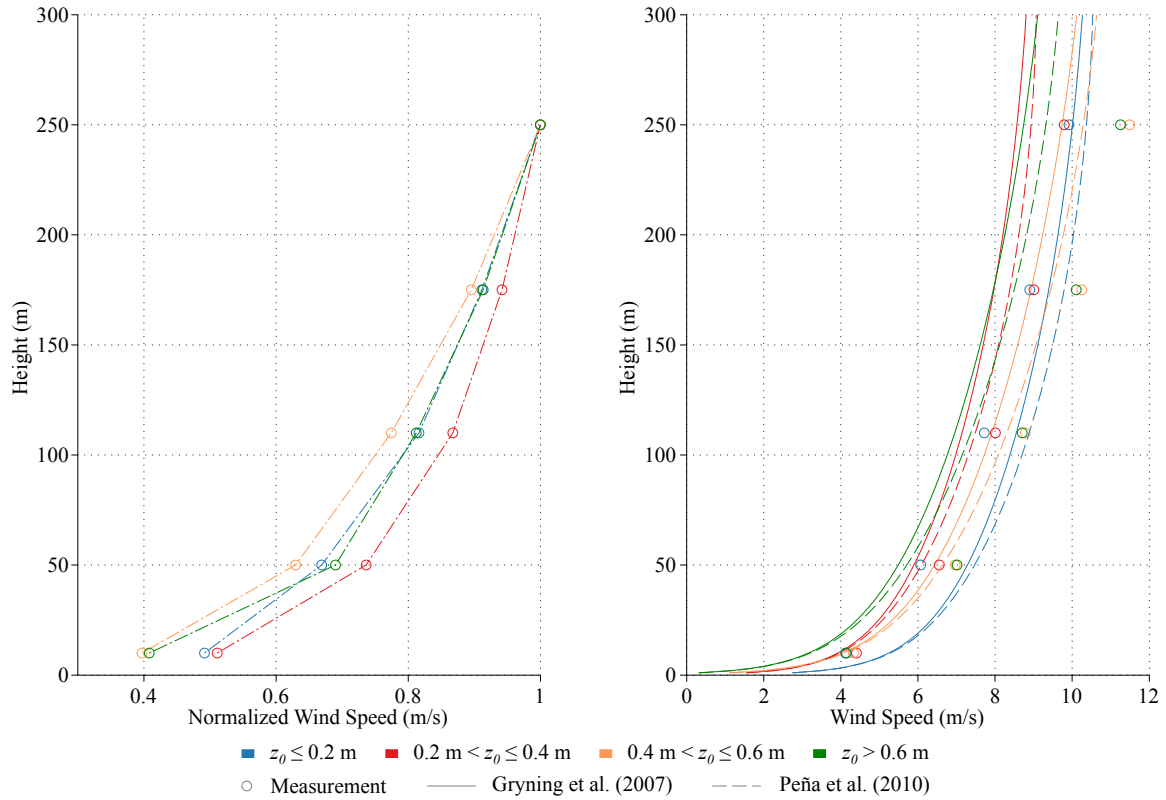
Figure 4.7: Measured and modeled wind profile at different surface roughnesses (colors). Left: average measured wind speed normalized with wind speed in 250 m. Right, comparison of measured (circles) and modeled wind speeds using the approach of Gryning et al. (2007) (solid lines) and Peña et al. (2010) (dashed lines).

The RMSE of wind speeds estimated by the model of Gryning et al. (2007) (Fig. 4.8a) is smallest (around 20%) in lower levels (10 m and 50 m) for medium surface roughnesses ($0.2\,\mathrm{m} < z_0 \leq 0.4\,\mathrm{m}$ and $0.4\,\mathrm{m} < z_0 \leq 0.6\,\mathrm{m}$). Comparatively large errors (more than 40%) can be found in the lowest roughness category ($z_0 \leq 0.2\,\mathrm{m}$) in those levels. Overall, the errors increase towards higher levels (above 110 m) and are almost of the same order in all categories in 250 m. The category with the largest errors throughout the entire profile is $z_0 > 0.6\,\mathrm{m}$. The estimated wind profiles at moderate surface roughnesses are in good agreement with the measurements in lower levels. Towards higher levels the errors are slightly larger. In case of more extreme values of surface roughness, the estimated wind profiles deviate more from the measurements. While the error decreases from more than 40% to about 25% with height for the smoothest roughness category ($z_0 \leq 0.2\,\mathrm{m}$), it is almost constant with height for the roughest category (around 0.3 for $z_0 > 0.6\,\mathrm{m}$).

The model of Gryning et al. (2007) overestimates wind speed for low surface roughnesses ($z_0 \leq 0.2\,\mathrm{m}$) in all heights. However, this deviation decreases with height from 25% to almost zero at 250 m in this category. In all other categories an underestimation of wind speed by 10 to 25% can be found which is almost constant with height (see Fig. 4.8b).
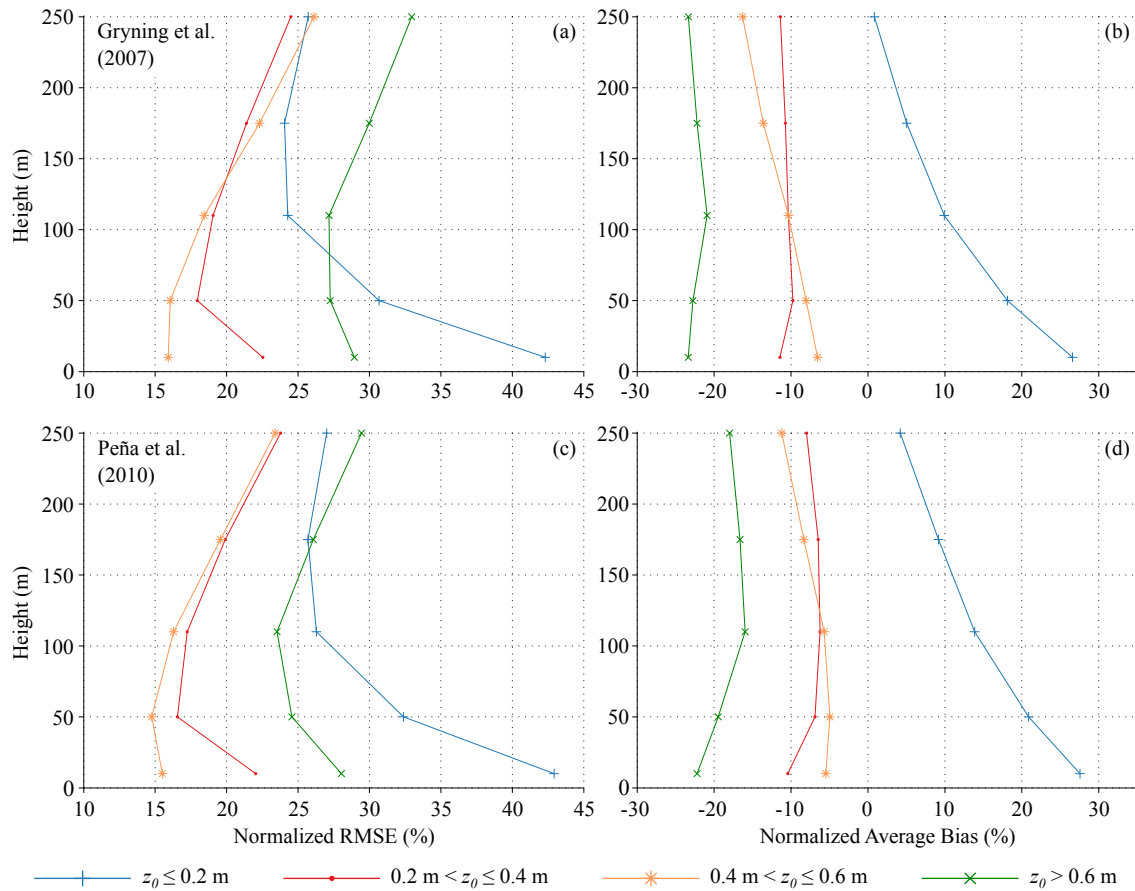
Figure 4.8: Error estimates of model results from comparison with measurements. Top row: the approach proposed by Gryning et al. (2007), bottom row: the approach proposed by Peña et al. (2010). The normalized RMSE is depicted in the left column, the normalized average bias in the right column. The bias is calculated by: $u_{\text{est}} - u_{\text{meas}}$.

When evaluating the wind speed estimated with the Peña et al. (2010) approach, the RMSE (Fig. 4.8c) overall shows characteristics similar to the Gryning et al. (2007) model. The errors of the roughest category ($z_0 > 0.6$ m) are smaller above 50 m (around 25–30%, compared to 28–32%). The RMSE of the smoothest category, on the other hand, is of the same order in lower levels but slightly higher than that of the Gryning et al. (2007) approach above 110 m (25–27%, compared to 24–26% before). As can be deducted from the bias between the measured wind speed and the wind speed estimated by the Peña et al. (2010) model (Fig. 4.8d), the wind speed is underestimated for most categories and only overestimated if the surface roughness is small ($z_0 \leq 0.2$ m). Overall, no considerable improvement of the Peña et al. (2010) model over the Gryning et al. (2007) model can be found.

After evaluating the wind profile models in this section, the impact of recalculating u_* (Sect. 4.2) can be assessed by means of the model error estimates. In the previous section, u_* has been recalculated
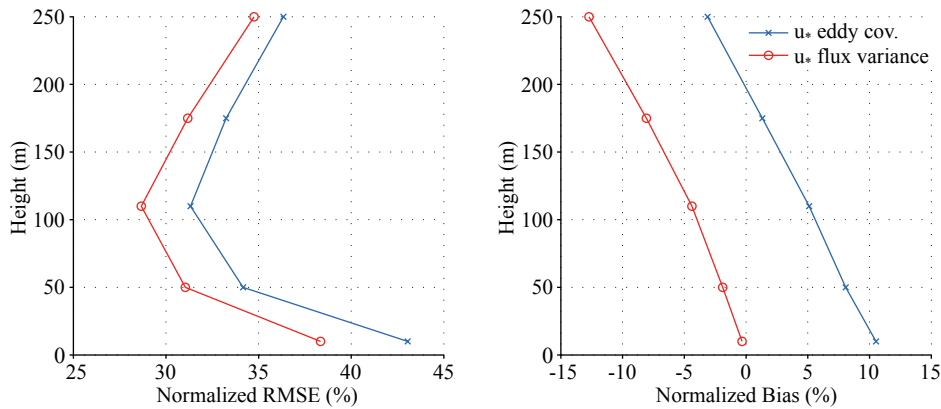
Figure 4.9: Comparison of input parameters for Gryning et al. (2007) model. Different u_* values are compared at neutral stratification. Remaining input parameters are identical. Left: normalized RMSE in %, right: normalized bias in %.

using flux variance similarity. There, the comparison between u_* and wind speed measurements only shows slight improvement of agreement.

In Figure 4.9, the model by Gryning et al. (2007) is evaluated for different u_* input parameters for all stratifications. The remaining input parameters z_0 and L are identical in both runs. In this case, the impact of varying friction velocities can be assessed. In this evaluation of error estimates of the models, it is obvious that the recalculation of u_* reduces the RMSE by about two percentage points and the bias by approximately twelve. In comparison with the errors found above (Fig. 4.8), this is a considerable effect since the RMSE in the roughness category $0.2\,\text{m} < z_0 \leq 0.4\,\text{m}$ only ranges between 18 and 23%. These errors would have been larger, if u_* from eddy covariance measurements was used. Results are similar when comparing u_* input parameters with the Peña et al. (2010) model. In conclusion, it can be stated that the determination of u_* by means of flux variance similarity is superior to the eddy covariance measurements in case of the data set at hand. Friction velocity from flux variance similarity improves the wind profile estimations by the models of Gryning et al. (2007) and Peña et al. (2010).

In conclusion, this chapter addresses the estimation of surface roughness in terms of the roughness length. Additionally, the measured wind profiles at varying roughnesses are compared to the estimated wind speeds from models.

- Friction velocity is derived from flux variance similarity. The drag coefficient $C_{\text{D}} = (u_*/\overline{u})^2$ links friction velocity and wind speed by a proportionality constant. This is used to examine the derived friction velocity. The calculated values are in good agreement with the measured wind speeds.

- The roughness length z_0 is estimated by comparison of wind profile measurements with the logarithmic wind profile. This method is highly sensitive to the heights used for this analysis. Interestingly, this effect only occurs for some wind directions while at others, the logarithmic wind profile is a very good description of the measured wind profile in neutral stratification.

- To reduce the sensitivity to the number of levels of the determination of roughness length from profile measurements a linear term is introduced into the wind profile. This extension leads to the effective roughness length $z_{0,e}$. The derived values are in good agreement with previous studies. It is advisable to use $z_{0,e}$ for sites with inhomogeneous surroundings and with measurements from tall masts.

- The ratio of linear and logarithmic portion in the log-linear wind profile is sensitive to wind speed in some directions. With increase of wind speed, the importance of the linear term decreases. But only at wind speeds larger than $5\,\mathrm{m\,s^{-1}}$ is the linear term 15% or less in magnitude compared with the logarithmic portion of the wind profile. The effective roughness length is in general insensitive to wind speed.

- The model approaches of Gryning et al. (2007) and Peña et al. (2010) are validated with measured wind profiles at neutral stratification. Both models underestimate the wind speed at the Wettermast Hamburg by 5–25% in most cases. Only for small roughness length is wind speed overestimated by both models. No considerable improvement of the Peña et al. (2010) model over the Gryning et al. (2007) model can be found.

5

Stratification of the Boundary Layer

As described in Section 2.2.1, the stratification of the boundary layer influences the shape of the wind profile. Strong inversions during stable stratification can inhibit the vertical exchange and result in a very shallow boundary layer, whereas instability enables convection and thus vertical mixing.

One measure to characterize atmospheric stratification is the Obukhov length L. Different ways of determining values of L are described and evaluated in Section 5.1. To assess possible limitations of the wind profile models by Gryning et al. (2007) and Peña et al. (2010), the impact of L as an input parameter for these models on wind speed estimations is evaluated in Section 5.2.

To be able to interpret the wind profile's dependency on atmospheric stability, knowledge of the characteristics of the atmospheric stratification at the Wettermast Hamburg site is necessary. These are described in Section 5.3 in terms of potential temperature gradients. Here, both the temperature gradients near the ground (10 m to 110 m) and the combined distribution of the temperature gradients in the two layers (10 m to 110 m and 110 m to 250 m) are analyzed. The common approach to account for atmospheric stability in wind profile estimations is to evaluate the stratification in the lowest layer of the atmosphere. However, the analysis of the wind profile in this work not only focuses on the levels close to the ground, but also considers wind speeds at the heights of potential future hub heights, above 100 m and up to 250 m. Therefore, the atmospheric stability in this upper layer will also be evaluated.

To assess the impact of atmospheric stability on wind profiles, observed wind profiles at different stability categories are characterized in Section 5.4. This analysis is conducted for wind profiles at uniform stratification throughout the entire mast height. In addition, it is investigated how large the impact variations of lower or upper layer stability is on the wind profile.

It is usually desired to estimate wind profiles from measurements close to the surface. Two mixing length models (Gryning et al. (2007); Peña et al. (2010), see Sect. 2.3) have been proposed previously for this estimation. To test the model performance at different atmospheric stratifications, the

model estimates of wind speed at varying stabilities are compared to measurements at the Wettermast Hamburg site in Section 5.5.

5.1 Obukhov Length

The Obukhov length is a widely used stability parameter (c.f. Sect. 2.2). It incorporates shear and buoyancy effects. It is defined in Stull (1988) as

$$L = -\frac{\overline{\theta}}{\kappa g} \frac{u_*^3}{\overline{w'\theta'}} \quad . \tag{5.1}$$

Here, $\overline{\theta}$ is the mean potential temperature, κ is the dimensionless Kármán constant, g the acceleration of gravity, u_* the friction velocity, and $\overline{w'\theta'}$ is the turbulent vertical transport of sensible heat which proportional to the turbulent sensible heat flux ($H = \rho c_p \overline{w'\theta'}$; ρ is the density of air, c_p is specific heat at constant pressure).

At measurement heights z close to the surface ($z \ll |L|$), shear effects dominate over buoyancy effects. On the other hand, at heights $z \gg |L|$, turbulence due to buoyancy becomes more influential than shear-induced turbulence. L and ultimately the stability parameter $\zeta = z/L$ give an estimate of the ratio between buoyancy and shear effects in the lower boundary layer. In the unstable boundary layer, the turbulent sensible heat flux is directed upward and therefore positive. This results in $\zeta < 0$. In stably stratified boundary layers with downward heat flux is $\zeta > 0$.

The Obukhov length can be directly determined by eddy covariance measurements. To this end, fluctuations of vertical and horizontal wind speed (w' and u' in case of turbulent flux of momentum) or fluctuations of vertical wind speed and temperature (w' and θ' in case of turbulent flux of sensible heat) are measured with ultrasonic anemometers at sufficiently high sampling frequency. The product of these fluctuations is averaged to covariances of these fluctuations ($\overline{w'u'}$ and $\overline{w'\theta'}$ respectively). The suitable averaging interval, strictly speaking, depends on atmospheric stratification. However, Foken (2006b) points out that at averaging intervals of 30 minutes the error should be reasonably small. Foken further mentions that the eddy covariance method produces best results if conditions are horizontally homogeneous, stationary and no obstacles disturb the flow which could lead to internal boundary layers. From these considerations some sources of uncertainty in eddy covariance calculations at the Wettermast Hamburg become apparent. The surroundings around the site are far from homogeneous (Sect. 3.3). Additionally, the averaging interval for operational calculation of turbulent fluxes at the Wettermast Hamburg site is typically shorter than 30 minutes. Schmidt (2012) confirms the dependency of calculated values of turbulent fluxes at the Wettermast Hamburg on averaging interval. These limitations have to be kept in mind when interpreting eddy covariance measurements.
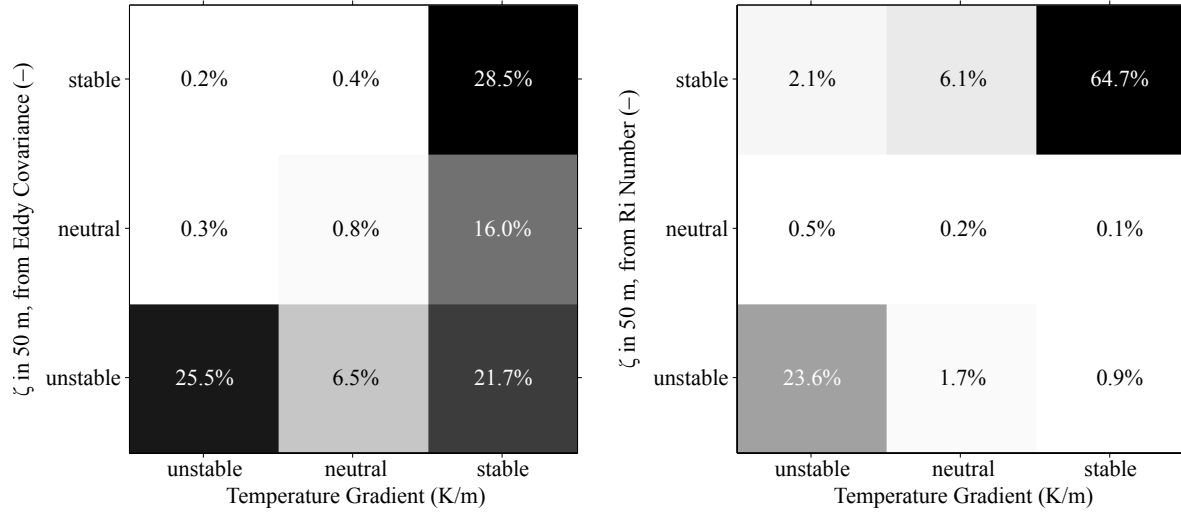
Figure 5.1: Frequency of occurrence of stability categories. $\zeta = z/L$ at 50 m versus $\Delta\theta/\Delta z$ between 70 m and 10 m. Left: ζ with Obukhov length from eddy covariance measurements; right: ζ with Obukhov length derived from the gradient Richardson number. The thresholds for the neutral categories are set to $|\zeta| \geq 0.01$ and $|\Delta\theta/\Delta z| \geq 0.001$ K/m.

Another measure for atmospheric stratification is the gradient of potential temperature $\Delta\theta/\Delta z$. Although both stability parameters cannot be directly converted into each other, it is expected that classification by both parameters generally are consistent. If, for example, the state of the boundary layer is classified as unstable by one parameter, it should also be assessed as unstable by the other. To assess the consistency between the stability parameters ζ and the temperature gradient, simultaneous measurements are evaluated regarding their stratification information. This information is categorized into three stability classes: unstable ($\zeta < -0.01$, $\Delta\theta/\Delta z < -0.001$ K/m), neutral ($|\zeta| \leq 0.01$, $|\Delta\theta/\Delta z| \leq 0.001$ K/m), and stable ($\zeta > 0.01$, $\Delta\theta/\Delta z > 0.001$ K/m). Since in nature no distinct boundaries exist between stability categories, these thresholds are chosen somewhat arbitrarily. However, they are in the order of magnitude of values commonly used for stability categorization (Mohan and Siddiqui, 1998; Peña et al., 2010).

As can be seen in Figure 5.1 (left), the deviation from consistent stability classification from those two quantities is quite large. The exact values in each category, however, depend on the thresholds used to determine the stability class. Therefore, deviations by one stability category might occur due to the values of those particular category thresholds. In 54.8% of the cases (25.5% both unstable, 0.8% both neutral, an 28.5% both stable) the determined stability categories coincide. In 23.3% the stability categories deviate by one. Those cannot be interpreted with certainty. However, in 21.9% of the cases the stratification according to Obukhov length is unstable and the stratification according to temperature gradient is stable or vice versa. Those deviations can be regarded as real deviations.

Since the stratification is determined considerably different by those two stability parameters, the Obukhov length L is recomputed using the gradient Richardson Number Ri:

$$\text{Ri} = \frac{g}{\theta}\frac{\partial\theta}{\partial z}\left(\frac{\partial u}{\partial z}\right)^{-2} \quad . \tag{5.2}$$

To calculate the gradient Richardson number Ri from measurements, knowledge of gradients of the temperature profile and the wind profile are required. As suggested by Businger et al. (1971), second order polynomials are fitted to measured potential temperature and wind speed profiles and gradients at the evaluation height $z_{\text{eval}} = 50\,\text{m}$ are determined from the first derivative of the fitted function.

The relation between gradient Richardson number Ri and Obukhov length L at the height z can then be described by (Golder, 1972; Irwin and Binkowski, 1981; Arya, 2001):

$$\frac{z}{L} = \begin{cases} \text{Ri} & \text{Ri} < 0 \\[2mm] \dfrac{\text{Ri}}{1-5\text{Ri}} & 0 \leq \text{Ri} < 0.2 = \text{Ri}_{\text{c}} \end{cases} \quad . \tag{5.3}$$

Values larger than the critical Richardson number of $\text{Ri}_{\text{c}} = 0.2$ have been discarded, as those indicate a state of the boundary layer, where the stable stratification inhibits turbulent mixing and the flow can be considered as laminar (Foken, 2006b).

The stability parameter L derived from the Richardson number (Fig. 5.1, right) is in much better agreement with the temperature gradient. Overall, 88.5% of the data result in coinciding stability categories, in 8.4% of the cases the two stability parameters deviate from one another by one category and in only 3% of the cases they deviate completely. As mentioned before, the absolute values of cases in each category depend on the chosen thresholds. Naturally, if thresholds for neutral stratification were relatively wide, almost all cases would fall in the neutral category and inevitably coincide. However, the deviation of stability categories still occurs if thresholds are twice or half as large and the improvement of L due to calculation from Richardson number still is present (not shown).

During the derivation of the Obukhov length as described above, the number of available profiles is further reduced (c.f. Sect. 3.4), since complete temperature profiles are necessary (in addition to complete wind profile measurements) and also due to the requirement of Equation (5.3) that $\text{Ri} < \text{Ri}_{\text{c}}$. Therefore, additional 54 807 profiles have to be omitted. This leads to a total of 319 959 (53% of the maximum possible measurements) data sets from the time period between October 2000 and March 2012. Before this reduction, 374 766 (62% of the maximum possible measurements) complete profiles were available.

It can be concluded that the Obukhov length that is derived by means of the Richardson number is in much better agreement with the stability derived from temperature gradients than the Obukhov length from eddy covariance measurements. Therefore, the newly derived Obukhov length will be used as

input parameter for the models of Gryning et al. (2007) and Peña et al. (2010) and it will be used to categorize measured stratification for comparisons of the wind profile with model results.

5.2 Model Sensitivity

When estimating the wind speed profile with the equations proposed by Gryning et al. (2007) or Peña et al. (2010), one has to keep in mind that these equations might comprise some limitations. Therefore, the relevant equations will be revisited in this section and their limitations will be assessed.

For stable cases wind speed in the Gryning et al. (2007) model is determined by:

$$\frac{u(z)}{u_{*0}} = \frac{1}{\kappa} \left[\ln\left(\frac{z}{z_0}\right) + b\frac{z}{L}\left(1 - \frac{z}{2z_i}\right) + \frac{z}{L_{\text{MBL}}} - \frac{z}{z_i}\left(\frac{z}{2L_{\text{MBL}}}\right) \right] \qquad \text{(2.13 revisited)}$$

In very stable cases, which is equivalent to very small positive values of L, the length scale L_{MBL} (c.f. Eq. (2.11)) becomes very large and consequently the third and fourth summand of Equation (2.13) are small. The second term inside the brackets in (2.13) becomes very large and is therefore dominant. This results in very high predicted wind speeds that are much larger than the measured wind speeds in those cases (Fig. 5.2, top left). Since the basic structure of the equations proposed by Peña et al. (2010) is similar, the same holds true for the respective wind speed determination of this model:

$$u(z) = \frac{u_{*0}}{\kappa} \left[\ln\left(\frac{z}{z_0}\right) + b\frac{z}{L}\left(1 - \frac{z}{2z_i}\right) + \frac{1}{d}\left(\frac{\kappa z}{\eta}\right)^d - \left(\frac{1}{1+d}\right)\frac{z}{z_i}\left(\frac{\kappa z}{\eta}\right)^d - \frac{z}{z_i} \right] \qquad \text{(2.19 revisited)}$$

Here, in very stable cases with very small positive values of L, the second term of the sum gets very large as well. This again results in very high predicted wind speeds (Fig. 5.2, top right). Since the length scale η in this model is not as influenced by small values of L, the effect is smaller in this model than in the Gryning et al. (2007) model.

To test the boundary values for stability which can be used in equations $(2.12)-(2.14)$ and $(2.18)-(2.20)$, limits of L have been tested and estimated wind speeds have been compared with measured wind speeds (Fig. 5.2, exemplarily for 110 m measuring height). When including almost all values of the Obukhov length ($|L| > 1$ m) for wind speed prediction (Fig. 5.2), modeled wind speeds reach values of up to $300\,\text{m\,s}^{-1}$. In case of wind speed estimated by means of the model by Gryning et al. (2007) in 110 m, 4024 values (2.1% of the data) can be assessed as too high. Wind speeds are deemed as too high if the measured wind speed is below $10\,\text{m\,s}^{-1}$ and the modeled wind speed exceeds $15\,\text{m\,s}^{-1}$. These values are chosen arbitrarily. However, as can be seen in Figure 5.2, they identify the extreme wind speed values well. In case of the model proposed by Peña et al. (2010), 2908 cases (1.5% of the data) are assessed as too high. When reducing the included Obukhov length data to the limits that are
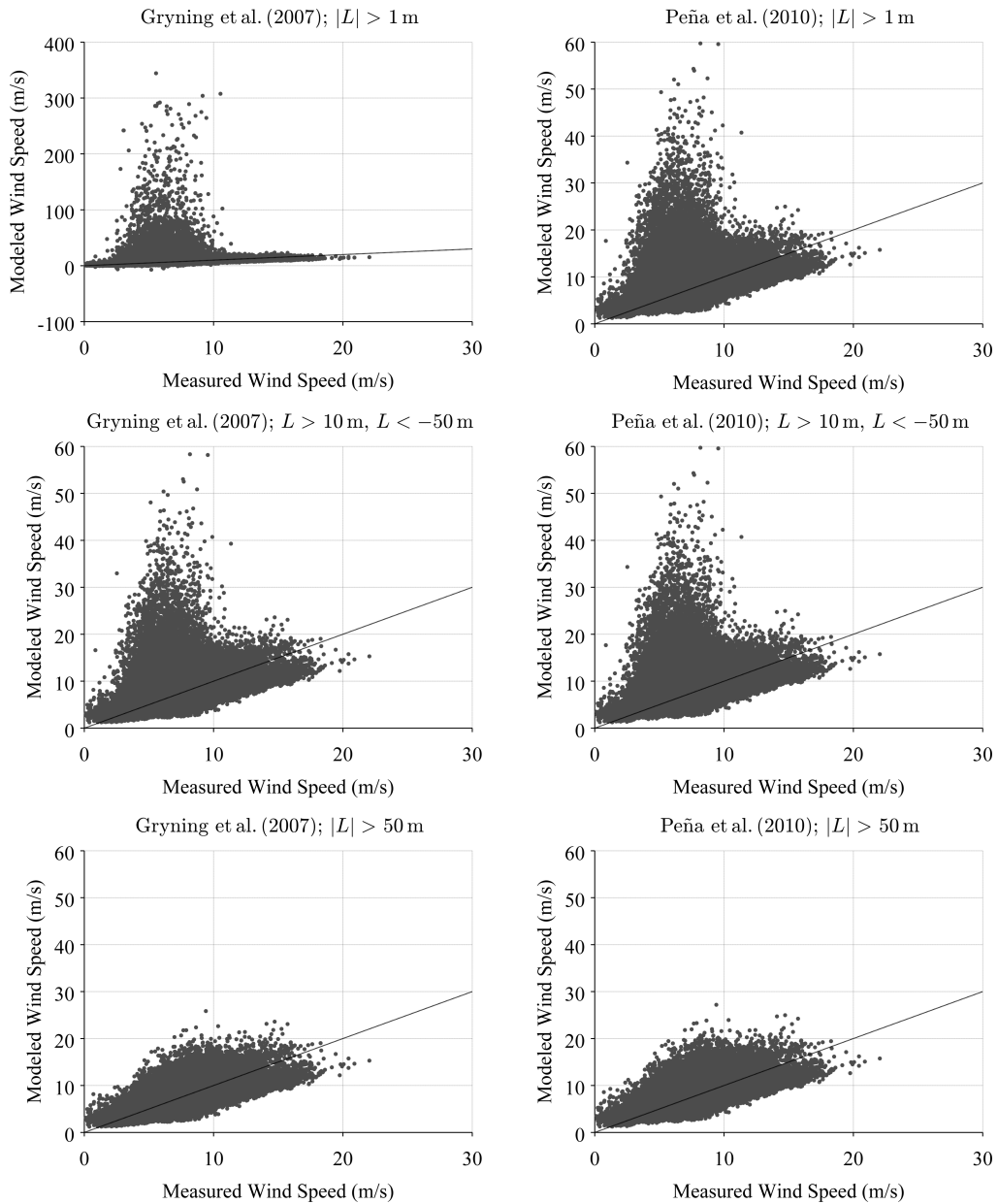
Figure 5.2: Comparison of measured and modeled wind speeds at 110 m height for different limits of the Obukhov length L and for both model approaches. Left column: model by Gryning et al. (2007), right column: model by Peña et al. (2010). Top row: $|L| > 1$ m as limit for included Obukhov lengths, middle row: $L > 10$ m and $L < -50$ m as limit for L, bottom row: $|L| > 50$ m.

suggested by Peña et al. (2010) $L > 10$ m or $L < -50$ m (Fig. 5.2, middle row), the effect of too high estimated wind speeds is smaller. However, some values are still out of line. The number of values that are assessed as too high in the Gryning et al. (2007) wind speed estimation is reduced approximately by half (now: 2235 cases, 1.2% of the data, again in 110 m), but has no effect on the Peña et al. (2010) wind speed estimates. When adjusting the stability input parameter boundaries further to $|L| > 50$ m, only 0.07% of the Gryning et al. (2007) wind speed estimates and 0.2% of the Peña et al. (2010) wind speed estimates could be assessed as too high (Fig. 5.2, bottom row).

One could argue that the original number of profiles in which the wind speed is considerably overestimated, is not very large (2.1% for the Gryning et al. (2007) model and 1.5% for the Peña et al. (2010) model). However, this overestimation is only an issue in very stable stratification. In this stratification category the sample size is already relatively small to begin with. Therefore, even those seemingly few cases, in which the wind speed is extremely overestimated, have an impact on the results in those stability category and should be avoided.

Based on the analysis in this section it can be concluded that the Obukhov length used for the wind speed estimation in either model should comply $|L| > 50$ m. This has been implied by Gryning et al. (2007), by only using $L > 50$ m or $L < -100$ m in their analysis of the Hamburg data, but is not stated explicitly. Peña et al. (2010) however, use stability categories with 10 m $\leq L \leq 50$ m as very stable and -100 m $\leq L \leq -50$ m as very unstable stratification. At least for the Wettermast Hamburg data, values of 10 m $\leq L$ seem to be too low, which can result in an overestimation of wind speed by the two models.

5.3 Atmospheric Stability at the Wettermast Hamburg Site

To assess the stratification characteristics of the observed layers at the Wettermast Hamburg, gradients of potential temperature between two measuring heights are used:

$$\frac{\Delta \theta}{\Delta z} = \frac{\theta(z_2) - \theta(z_1)}{z_2 - z_1} \quad . \tag{5.4}$$

The temperature gradients are calculated for two layers: the lower layer (using $z_1 = 10$ m and $z_2 = 110$ m) and the upper layer (using $z_1 = 110$ m and $z_2 = 250$ m). The resulting temperature gradients are classified into seven categories according to Mohan and Siddiqui (1998) (cf. Table 5.1): very unstable (vu), unstable (u), near unstable (nu), neutral (n), near stable (ns), stable (s), and very stable (vs).

It has to be kept in mind that those classifications of stability are still somewhat arbitrary. It is therefore essential to allow for some inaccuracies in the categorization. For example, a temperature gradient of

Table 5.1: Stability parameter limits for temperature gradients $\Delta\theta/\Delta z$ and Obukhov length L. The limits are based on Mohan and Siddiqui (1998) (temperature gradient) and Peña et al. (2010) (Obukhov length). The derivation of these two stability parameters is based on different principles. The parameters can therefore not necessarily be converted into each other, but both give a reasonable classification of stability.

	Temperature gradient interval (K/m)			Obukhov length interval (m)		
very unstable (vu)		$\Delta\theta/\Delta z$	≤ -0.009	$-50 \geq$	L	> -100
unstable (u)	$-0.009 <$	$\Delta\theta/\Delta z$	≤ -0.007	$-100 \geq$	L	> -200
near unstable (nu)	$-0.007 <$	$\Delta\theta/\Delta z$	≤ -0.005	$-200 \geq$	L	> -500
neutral (n)	$-0.005 <$	$\Delta\theta/\Delta z$	≤ 0.005		$|L|$	≥ 500
near stable (ns)	$0.005 <$	$\Delta\theta/\Delta z$	≤ 0.025	$500 \geq$	L	> 200
stable (s)	$0.025 <$	$\Delta\theta/\Delta z$	≤ 0.05	$200 \geq$	L	> 50
very stable (vs)	$0.05 <$	$\Delta\theta/\Delta z$		$50 \geq$	L	> 10

0.006 K/m could very well be considered as neutral as a temperature gradient of 0.004 K/m, although the former is categorized as near stable in Table 5.1 and the latter is categorized as neutral. These classifications and the resulting numbers and frequencies must therefore not be regarded as absolute statements but as indicators. Nevertheless, since atmospheric stability in nature is not categorized but happens and evolves gradually, this classification is as good as any to estimate stability's influence on the wind profile.

5.3.1 Temperature Gradient Close to the Surface

The temperature gradient between 10 m and 110 m (lower layer stability) is used to assess the stratification near the ground. The frequency distribution of temperature gradients over all wind directions shows a maximum that lies within the neutral stratification category (Fig. 5.3). Also, a considerable amount of data fall into the near stable and into the stable categories. Therefore, the most frequent stability category is neutral (225 813 cases), followed by near stable (102 521), and stable (19 436). As can be seen on the right-hand side of Figure 5.3, stable stratification mainly occurs during nighttime (22 – 04 CET), corresponding to a nocturnal boundary layer structure. The bulk of the neutral stratification cases, on the other hand, happens during daytime (10 – 16 CET).

If measurements from all wind directions are used for the wind profile analysis in the following sections, a superposition of the stability's influence and possible influences of surface roughness would be possible. Therefore, the measurement data are sorted according to wind direction to account for the varying surrounding surface characteristics (see Sect. 3.1 and Tab. 3.2). The frequency of occurrence of the different stability classes is also dependent on the wind direction. In Figure 5.4, the three stable categories (very stable, stable, near stable) are combined into one, as well as the three unstable
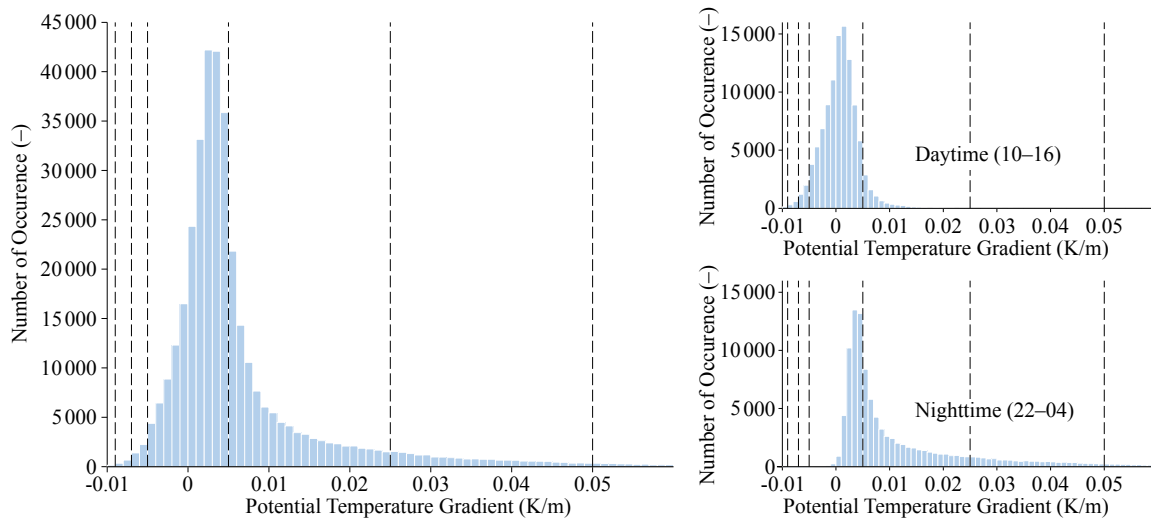
Figure 5.3: Frequency distribution of temperature gradients between 10 m and 110 m for the entire time series (left) and distinguished between daytime, i.e. 10 – 16 CET (right, top) and nighttime, i.e. 22 – 04 CET (right, bottom). Dashed lines denote the stability category borders according to Table 5.1. Percentages in each stability category for entire time series: very unstable: 0.09%; unstable: 0.30%; near unstable: 1.17%; neutral: 67.14%; near stable: 27.98%; stable: 3.02%; very stable: 0.31%.

categories (very unstable, unstable, near unstable). The frequencies of each direction and each wind speed category are normalized with the total number of cases in that category. The wind direction and wind speed is taken at 50 m measuring height.

As can be seen in Figure 5.4, the unstable categories are the least frequent. The fraction of these is around 1–2% in all wind direction sectors at wind speeds below $6\,\mathrm{m\,s^{-1}}$ and up to 4% for wind speeds above $6\,\mathrm{m\,s^{-1}}$. This increase of frequency, however, occurs assumably mainly due to the decrease of overall number of cases in these categories and the consequential larger statistical scattering of the data. In Figure 5.3 it is already shown that unstable stratifications are the overall least frequent stability categories. From Figure 5.4 it can now be deduced that those mainly occur at lower wind speeds. This is reasonable, since higher wind speeds reduce large temperature gradients and thus instability dissolves.

The fraction of neutral stratification at wind speeds below $3\,\mathrm{m\,s^{-1}}$ is distributed over all wind direction sectors between 40–60%. Between $3\,\mathrm{m\,s^{-1}}$ and $9\,\mathrm{m\,s^{-1}}$, it is larger for westerly directions (between 60 and 90%) and less in southeasterly directions (40–50%). Accordingly, the fraction of stable stratification categories is more or less equally distributed at wind speeds below $3\,\mathrm{m\,s^{-1}}$. For larger wind speeds, the stratification is stable more often in southeasterly wind directions and considerably less often in westerly directions. At wind speeds larger than $9\,\mathrm{m\,s^{-1}}$, the stratification is mainly neutral in all wind direction sectors. The variations of fraction of the stability categories between wind direction sectors can be attributed to the smaller sample size and thus higher uncertainty in this wind speed
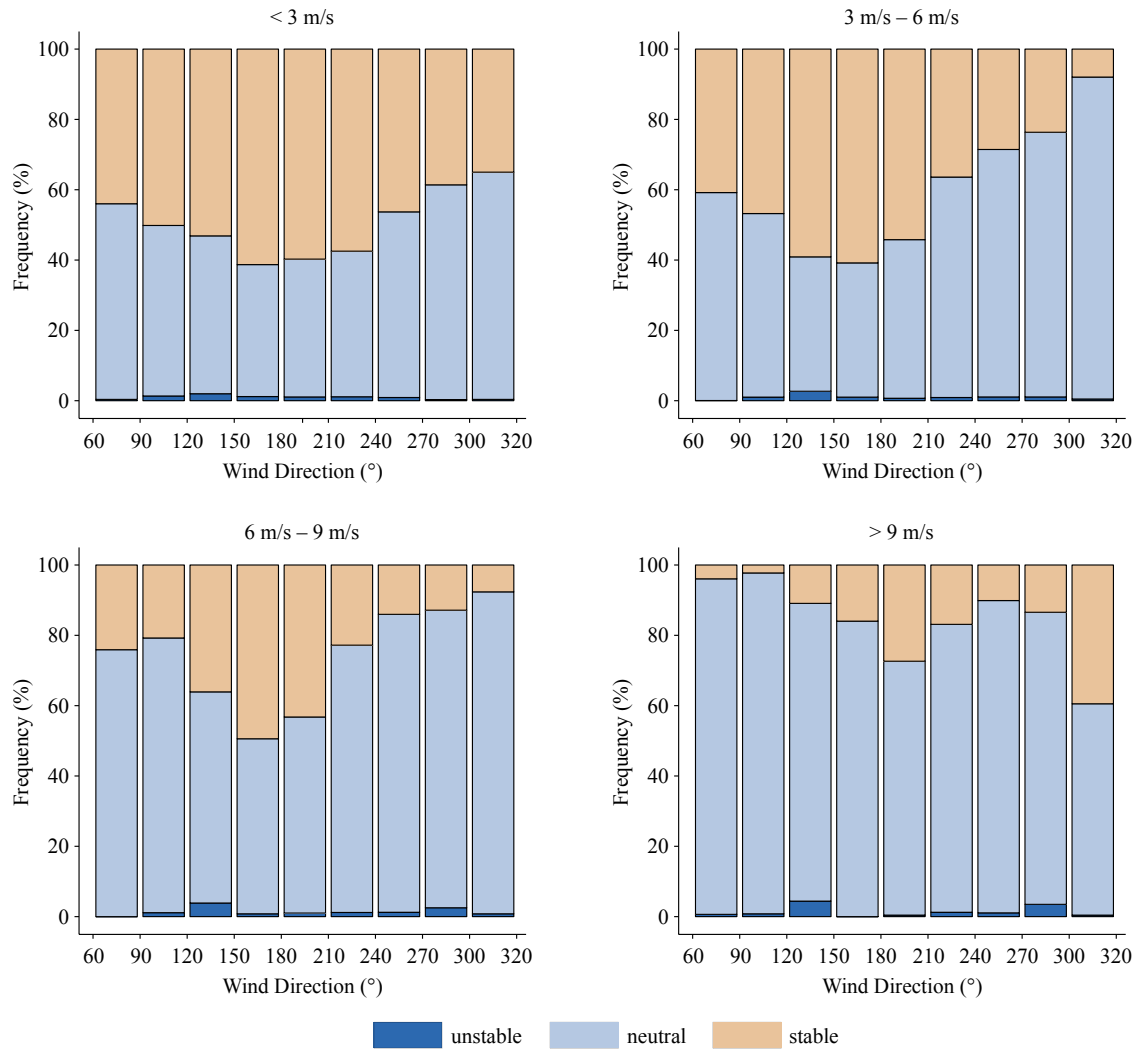
Figure 5.4: Frequency of occurrence of unstable, neutral, and stable stratification cases according to temperature gradients between 10 m and 110 m height per wind direction sector at varying wind speed categories: (a) less than $3\,\mathrm{m\,s^{-1}}$, (b) between 3 and $6\,\mathrm{m\,s^{-1}}$, (c) between 6 and $9\,\mathrm{m\,s^{-1}}$, (d) more than $9\,\mathrm{m\,s^{-1}}$. The wind direction and wind speed are taken from 50 m measurements. Wind directions between $320°$ and $60°$ are excluded due to disturbances induced by the mast structure.

category. This corresponds well with the fact, that during high wind speed situations within a well mixed boundary layer the development of strong temperature gradients is inhibited (Stull, 1988).

The relative frequency of occurrence for stable cases varies considerably between the different sectors. Overall, most cases of stable stratification occur at lower wind speeds which has to be expected since strong inversions only develop with sufficiently weak turbulent mixing. However, it is quite surprising that during flow from westerly directions ($210° - 320°$) at wind speeds larger than $3 \, \mathrm{m \, s^{-1}}$, the fraction of stable stratification is quite small. Only 36% of the cases with wind direction from $210° - 240°$ at $3 - 6 \, \mathrm{m \, s^{-1}}$ are stably stratified. Even less cases can be found in other sectors (i.e. $240° - 270°$: 29%; $270° - 300°$: 24%; $300° - 320°$: 8%). On the other hand, about 54 to 61% of the cases with wind from southeasterly directions and wind speeds between 3 and $6 \, \mathrm{m \, s^{-1}}$ are stably stratified.

Up until now, one can only speculate about the reasons for this phenomenon. One approach to explaining this would be that at westerly wind directions the flow always first passes the city of Hamburg which poses a source for turbulence due to the higher roughness elements present here. This causes turbulent mixing, even at lower wind speeds, and the development of stable stratification would be inhibited. Another possible explanation could be the observation that the wind direction in the levels close to the surface is easterly during stable nights, while the overlying air flows from westerly directions. These observed events, however, are very shallow and often restricted to the lowest 50 m. The above analysis is conducted for wind speeds and wind directions at 50 m measuring height. Anyway, the effect of considerably less cases of stable stratification during westerly winds is also present in observations at all other measurement levels. This contradicts the above described phenomenon of nightly easterly winds below a westerly flow as the reason behind this.

To minimize the effect of changing surface roughnesses at different wind directions, the stability dependence in the following sections is only investigated within one wind direction sector ($90° - 150°$) which features relatively uniform surface roughnesses (see Sect. 4) and also shows a similar frequency of occurrence for the different stability categories (5.4). Furthermore, according to Brümmer et al. (2012), this direction range is the second most frequent, ensuring an adequate large data set for the analysis.

5.3.2 Temperature Gradient in Two Layers

To assess the influence of varying atmospheric stability in higher levels, in addition to the temperature gradient in the lower layer ($10 - 110 \, \mathrm{m}$), also the temperature gradient in the upper layer ($110 - 250 \, \mathrm{m}$) is determined. The corresponding frequency distribution of the temperature gradients for the two separate levels is shown in Figure 5.5. The most frequent combination of the stability in the lower and upper part is neutral (n) stratification in both layers (23 770 cases in the $90° - 150°$ sector). The com-
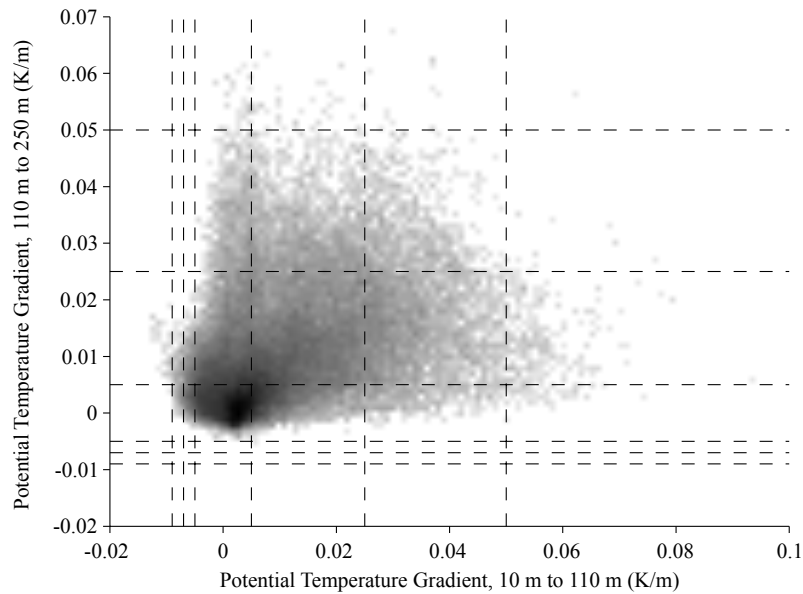
Figure 5.5: Frequency distribution of temperature gradients for the lower (10 m to 110 m) and the upper (110 m to 250 m) part of the mast for wind directions between 90° and 150°. The gradients are calculated from 10-minute means. Shades denote data density. Dashed lines denote the stability classifications according to Table 5.1.

bination of near stable (ns) stratification in both layers is also very common (19 723 cases). Towards instability the frequency distribution of temperature gradients has a sharp boundary. Almost no gradients are smaller than -0.002 K m^{-1} in the upper part. The temperature gradients at stable stratification are spread over a wider range of values. No cases exist in which stratification in the upper layer is very unstable (vu). In General, instability in the upper layer only occurs during neutral or near stable conditions in the lower layer. This is plausible, since unstable stratification forms due to heating from the surface. Because this heating from below is not present in the upper layer, instability only rarely develops.

From Figure 5.5 it becomes quite obvious that the atmospheric stability which is determined below 110 m in the lower part of the boundary layer is not always representative for the stratification in the layer above. In 57.5% of the observed cases, the stratification in the upper and the lower layer correspond. During 37.3% of the cases the stratification deviates by only one stability class. However, for 5.1% of the cases the difference in stratification between both parts is larger than one stability class. In the following section the impact of non-uniform stratification in both layers on the wind profile is investigated.

5.4 The Wind Profile at Different Stabilities

The atmospheric stratification influences the shape of the wind profile (Sect. 2.2.1). In an unstable, well mixed boundary layer the turbulent eddies induce the exchange of momentum from the higher layers of the boundary layer downward. The wind speed increase with height is therefore smaller compared to neutral stratification. In a stable boundary layer on the other hand, the exchange of momentum between the layers is reduced and the increase of wind speed with height is larger, because the wind speed close to the ground is slowed down due to surface friction and the wind speed in the upper layers is mainly influenced by the overlying geostrophic wind.

To analyze the behavior of the wind profile at different stabilities, the wind speed is normalized with the measurement value at 250 m height (Fig. 5.6) to minimize the effect of different wind speeds in the stability categories. The wind speed measurements from 250 m height are selected for homogenization because in this height the influence of the surface is smallest of all measurement heights. Thus these wind speeds are least affected by surface friction. The profiles are classified according to the stability categories in Table 5.1 and are averaged for each stability class. To eliminate the influence of different surface roughnesses, only the wind direction range $90° - 150°$ is used in this section. However, the following analyses match the stability dependent profiles for the other wind direction sectors as well. Since commonly only one stability information from the lower boundary layer is used to obtain the relevant stability for the expected wind profile and this stratification is assumed to be uniform throughout the entire surface layer, only cases with uniform stability in the lower and the upper part are used.

5.4.1 Wind Profiles at Uniform Stratification

As can be drawn from Figure 5.5, no cases with uniform stratification in both layers exist for unstable categories (very unstable, unstable, near unstable). In cases where stratification in the lower part is unstable (vu, u, nu), stratification in the upper part is neutral to stable. Therefore, only the mean profiles of neutral and stable cases (neutral, near stable, stable, very stable) are used in this analysis.

The normalized wind profiles u/u_{250m} for uniform stability categories neutral to very stable are depicted in Figure 5.6. The wind speed increase with height is considerably larger at inversions (near stable, stable and very stable) than at neutral stratification. At stable (s) stratifications the wind speed increases strongly with height up to 175 m and remains almost constant above. This indicates that the height of the boundary layer often is below the highest measurement height of the Wettermast Hamburg in these cases. The unevenness of the very stable (vs) profile could be explained by the small number of cases that contribute to this average (15, compared to 1807 in uniformly stable stratification). However, at very stable stratification it is also possible that low level jets around the height of 175 m could cause these high wind speeds.
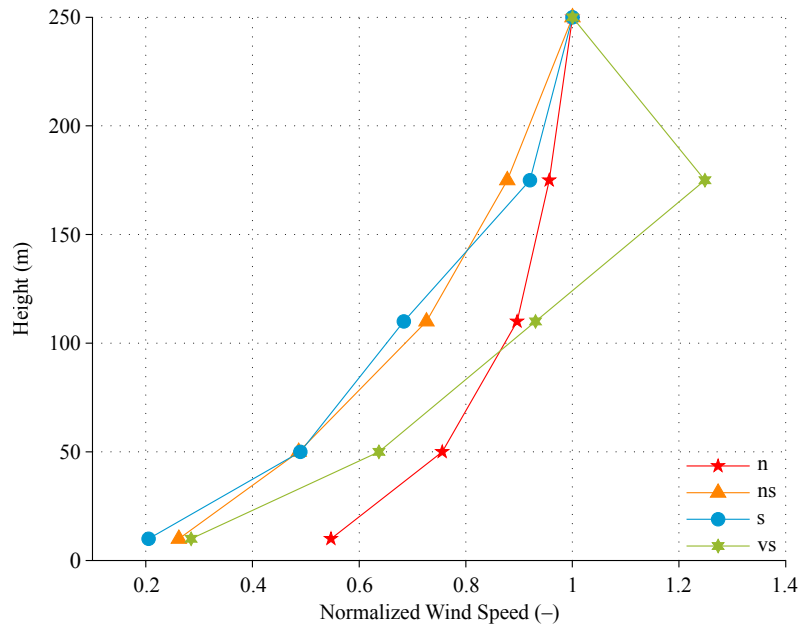
Figure 5.6: Average wind speeds normalized with wind speed in 250 m for different stability categories (Tab. 5.1). To eliminate the influence of different surface roughnesses, only the wind direction range $90° - 150°$ is considered. The characteristics of the profiles in other wind direction sectors correspond.

The wind speed increase with height (wind speed gradient) below 110 m at neutral stratification is only weak, but increases towards more stable stratifications, especially at stable and very stable stratification. The wind speed increase above 110 m is very small at neutral and only slightly stronger at near stable and stable stratification. This is, however, considerably less distinct than below 110 m. From this analysis, it can be deduced that changes in stability mostly results in changes of wind speed gradients in lower levels.

Overall, the shape of the wind speed profiles at different stabilities agree with the expectations (c.f. Sect. 2.2.1) with larger wind speed gradients at stable stratification. At neutral stratification, the boundary layer is reasonably well mixed and momentum is exchanged between higher and lower levels. Therefore, no strong wind speed gradients develop. Increasing stability, however, suppresses vertical mixing and thus inhibits the exchange of momentum between the levels which results in larger wind speed gradients. Holtslag (1984), Monahan et al. (2011) and Floors et al. (2011a) describe a similar behavior of wind profiles at varying stabilities. In these studies, wind speed gradients are weaker at unstable to neutral stratification and gradients increase towards stronger stability.

The standard deviation σ_u (see App. A.1 for method of calculation) of the distribution of the wind speed ratio u/u_{250m} is used to describe the variability of the wind speed (Fig. 5.7, left). Overall, the standard deviation increases with increasing stability from neutral to stable stratification and decreases slightly towards very stable stratification. The largest standard deviation, and thereby the highest vari-
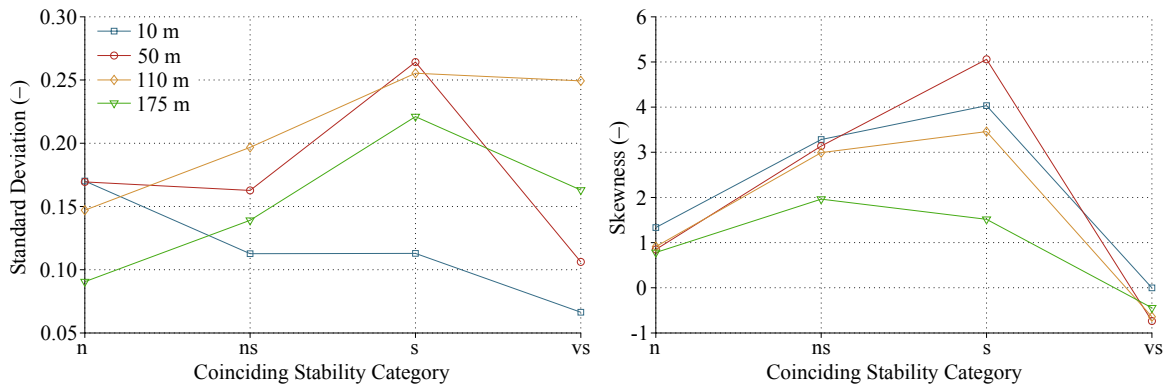
Figure 5.7: Standard deviation (left) and skewness (right) of the distribution of wind speed ratio u/u_{250m}. Stability classes are determined according to Table 5.1 and represent uniform stratification in lower (10 to 110 m) and upper layer (110 to 250 m).

ability in the distribution, is found at 50 m and 110 m height at stable stratification. In 10 m height, however, variability of wind speed decreases with increasing stability continuously. As mentioned above, care must be taken when interpreting results from the very stable stratification category. The very small sample size in this category can lead to results that are not representative.

Several studies investigate wind speed distributions at varying surface stabilities at towers in Cabauw, Netherlands (e.g. Monahan, 2010; Monahan et al., 2011; He et al., 2013). In general, they mention similar effects of stability on standard deviation and skewness (see next paragraph) of the wind speed distribution as is found in this thesis. Monahan et al. (2011) describe a decrease of variability in wind speed in heights close to the surface as well. They attribute this to generally weaker surface wind speeds which results in less variability. Also, the increase of variability at higher levels with increasing stability is noted in this study. The authors state that this effect is a result of larger variation of wind regimes in this level. Depending on the vertical extent of the boundary layer, this measurement levels often lie above the surface layer or even above the boundary layer. In this case low level jets often develop. This relatively large variety of regimes is the reason for larger wind speed variability in these levels.

While the vertical variation of average wind speed is relatively well investigated, the vertical variation of the wind distribution shape is still subject to research (Kelly et al., 2014). Oftentimes, the Weibull shape parameter is used to describe the distribution's shape (Emeis, 2013; Gryning et al., 2013, 2014). However, Monahan et al. (2011) point out that, especially at stable stratification, the shape parameter only insufficiently describes the shape of the distribution. Therefore, skewness (App. A.1) is used in this thesis to describe the shape of the distribution at varying stratification. At positive values, the right tail of the distribution is longer than the left one. This means that the distribution consists of many measurements with relatively small values and some extremely high measurements. This shape is expected for a quantity like the wind speed, because it is naturally limited to values larger than zero.

As can be seen on the right-hand side of Figure 5.7, the skewness of all distributions is mostly positive. It is relatively small to slightly negative at very stable stratification, which suggests a mostly symmetrical or slightly left-tailed distribution where the amount of extremely high wind speed ratios is relatively small. For neutral conditions, the skewness is largest at 10 m and decreases with height. At 175 m, the distribution is comparatively symmetric with not too many extreme values. The skewness is highest at stable stratification in almost all heights. This indicates a relatively large number of extremely high wind speeds in this stability category which occur due to the large variety of regimes in this stability category. Whether or not the true wind speed distribution becomes more symmetrical with decreasing skewness at very stable stratification is not known. Most probably, this effect results from the small sample size in this category and cannot be interpreted with certainty.

Monahan et al. (2011) investigate the shape of the wind speed distribution at varying stratification by analyzing the wind speed distribution's skewness. They state that skewness increases in lower levels with increasing stability. At higher levels, on the other hand, skewness of wind speed distributions is found to decrease with stability. Even slightly negative skewness values are found, indicating a shift of the bulk of the wind speed distribution towards higher wind speeds with only little small wind speed values. Therefore, even if the sample size of the very stable category for the Wettermast Hamburg data is very small, the decrease of skewness might be an indication of the true distribution shape as this is supported by Monahan et al.'s findings as well.

Overall, the average normalized wind speeds vary according to the stratification with larger wind speed gradients in stable stratification and considerably smaller gradients in neutral stratification. The variability of the wind speed distribution is smaller near the ground. At higher levels, it increases with increasing stability. The shape of the distribution is generally right-tailed, implying that it mostly consists of relatively low wind speeds and only little extreme high values. The skewness is smallest in neutral stratification. This indicates that the distribution in those categories is more symmetrical and that more relatively high wind speeds occur at stable stratification. In conclusion, the results of wind speed gradients, variability and shape of the wind speed distribution at varying atmospheric stratification are in good agreement with previous works.

5.4.2 Characteristics of Wind Profiles at Non-Uniform Stratification

Usually, when estimating the wind profile from measurements, only the stratification characteristics close to the ground are taken into account and are assumed to be uniform throughout the entire surface layer. This section gives an overview of how well those estimations represent the properties throughout the entire height of the Wettermast Hamburg and how this influences the wind profile.

As shown in Section 5.3.2, only in 53.3% of the time, stratification is uniform in both layers. This leaves about 46% of the data that deviate from this ideal concept. Therefore, those cases are inves-

tigated to assess how and in which manner this deviation results in differences in wind profiles. The average normalized wind speed and the standard deviation of the wind speed distribution are analyzed for non-uniform stability categories in the lower and the upper layer. Furthermore, the deviations between wind speeds due to the misestimation of the stratification are quantified.

The deviation of stratification from uniformity results in differences in the average normalized wind speeds (Fig. 5.8). The average normalized wind speeds vary between 0.2 and 0.1 in 10 m and between 0.8 and 1.6 in 175 m at different stabilities. Overall, the normalized wind speed is lower at stable lower layer stability and higher at unstable lower layer stability, indicating stronger gradients during stable and weaker gradients during unstable stratification. As mentioned in previous sections (Sect. 2.1, Sect. 5.4.1), wind speed gradients are weaker during unstable stratification due to stronger mixing within the boundary layer. Stable stratification, on the other hand, suppresses vertical exchanges and thus allow for stronger gradients to develop. However, it is interesting that, for example, at neutral lower layer stability the average normalized wind speed in all heights decreases (wind speed gradients increase) with increasing upper layer stability. Here, the inhibition of turbulence due to increasing stability only in the upper layer produces stronger wind speed gradients throughout the entire height.

The standard error of the mean (Fig. 5.8) is estimated by bootstrap resampling the mean of each stability category and calculating the standard deviation of its distribution (see App. A.3). The standard deviation of the distribution of those resampled averages is used to estimate the interval in which the true mean lies with 68.2% probability. The values of the standard error show roughly the influence of the sample size in each category. The magnitude of the standard error in each category increases with height. This indicates that the calculated averages at higher levels provide a less accurate estimation of the true average value. However, overall the error is reasonably small, which indicates that the average is a good estimator of the typical value of the distributions.

When comparing the results in Figure 4.7 and Figure 5.8, it can be seen that the influence of changing stratification is larger than influences due to varying surface roughnesses. In 10 m, the normalized average wind speed $u_{10\,m}/u_{250\,m}$ at different surface roughnesses ranges between 0.4 and 0.5. In the same height, normalized average wind speeds at varying stratification are between 0.2 and 0.7. Also in 110 m, variation due to changes between stable stratification classes is larger than those due to changing surface roughness. Normalized wind speed in 110 m $u_{110\,m}/u_{250\,m}$ ranges between approximately 0.6 and 1 for different stratification. On the other hand, at varying roughness lengths the normalized wind speed in 110 m is between 0.75 and 0.85. This shows that varying stratifications have larger impacts on wind speeds than varying surface roughnesses.

The standard deviation as a measure of variability within the wind speed distribution is depicted in Figure 5.9. The variability within the distribution, determined by the standard deviation, is low at unstable and largest at stable lower layer stability. In all unstable lower layer stability categories (very unstable, unstable, near unstable), the standard deviation is of approximately the same order of mag-
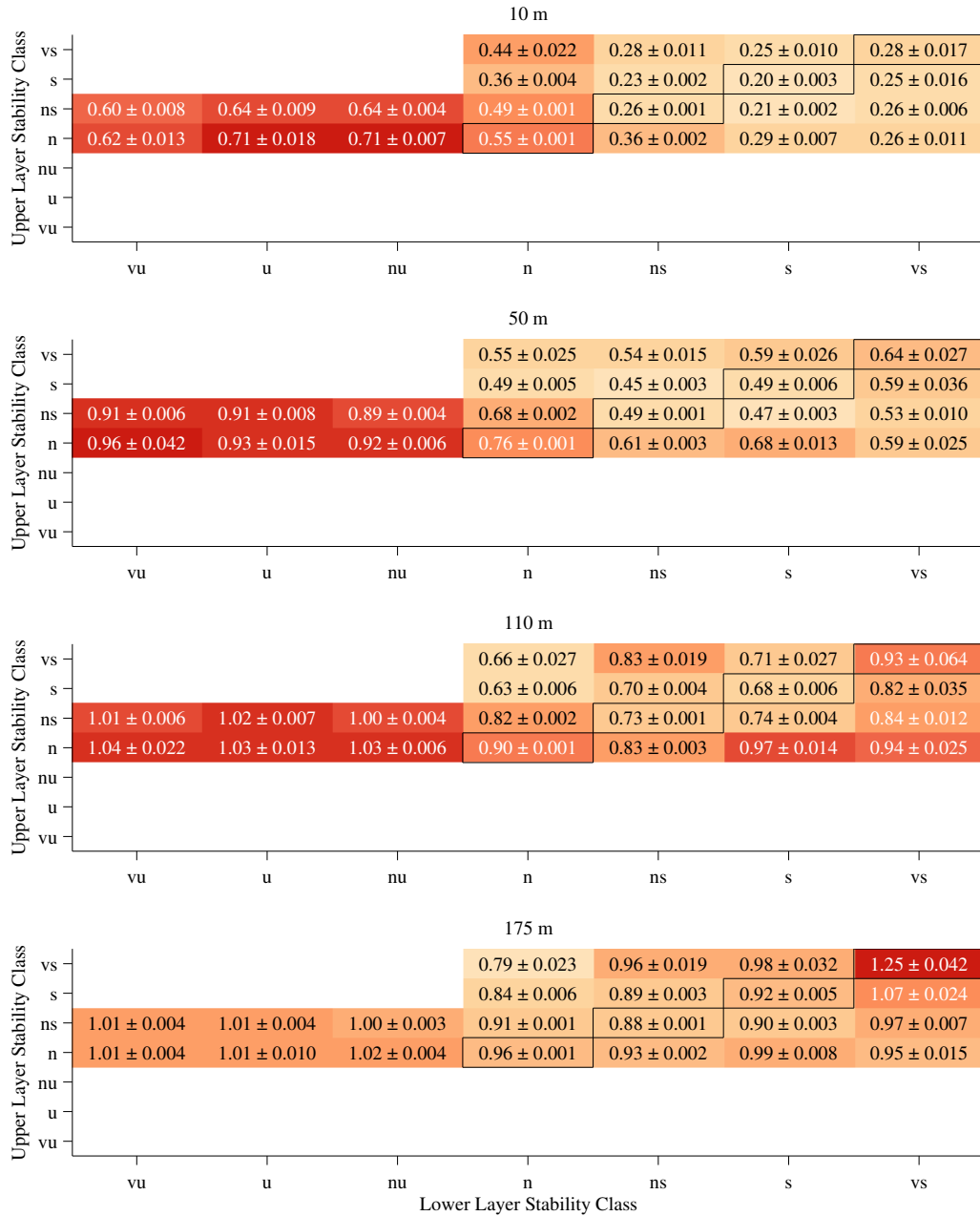
10 m

Upper Layer Stability Class	vu	u	nu	n	ns	s	vs
vs				0.44 ± 0.022	0.28 ± 0.011	0.25 ± 0.010	0.28 ± 0.017
s				0.36 ± 0.004	0.23 ± 0.002	0.20 ± 0.003	0.25 ± 0.016
ns	0.60 ± 0.008	0.64 ± 0.009	0.64 ± 0.004	0.49 ± 0.001	0.26 ± 0.001	0.21 ± 0.002	0.26 ± 0.006
n	0.62 ± 0.013	0.71 ± 0.018	0.71 ± 0.007	0.55 ± 0.001	0.36 ± 0.002	0.29 ± 0.007	0.26 ± 0.011
nu							
u							
vu							

50 m

Upper Layer Stability Class	vu	u	nu	n	ns	s	vs
vs				0.55 ± 0.025	0.54 ± 0.015	0.59 ± 0.026	0.64 ± 0.027
s				0.49 ± 0.005	0.45 ± 0.003	0.49 ± 0.006	0.59 ± 0.036
ns	0.91 ± 0.006	0.91 ± 0.008	0.89 ± 0.004	0.68 ± 0.002	0.49 ± 0.001	0.47 ± 0.003	0.53 ± 0.010
n	0.96 ± 0.042	0.93 ± 0.015	0.92 ± 0.006	0.76 ± 0.001	0.61 ± 0.003	0.68 ± 0.013	0.59 ± 0.025
nu							
u							
vu							

110 m

Upper Layer Stability Class	vu	u	nu	n	ns	s	vs
vs				0.66 ± 0.027	0.83 ± 0.019	0.71 ± 0.027	0.93 ± 0.064
s				0.63 ± 0.006	0.70 ± 0.004	0.68 ± 0.006	0.82 ± 0.035
ns	1.01 ± 0.006	1.02 ± 0.007	1.00 ± 0.004	0.82 ± 0.002	0.73 ± 0.001	0.74 ± 0.004	0.84 ± 0.012
n	1.04 ± 0.022	1.03 ± 0.013	1.03 ± 0.006	0.90 ± 0.001	0.83 ± 0.003	0.97 ± 0.014	0.94 ± 0.025
nu							
u							
vu							

175 m

Upper Layer Stability Class	vu	u	nu	n	ns	s	vs
vs				0.79 ± 0.023	0.96 ± 0.019	0.98 ± 0.032	1.25 ± 0.042
s				0.84 ± 0.006	0.89 ± 0.003	0.92 ± 0.005	1.07 ± 0.024
ns	1.01 ± 0.004	1.01 ± 0.004	1.00 ± 0.003	0.91 ± 0.001	0.88 ± 0.001	0.90 ± 0.003	0.97 ± 0.007
n	1.01 ± 0.004	1.01 ± 0.010	1.02 ± 0.004	0.96 ± 0.001	0.93 ± 0.002	0.99 ± 0.008	0.95 ± 0.015
nu							
u							
vu							

Lower Layer Stability Class

Figure 5.8: Average wind speeds normalized with wind speed in 250 m for seven stability classes (Tab. 5.1) in lower and upper layer at the Wettermast Hamburg. To eliminate the influence of different surface roughnesses, only the wind direction range $90° - 150°$ is considered. Additionally, standard errors of the mean from bootstrapping are given. Boxes indicate cases with uniform stratification in both layers. Colors are given according to average wind speed value in separate color scales in each height.
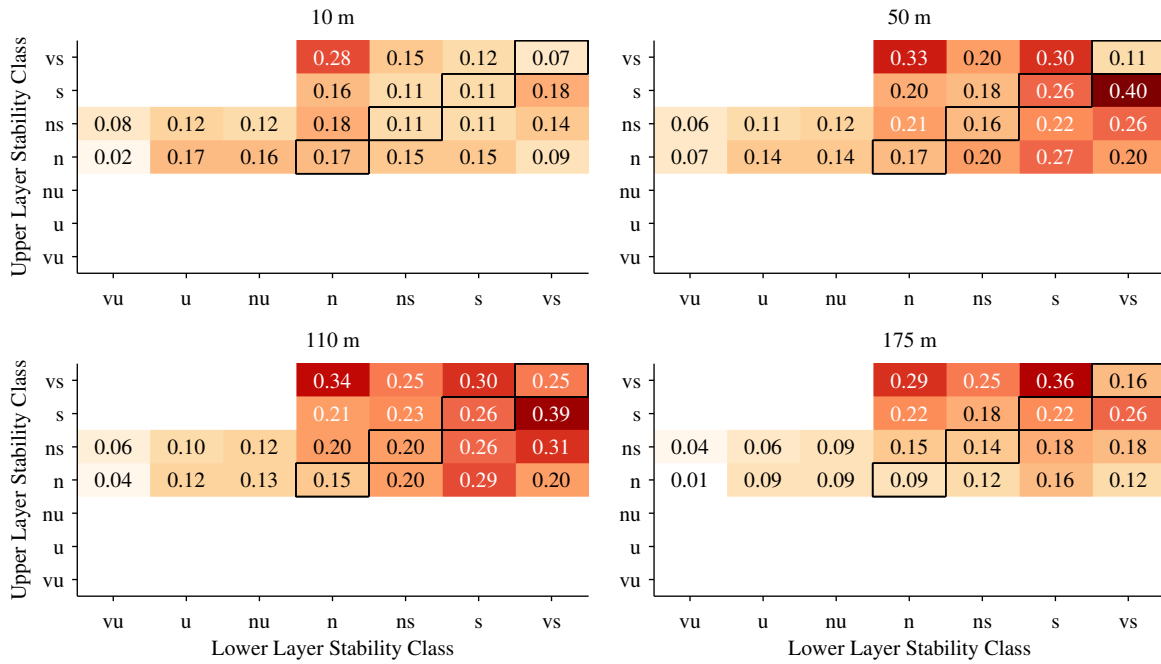
Figure 5.9: Standard deviation of wind speed distribution at varying stratification categories. Boxes indicate cases with uniform stratification in both layers. Colors are given according to standard deviation value in separate color scales in each height.

nitude in each height and for both occurring upper layer stability categories. This indicates that the variability in all heights is not influenced much by those relatively small variations in stability. In neutral to stable lower layer stability, on the other hand, the variability estimated by the standard deviation increases with increasing upper layer stability. Only standard deviation in 10 m decreases with stability as mentioned in the previous section. Interestingly, also an increase of upper layer stability can result in a change of standard deviation in 10 m. However, the effect is relatively small. If the lower layer stratification is stable, a variation of the upper layer stability does not result in any major changes in the standard deviation, except in 50 m. Here, the standard deviation ranges between 1.4 (s|vs) [1] and 2.5 (s|n).

Overall, an increase of lower layer stability results in a larger variability in the wind speed distribution regardless of the upper layer stability in all heights but 10 m. This corresponds to the findings in the previous section where the variability increases with increasing stability. The effect of variation of upper layer stability on the other hand cannot as easily be summarized. Generally, the magnitude of standard deviation change due to changes in upper layer stability is smaller than that due to lower layer stability changes. However, an influence of upper layer stability on the average wind speed and the variability is present. Basically, the same mechanisms that influence the variability of wind speed

---

[1] In this section, the combination of stratification conditions will be denoted as (lower layer stability | upper layer stability). For example, the combination of stable (s) lower layer stability and very stable (vs) upper layer stability is denoted as (s|vs).
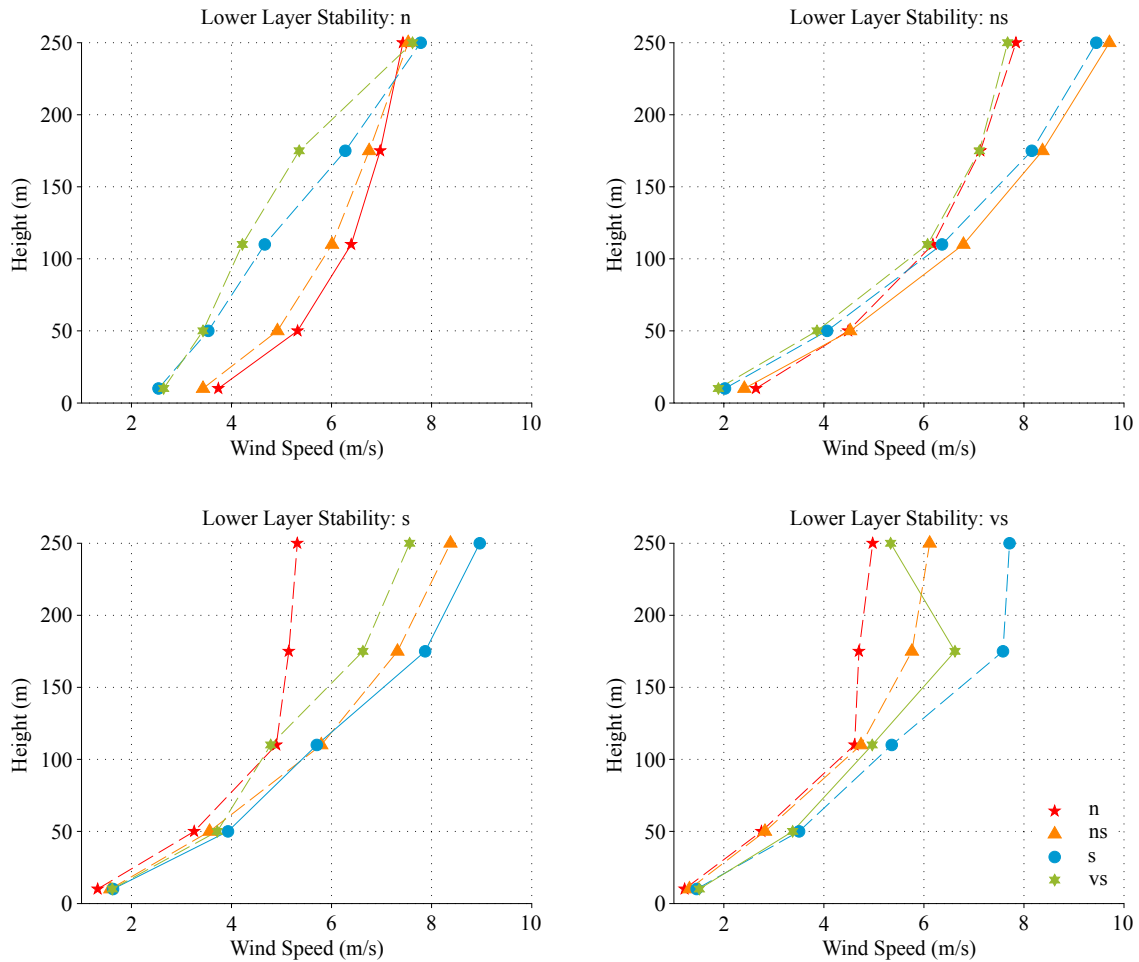
Figure 5.10: Profiles of average wind speeds. Each subfigure depicts profiles at one fixed lower layer stability and varying upper layer stability. Wind profiles at uniform stratification are drawn with solid lines, profiles at deviating stratification with dashed lines.

that are mentioned in the previous section also matter in separate changes of lower layer stability and upper layer stability. In 10 m at weaker surface wind speeds, the variability is generally low. At higher levels, however, the effect of larger variability of wind speed with increasing stability is also present if only upper layer stability changes. As mentioned above, in stable stratification a larger variety of wind regimes is present due to varying boundary layer heights.

Deviations from uniform stratification affect the measured wind profiles in all measurement levels (Fig. 5.10). In cases of neutral lower layer stability, increase of upper layer stability results in changes in wind speeds in all measurement height. If the lower layer is stably stratified (near stable, stable, and very stable), wind speed in lower levels is influenced a little, but the majority of changes occurs in the upper levels.

To quantify the previously mentioned deviation of wind speed due to separately varying stabilities,
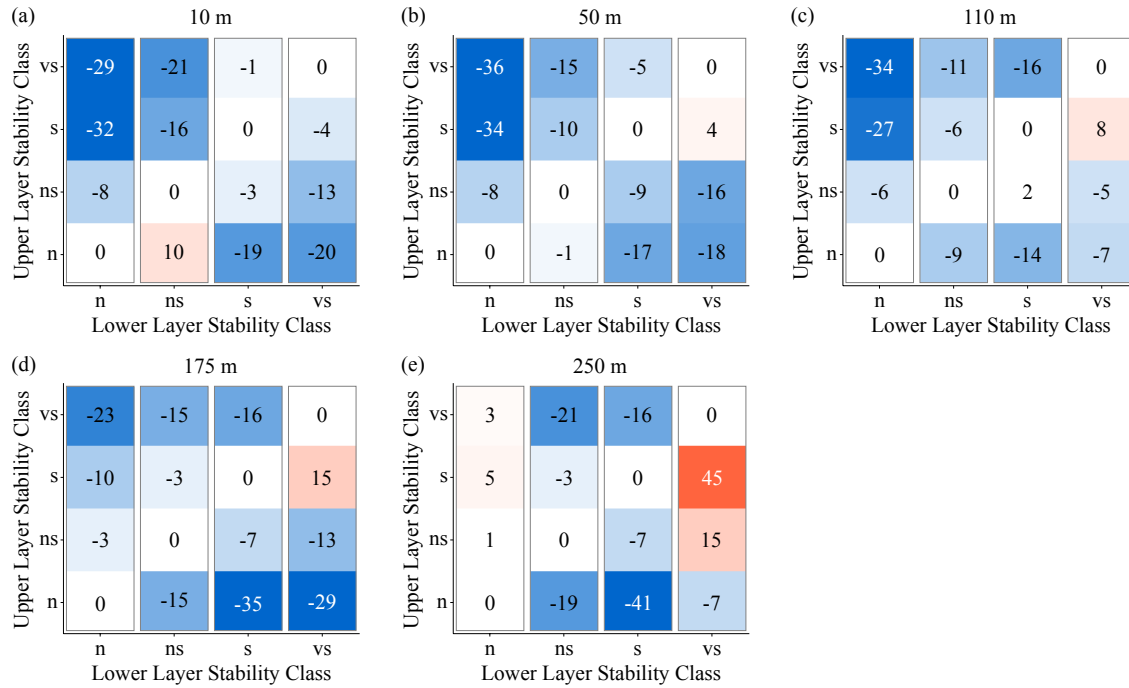
Figure 5.11: Relative differences of wind speed for varying upper layer stability in %. The difference is calculated between the average wind speed at uniform stratification (diagonal entries) and the average wind speed at the same lower layer stability but different upper layer stability (variation along ordinate) and normalized with average wind speed at uniform stratification in 10 m (a), 50 m (b), 110 m (c), 175 m (d), and 250 m (e). Positive values indicate higher wind speeds than at uniform stratification and negative values indicate lower wind speeds.

relative difference are calculated in each height. Those are taken between the expected wind speed at uniform stratification (diagonal entries in Fig. 5.11) and the wind speed at the same lower layer stability and different upper layer stability (variation along ordinate in Fig. 5.11). For example, in case of the (n|ns) category, the relative difference is calculated using:

$$\Delta \overline{u}_{(n|ns)} = \frac{\overline{u}_{(n|ns)} - \overline{u}_{(n|n)}}{\overline{u}_{(n|n)}} \quad . \tag{5.5}$$

Here, positive values indicate higher wind speeds and negative values indicate lower wind speeds than at uniform stratification.

The wind speed at varying upper layer stability is smaller than the expected wind speed at uniform stratification in almost all cases. The amount of these differences varies with height and stability category. Large deviations occur if neutral stability is assumed and the upper layer stability is stable or very stable. In these cases the wind speed in lower levels (10 to 110 m) is about 30% smaller than assumed. However, this deviation is smaller in 175 m and even inverse in 250 m. Here, the wind speed is about 5% larger than assumed in case of neutral stratification in the lower layer and stable stratification on top (n|s).
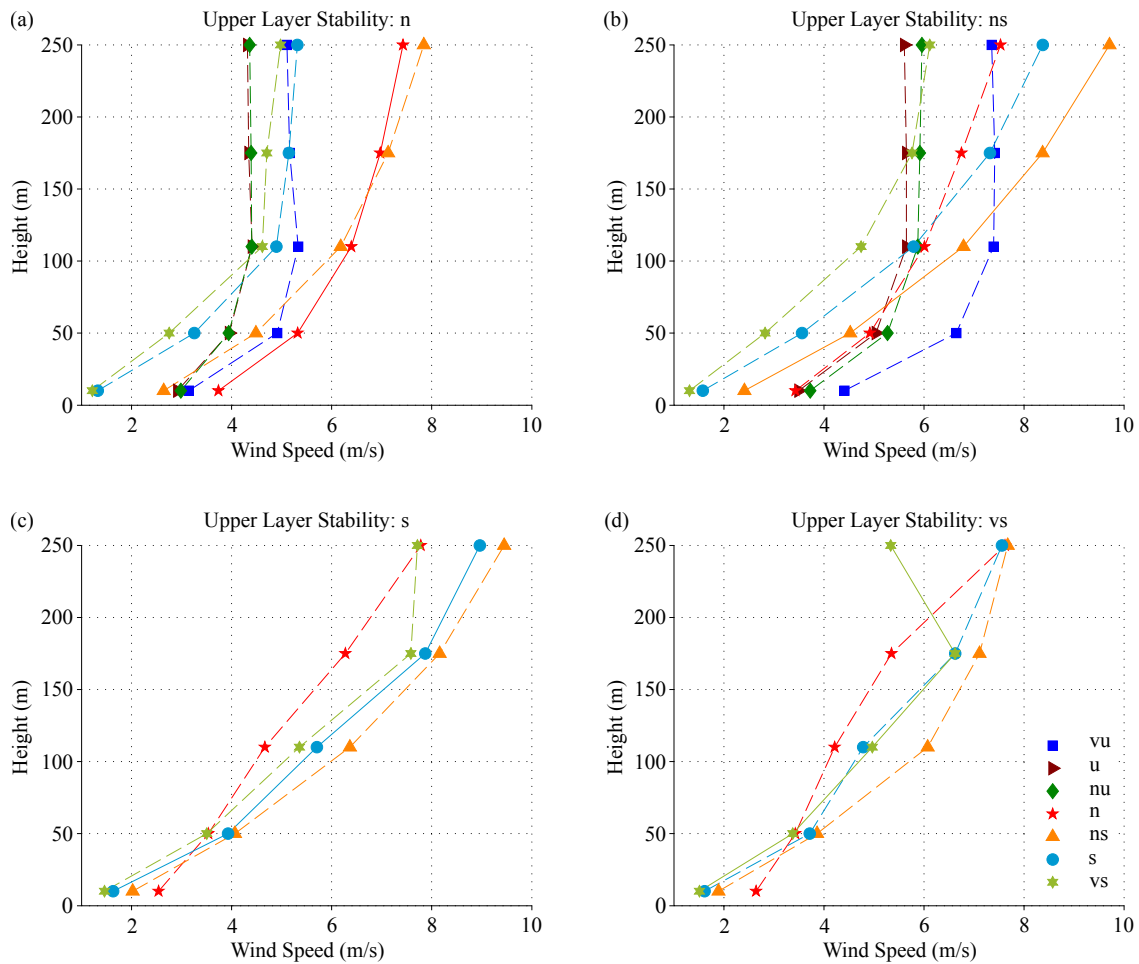
Figure 5.12: Profiles of average wind speeds. Each subfigure depicts profiles at one common upper layer stability and varying lower layer stability. Wind profiles at uniform stratification are drawn with solid lines, profiles at deviating stratification with dashed lines.

In all other stability categories, the deviation in upper layer stability results in lower wind speeds than expected. Large deviations occur in the category (s|n). Here, the wind speed is between 14% and 41% lower than expected. Care must be taken when interpreting results from the very stable lower layer stability category. These deviations appear to be the overall largest. As can be seen in Figure 5.8, the average wind speed in the (vs|vs) stability category has a large uncertainty of 1.25 ± 0.042 because it consists of only 15 data samples.

A general overestimation of wind speeds can be seen in Figure 5.11. Since no unstable stratification occurs in the upper layer (Sect. 5.3.2), it can only be stated that a misinterpretation of upper layer stability leads to overestimation of wind speed. Overall it can be concluded that, if the stratification in the upper layer is less stable than assumed based on the conditions in the lower layer, the wind speed in all heights is smaller than the one in the comparison category. Generally, if upper layer stability is ignored and only lower layer stability is taken into account, the wind speed would be overestimated in almost all cases.
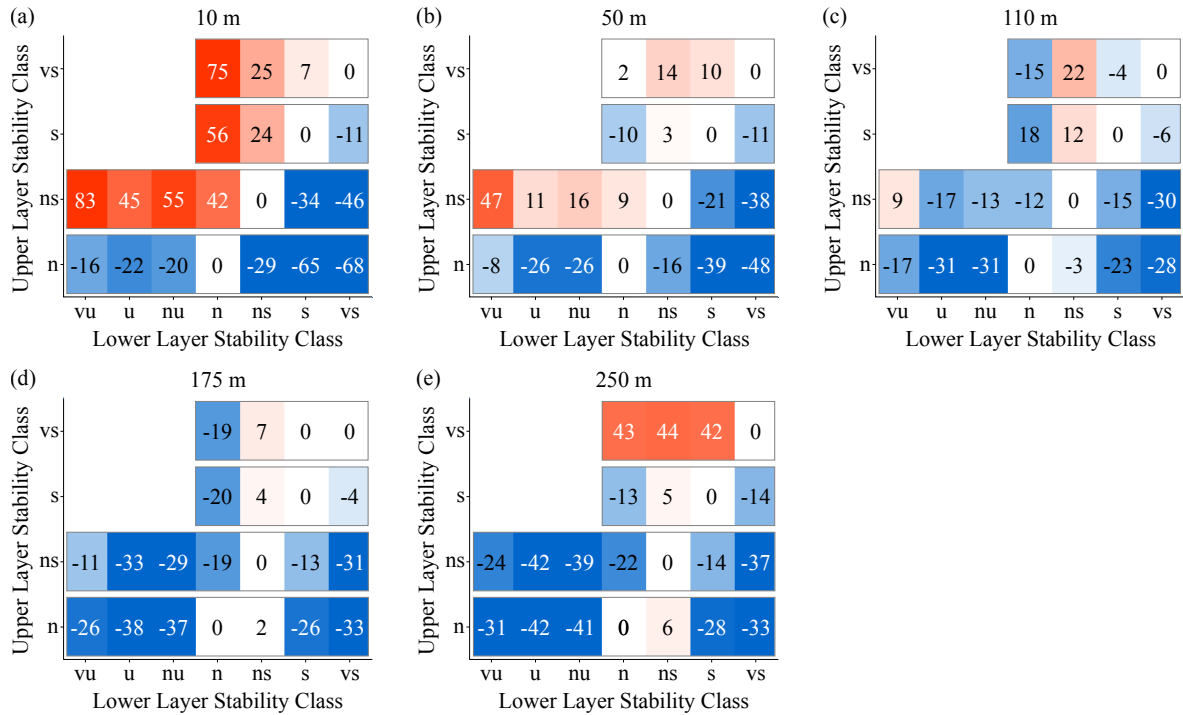
Figure 5.13: Relative differences in %, same as Fig. 5.11 but for deviation of lower layer stability from uniform stability throughout the entire mast height.

Naturally, the change in lower layer stability also has an impact on the wind profile. As can be seen in Figure 5.12 change of lower layer stability at constant upper layer stability, affects the wind profiles in all heights. In Figures 5.12a and b it is obvious that the lower layer stability determines the shape of the wind profile with little increase of wind speed for unstable lower layer stability and larger increase for stable lower layer stability. However, also in Figure 5.12c and d it is visible that the variation of lower layer stability influences the wind speed at higher levels as well. In fact, the range of variation of the relative differences due to those changes (Fig. 5.13) is even larger than the above described variation of wind speed due to changing upper layer stability.

The highest impact can be found in lower measurement levels (10 and 50 m). Here, if the stratification is more unstable than assumed, the wind speed is larger by as much as 83%. This means that at unstable lower layer stability and neutral to stable upper layer stability wind speed close to the ground is still increased, even if the exchange with higher layers is inhibited by inversions. In higher measurement levels (110 m and above) and in cases with unstable lower layer stability and neutral to stable upper layer stability, the wind speed is smaller than at uniform stratification. This could indicate, that at neutral upper layer stability, which neither inhibits nor enhances vertical exchange of momentum, the increased turbulence close to the ground extracts momentum from the higher measurement levels. However, care must be taken when interpreting the strong increase of wind speed at very stable upper layer stability. The category (vs | vs) only consists of 15 profiles which results in higher uncertainty of the values.

Exemplarily, the relative deviation of wind speed due to varying upper layer stability can be calculated with absolute wind speeds. The average absolute wind speed in 110 m in uniform neutral stratification (n|n) is $6.4\,\mathrm{m\,s^{-1}}$. If one would assume this stratification for wind profile estimation, the deviation of -34% in the (n|vs) stability category would result in a wind speed of $4.2\,\mathrm{m\,s^{-1}}$. In 175 m, the relative differences of wind speed are of approximately the same order. However, the average wind speeds increase with height. If one would like to predict the wind speed at 175 m and (s|s) stability is assumed, the relative deviation is -35% (in case of true (s|n) stability). Therefore the wind speed would be expected to be $8.0\,\mathrm{m\,s^{-1}}$, while it only is $5.1\,\mathrm{m\,s^{-1}}$. In 250 m, the average wind speed in (s|s) stability is $9.0\,\mathrm{m\,s^{-1}}$. If the upper layer stability would be ignored in wind speed estimation in this stability category, the deviation can be as large as -41%, if the true upper layer stability was neutral. This would mean an actual wind speed of $5.3\,\mathrm{m\,s^{-1}}$. Overall, disregarding variation in upper layer stability mostly results in overestimations of wind speed in all levels.

The deviations of average wind speeds due to the assumption of uniform stabilities throughout the entire height are even larger for variations in lower layer stability. It is therefore essential to estimate the correct stability in this layer. Nevertheless, variations in upper layer stability mainly lead to overestimations of the wind speed. In these cases the true wind speed would be up to 41% less than assumed.

When estimating the wind speed at larger heights, that are sometimes well above the surface layer, the upper layer stability becomes more important with increasing height. For yield projections above the current hub heights ($> 100\,\mathrm{m}$), an overestimation due to varying upper layer stability would result in overprediction of the possible earnings. Whereas, for wind load estimations at higher levels an underestimation of the expected wind speeds due to varying upper layer stability would lead to an underestimation of the expected load on structures.

5.5 Modeling Wind Profiles at Varying Stratification

Both Gryning et al. (2007) and Peña et al. (2010) propose models to predict the wind profile from measurements at or close to the surface: roughness length z_0, friction velocity u_* from 10 m measurements, and the Obukhov length L evaluated at 50 m (cf. Sect. 2.3). Their suggestions are evaluated by comparison with measurements at the Wettermast Hamburg site in the course of this section.

5.5.1 Modeled Wind Profiles at Uniform Stratification

The necessary input parameters u_*, L, and z_0 (Sect. 4) are determined at every available time step and a wind profile between 1 m and 300 m is calculated from both models. The average wind speeds for the
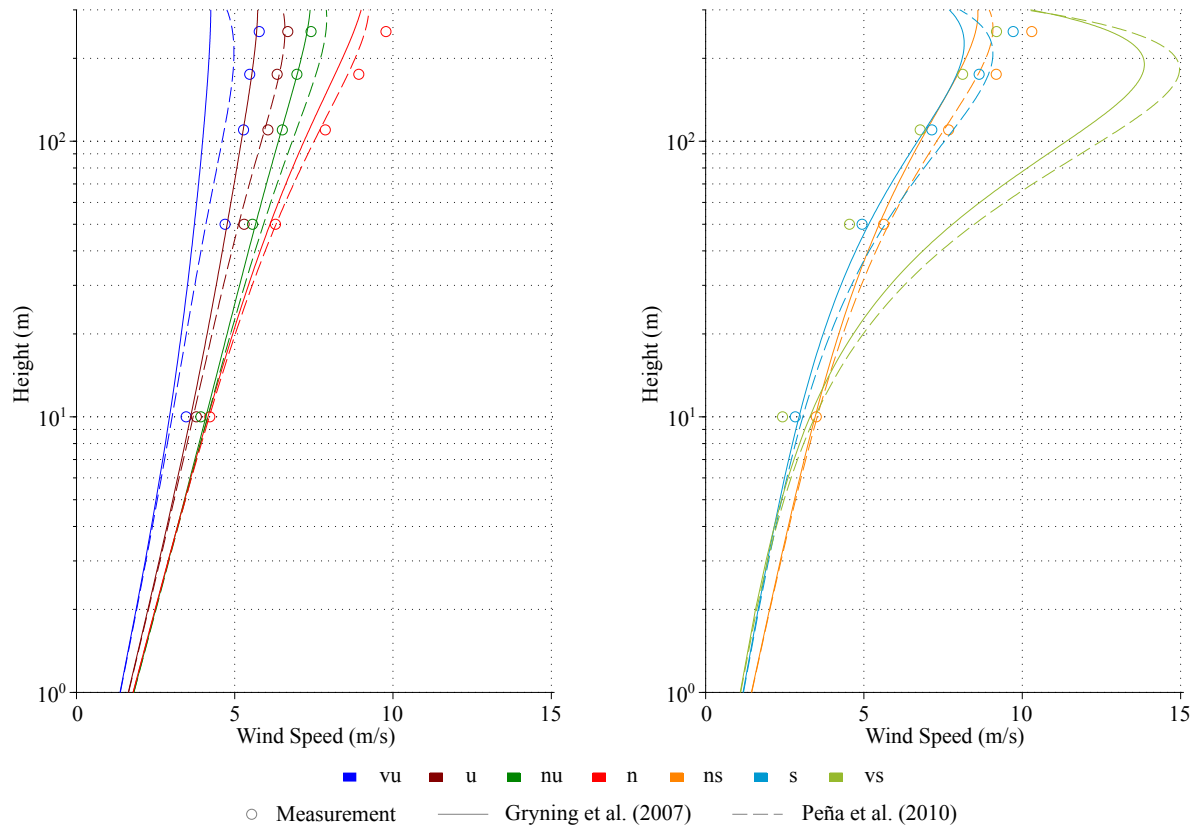
Figure 5.14: Wind speed profiles measured at Wettermast Hamburg (circles) and estimated by the approach of Gryning et al. (2007) (solid lines) and Peña et al. (2010) (dashed lines) for wind directions between 90° and 150° ($\overline{z_0} = 0.16$ m). The colors denote the stability categories according to Table 5.1. Left: unstable and neutral stratification, right: stable stratification.

seven stability categories (Tab. 5.1) from both models and measurements are depicted in Fig. 5.14. As in the above evaluation of the measured wind speed profiles, only the wind direction sector between 90° and 150° is used to eliminate any possible influence of varying surface roughnesses. Only friction velocities $u_* \geq 0.1\,\mathrm{m\,s^{-1}}$ are considered since this otherwise indicates an upward momentum flux which is an unusual state of the surface layer. The number of remaining profiles in each stability category are given in Table 5.2.

The estimated wind profiles show the same basic shape as the measurements. Below 110 m, the modeled wind speeds agree reasonably well with the measurements, with exception of very unstable and very stable categories. Here, the wind speed is systematically overestimated in case of very stable stratification and underestimated in case of very unstable stratification. Both models overestimate wind speeds in very stable stratification by about 5 m s^{-1}. As discussed in Section 5.2, the small positive values of the Obukhov length ($50 \geq L > 10$) in the very stable stratification category can lead to unreasonably large wind speeds. Therefore, this category is excluded in further investigations.

Table 5.2: Number of available profiles within the 90° and 150° wind direction sector for each stability category according to Table 5.1

Stability category	vu	u	nu	n	ns	s	vs
Number of profiles	2 266	2 382	2 247	14 342	7 930	7 063	2 138

To quantify the deviations between the predicted wind profiles and the measurements, the root mean square error (RMSE) and the average bias are calculated (Fig. 5.15 and excerpts for 110 m and 175 m in Tab. 5.3). The bias is calculated by subtracting the measured wind speed from the estimated wind speed $u_{est} - u_{meas}$. Thus, negative bias values indicate that the predicted wind speed is smaller than the measured one, i.e. the model is underestimating the wind speed. To account for the effect that at higher average wind speeds also the errors can be larger, both are normalized with the average wind speed in each height.

The RMSE of the Gryning et al. (2007) approach (Fig. 5.15a) is overall smallest at near unstable stratification with about 27% in 10 m, decreasing to 16% in 110 m and 175 m, and increasing again further up. For unstable and very unstable stratification the nature of the RMSE is essentially the same but with slightly higher values (between 24% and 18% (u) and between 28% and 21% (vu)). At neutral and towards near stable and stable stratification the RMSE is of the same order as in the above mentioned stability categories, but the error increased stronger towards higher measuring heights. In stable stratification the error is smallest of all stability categories in 10 m but increases strongly towards higher levels. This indicates that the wind speed in all heights is comparatively well represented by the Gryning et al. (2007) approach for neutral and unstable stratifications, but, as already described above, in stable stratification and at higher levels the deviations from the measurements are larger.

The average bias between the Gryning et al. (2007) model and the measurements (Fig. 5.15b) shows that the wind speed is underestimated in almost all stability categories and in all heights. One exception is the wind speed below 110 m during stable and near unstable stratification in all heights. Here, the bias is approximately zero or slightly positive. At all three unstable categories and in neutral stratification the bias is more or less constant with height. This indicates that the Gryning et al. (2007) approach is a good estimate for unstable and neutral conditions, regardless of the height. In stable stratifications, on the other hand, the estimate is even better in the lower levels. However, the bias increases towards larger negative values with increasing measurement height. Nevertheless, even at 250 m the lowest bias in near stable stratification is of the same order of magnitude as the bias for very unstable stratification.

The characteristics of the RMSE of the Peña et al. (2010) approach for different stabilities (Fig. 5.15c) are similar to the above described RMSE of the Gryning et al. (2007) approach. The error is smallest in 110 m and 175 m height at unstable stratification (near unstable, unstable, and very unstable). At
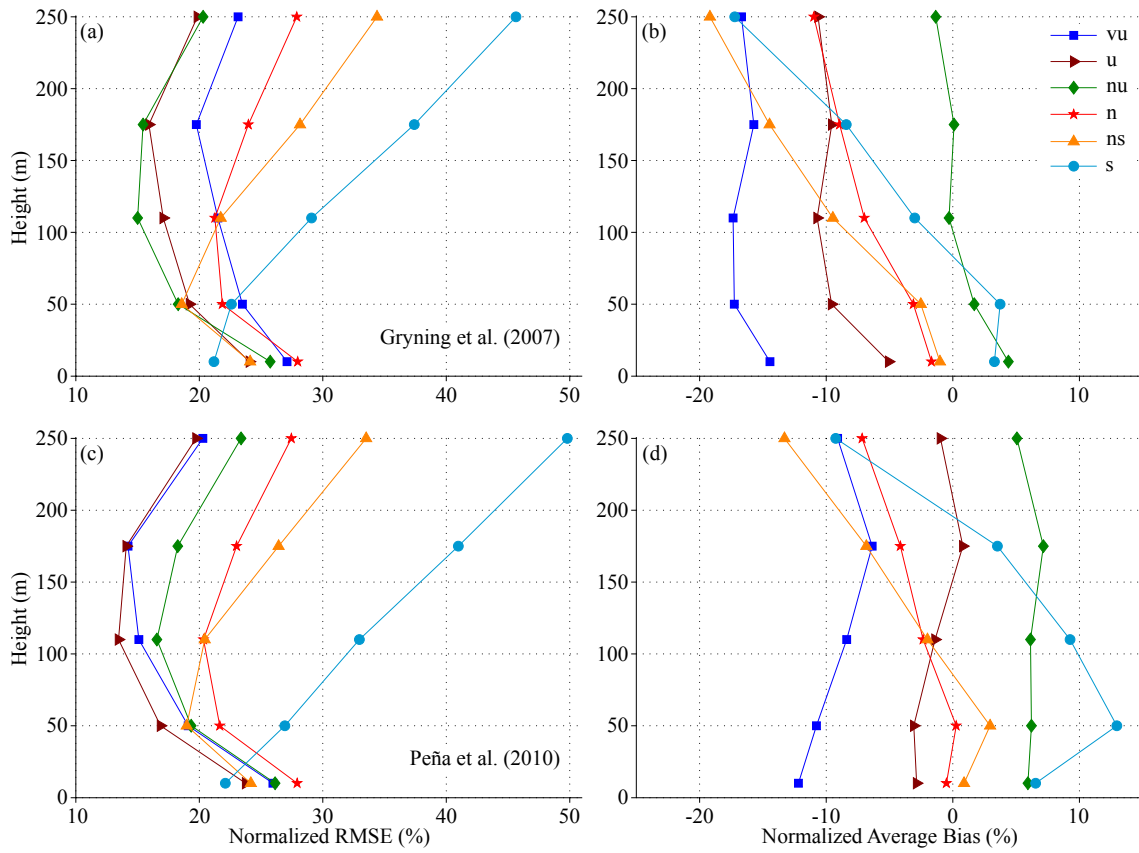
Figure 5.15: Error estimates of model results from comparison with measurements. Top row: the approach proposed by Gryning et al. (2007), bottom row: the approach proposed by Peña et al. (2010). The normalized RMSE is depicted in the left column, the normalized average bias in the right column. The bias is calculated as $u_{est} - u_{meas}$.

neutral and near stable stratification the error is reasonably small in the lower levels as well, but increases towards higher levels. In stable stratification the error is smallest of all stability categories in 10 m but already in 50 m the error is larger than in all other stability categories and increases even further towards higher levels. The overall values of the RMSE of the Peña et al. (2010) approach are – with exception of the stable stratification category – smaller than those of the Gryning et al. (2007) approach, indicating an overall better fit to the data.

The overall values of the average bias of the Peña et al. (2010) approach (Fig. 5.15d) are closer to zero than those of the Gryning et al. (2007) approach. The wind speeds in all heights are only underestimated in very unstable stratification, indicated by negative biases. In all other stability categories however, the bias is close to zero or even positive in some heights, which indicates an overestimation of wind speed. At unstable stratification the bias is closest to zero in all heights. Thus, this stability category is represented best by the Peña et al. (2010) model. Although the error estimates are smaller than those of the Gryning et al. (2007) approach, the model of Peña et al. (2010) still mostly underestimates the wind speed in all heights.

Table 5.3: Relative RMSE and bias from comparison of the models of Gryning et al. (2007) and Peña et al. (2010) with measurements exemplarily for 110 m and 175 m height. The RMSE and bias are normalized with the average wind speed in each height. Stability is categorized according to Tab. 5.1. Compare Fig. 5.15 for more comprehensive presentation of the model error estimates. Very stable (vs) stratification category is excluded, due to model sensitivity issues (Sect. 5.2).

RMSE (%)		vu	u	nu	n	ns	s
Gryning et al. (2007)	110 m	22	17	15	21	22	29
	175 m	20	16	15	24	28	37
Peña et al. (2010)	110 m	15	13	17	20	20	33
	175 m	14	14	18	23	26	41

Bias (%)		vu	u	nu	n	ns	s
Gryning et al. (2007)	110 m	−17.3	−10.7	−0.3	−7.0	−9.5	−3.0
	175 m	−15.7	−9.6	0.1	−8.9	−14.5	−8.4
Peña et al. (2010)	110 m	−8.4	−1.4	6.1	−2.3	−2.0	9.3
	175 m	−6.4	0.8	7.2	−4.1	−6.8	3.5

In conclusion, the error estimates of both models are lowest for unstable stratification, compared to the other stability categories. This can be explained by the fact that the convective boundary layer usually extends up to higher heights than the neutral or even the stable boundary layer. It can therefore be assumed that all measurement heights lie well within the boundary layer or even the surface layer during unstable conditions. During stable conditions, on the other hand, the top of the boundary layer can be as low as 10 m above ground (Foken, 2006b). However, this extremely low value is very unlikely in case of the measurements at Wettermast Hamburg, since the surface roughness of the surroundings induces turbulence which always expands the boundary layer (Zilitinkevich and Baklanov, 2002). Nevertheless, the top of the boundary layer in stable stratification that is determined by the Rossby-Montgomery formula (Sect. 2.3.1) and used within the models is often around 200 m in stable cases. The top measurement of the Wettermast Hamburg therefore often is above the boundary layer during stable stratification. This height corresponds further with the wind speed maximum of the predicted wind speeds in stable cases.

Sathe et al. (2011) investigate the agreement between the Gryning et al. (2007) model and offshore tower measurements. They state that for unstable and neutral stratification the model represents the measurements reasonably well. However, in stable stratification the deviation between model and measurements are larger at these offshore sites as well. Emeis (2013) compared both model approaches to one month of Sodar measurements. He found no considerable differences of performance between the two models. It can be concluded from this section that both mixing length models represent wind profile measurements well under unstable and neutral conditions. During stable stratification however,

the errors between models and measurements are larger. Overall, no model is superior over the other. In some stability categories the Gryning et al. (2007) model performs better, in others the Peña et al. (2010) model fits the measurements better.

––––––––––––––––––––

In conclusion, this chapter addresses the impact of the variable stratification of the atmosphere close to the ground on the wind profile. Stratification characteristics at the Wettermast Hamburg are discussed and the input parameter L, needed to predict the wind speed with the models of Gryning et al. (2007) and Peña et al. (2010), is reviewed.

- The Obukhov length L derived from eddy covariance measurements deviates considerably from the stability categorization by the gradients of potential temperature in 22% of the cases. Therefore, the Obukhov length is recalculated utilizing the gradient Richardson number. Only 3% of the measurements deviate from one another after recalculation of L. This indicates deficiencies of the eddy covariance measurements at the Wettermast Hamburg. Therefore, the consistency of the data set is improved by recalculating L from gradient Richardson number (Sect. 5.1).

- Wind speed models by Gryning et al. (2007) and Peña et al. (2010) are sensitive to very small positive values of L (extreme stability). This results in an overestimation of wind speed for those cases. Therefore, only profiles with stratification $|L| > 50$ m should be used for the model estimations (Sect. 5.2).

- Neutral stratification is the most frequent stability category at the Wettermast Hamburg. Diurnal differences of the frequency distribution of stability can be found. Stable stratification mainly occurs during nighttime, corresponding to a nocturnal boundary layer structure. The bulk of the neutral stratification cases happenes during daytime. Additionally, the frequency of occurrence of stability categories also varies with wind speed and wind direction. At higher wind speeds, more cases are neutrally stratified. During flow from westerly directions ($210° - 320°$), the fraction of stable stratification is quite small (Sect. 5.3).

- Additionally, atmospheric stratification at the Wettermast Hamburg is determined by gradients of potential temperature in two layers (10 m to 110 m and 110 m to 250 m). The most frequent stability category in both layers is neutral stratification. When discerning between the stratifications in the lower layer and the upper layer, it becomes obvious that in about 46% of the data upper layer stability is different from lower layer stability (Sect. 5.3).

- The average wind profile increases less with height at neutral stratification and stronger in stable stratification. Variability of the wind speeds is small in 10 m and decreases with increasing stability. In higher levels, variability is larger and increases with stability (Sect. 5.4).

- When discerning between stability in the lower and in the upper layer of the Wettermast Hamburg, the wind speed shows a strong response to changes in the lower layer stability with constant upper layer stability. Nevertheless, variations in upper layer stability with constant lower layer stability also causes wind speed deviations. These are mainly overestimations of wind speed. In these cases the true wind speed would be up to 41% less than assumed (Sect. 5.4).

- The wind speed between 1 m and 300 m is predicted, using models proposed by Gryning et al. (2007) and Peña et al. (2010). The wind speed is best predicted from both models for unstable stratification when the top of the boundary layer lies presumably well above the mast height. During stable stratification, the error between the modeled and the measured wind speed is reasonably small in lower levels but increases distinctly with height. This could be explained by the fact that the top of the boundary layer in those cases often lies below the highest measuring height and therefore not all measurements are taken within the boundary layer (Sect. 5.5).

6

Conclusions and Outlook

The scope of this thesis is the wind profile in heterogeneous terrain, in particular in the transition area between urban and rural terrain. It is the aim of the study to broaden the understanding of the boundary layer wind profile and to analyze different influencing parameters on the wind profile. The results can provide a deeper insight on the important factors for estimations of the wind profile, e.g. for wind energy applications.

The measurements used in this thesis were taken at the Wettermast Hamburg site which is located at the easterly outskirts of the city of Hamburg. Observations at five measurement levels between $10\,\mathrm{m}$ and $250\,\mathrm{m}$ from October 2000 until March 2012 are used. The data set is homogenized into complete, undisturbed profiles with wind speeds larger than $1\,\mathrm{m\,s^{-1}}$ in all heights. 62% of the maximum possible measurements comply with those prerequisites.

Atmospheric stratification is determined by Obukhov length L and gradients of potential temperature. The Obukhov length derived from eddy covariance measurements deviates in 21.9% of the cases from the stability categorization by the gradients of potential temperature. This deviations originate from shortcomings of operational eddy covariance calculations in the Wettermast Hamburg data. Therefore, the Obukhov length is recalculated utilizing the gradient Richardson number. In contrast to Obukhov length, no obvious inaccuracies of friction velocity u_* calculated from eddy covariance is found. Nevertheless, u_* is recalculated by means of flux variance similarity. This recalculation is performed to gain a coherent data set. The recalculated values of friction velocity are compared to wind speed measurements utilizing the definition of the drag coefficient. Those are in good agreement. It can therefore be concluded that those two approaches of replacing eddy covariance measurements are feasible and result in a homogenous data set.

The location of the Wettermast Hamburg site allows for the analysis of the wind profile at different surface roughnesses depending on the wind direction. Overall, the terrain to the west of the site is mostly urban. To the east it is mainly rural. The roughness length as surface characteristic is determined for

the surroundings of the Wettermast Hamburg from wind profile measurements at different heights and for 30°-wide wind direction sectors. The measured wind profile is analyzed in terms of influence of surface roughness and atmospheric stratification. Furthermore, two wind profile models are validated with measurements at the Wettermast Hamburg. Both model approaches utilize an expansion of the mixing length concept to allow for the estimation of wind speed above the surface layer.

Based on the analyses in this thesis, the questions specified in Chapter 1 are answered below.

What are important characteristics of the Wettermast Hamburg site and its observations?

To ensure adequate interpretation of observations at the Wettermast Hamburg site, comprehensive knowledge of the site characteristics and the climatological conditions is necessary. The Wettermast Hamburg itself is a solid cylindrical mast. The booms on which the instruments are mounted extend towards 190°. Anemometers are installed at the edge of these booms at a distance of 6.47 m from the mast's center.

Although the distance between mast and anemometers is comparatively large, disturbances of the flow due to mast circulation can still be detected. Turbulence intensity in undisturbed conditions characterizes the turbulence of the mean flow. In case of mast circulation an increase of turbulence caused by the mast's structure can be observed. Turbulence intensity values are mainly between 0.02 and 0.1 for most directions. However, they increase considerably for wind directions between 320° and 60° to values between 0.25 and 0.8. Until now, no reliable method of correction for this effect could be found. Therefore, wind directions between 320° and 60° have to be discarded to ensure reliable wind measurements.

The Wettermast Hamburg site is situated at the easterly outskirts of the city of Hamburg. The immediate surroundings of the site are far from homogenous. The terrain is dominated by different roughness elements, depending on distance from the mast and wind direction. The site is surrounded by allotment gardens (south), a gravel pit (east and north) and industrial buildings (west). The more distant area around the measurement site towards the west is characterized by industrial buildings and the city of Hamburg. East of the site the terrain is mainly rural.

One main prerequisite of traditional boundary layer theory is horizontal homogeneity. Apart from large steppes, deserts, large ice fields, or open water, probably no terrains meet this requirement. Nevertheless, it is equally as important to try to ascertain the boundary layer wind profile in heterogeneous terrain. In fact, wind turbines are seldom deployed at "ideal" sites where the flow is mainly undisturbed, but also in the vicinity of settlements or cities. Therefore, the results in this thesis can help to transfer theoretical assumptions to conditions closer to reality.

The prevailing wind directions at the Wettermast Hamburg site are westerly directions with overall higher wind speeds than from other directions. This can be attributed to the location of the measure-

ment site in the mid-latitudes. Southeasterly wind directions are second most frequent. This secondary maximum is more distinct in lower levels and at smaller wind speeds. It becomes less distinct with height, but even in 250 m measuring height, winds from southeast are more frequent than those from east or south.

Overall, wind speeds increase with height due to the reduction of surface friction. Low wind speeds occur, except for 10 m height, at all wind directions with the same frequency. High wind speeds, on the other hand, predominantly occur at westerly directions, Larger wind speeds (i.e. $> 10 \, \mathrm{m \, s^{-1}}$) are more frequent at 110 m and above. Even larger wind speeds ($> 15 \, \mathrm{m \, s^{-1}}$) also almost exclusively occur at westerly directions.

During winter (December, January, February), high wind speeds occur more frequently than during summer (June, July, August). Additionally, most cases with southeasterly wind directions occur during winter. In 110 m the most frequent wind direction is west with the highest wind speeds as well. Easterly directions are second most frequent here. The highest wind speeds ($> 20 \, \mathrm{m \, s^{-1}}$) only occur from westerly directions.

The reason for the frequent occurrence of southeasterly directions is still subject to research. Possible explanations for this would be local effects like canalization within the valley of the river Elbe, inflow into the nocturnal urban heat island, or local small-scale circulations at the measurement site. Up until now, this effect could not be explained completely.

In conclusion, wind measurements at the Wettermast Hamburg site are representative for a location in the mid latitudes with prevailing westerly wind directions. A secondary maximum in wind direction frequencies occurs for southeasterly directions. The measurement site is located in rather heterogeneous terrain in the transition area between urban and rural ares. Measurement at a tower poses challenges due to circulations of the structure. Therefore, an operational sector is identified.

How can the roughness length z_0 be derived from observations at tall masts in heterogeneous terrain?

To characterize a site, either for meteorological measurements or for deployment of wind turbines, a description of its surrounding surface properties is necessary. To this end, most often the roughness length z_0 is used. Several approaches exist to derive z_0 from meteorological measurements. In this thesis, variations of comparison with the logarithmic wind profile is used to estimate z_0.

The traditional approach to derive z_0 is to compare wind speed measurements with the logarithmic wind profile. When following this approach at a tall mast surrounded by heterogeneous terrain, some limitations of this method become obvious: the derived roughness length is highly sensitive to the levels that are used in the estimation. It can be seen from average profiles at the Wettermast Hamburg that wind speeds at neutral conditions in some directions deviate considerably from the theoretical

logarithmic shape. These deviations result in sensitivity of the calculated roughness length on the heights used for the estimation. Interestingly, this effect only occurs for some wind directions while in others, the logarithmic wind profile is a very accurate description of the measured wind profile in neutral stratification. At the Wettermast Hamburg, in the wind directions between $180° - 210°$ the resulting value of z_0 is found to more than double. If only heights from 10 to 110 m are considered, the resulting roughness length is 0.34 m. On the other hand, it is estimated as 0.82 m if all heights between 10 and 250 m are used. In other directions, however, this effect is not as large. In wind directions between $270°$ and $300°$, the roughness length is almost constant between 0.69 m (for heights 10 to 110 m) and 0.72 m (for heights 10 to 250 m). This is only a spread of 0.04 m.

This sensitivity to number and height of measurement levels can be reduced by adding a linear term to the logarithmic wind profile description. This extension leads to an effective roughness length $z_{0,e}$. The resulting equation describes the measured profiles much better. The effective roughness length values are in good agreement with the values that are proposed by several authors and are integrated over the inhomogeneous surface in the fetch area. It is advisable to use $z_{0,e}$ for sites with inhomogeneous surroundings and with measurements from tall masts.

In summary, the roughness length can be determined from average wind profiles. Sometimes, the situation at a site or the aim of an analysis requires measured wind profiles that extend above 110 m. In these cases, however, it is necessary to expand the logarithmic wind profile to include a linear term. This term accounts for a stronger increase of the wind speed at upper levels.

Is it sufficient to determine atmospheric stability for wind profile estimates by means of stratification close to the surface?

Several quantities exist that are used to characterize atmospheric stratification. In this thesis Obukhov length L and temperature gradient $\Delta\theta/\Delta z$ are used. As mentioned in Section 5.1, this method is prone to errors if the derivation of turbulent fluxes from eddy covariance measurements is not conducted carefully. Therefore, in this thesis gradients of potential temperature are used to characterize atmospheric stratification.

Stratification is determined by gradients of potential temperature in two layers (10 m to 110 m and 110 m to 250 m). The most frequent stability category in both layers is neutral stratification. When discerning between the stratifications in the lower layer and the upper layer, it becomes obvious that in about 42% of the data upper layer stability is different from lower layer stability.

The most frequent combination of stability in the lower and upper part is neutral stratification in both layers (23 770 cases in the $90° - 150°$ sector, 30%). The combination of near stable stratification in both parts is also very common (19 723 cases, 25%). Towards instability the frequency distribution of temperature gradients has a sharp boundary. Almost no gradients are smaller than -0.002 K m^{-1} in the

upper part. The temperature gradients at stable stratification on the other hand, are spread over a wider range of values. No cases at all exist where the stratification in the upper layer is very unstable. In general, instability in the upper part only occurs during neutral or near stable conditions in the lower part. This is plausible, since unstable stratification mainly forms due to heating from the surface. Since this heating from below is not present in the upper layer, instability only rarely develops.

Stability which has been determined below 110 m in the lower part of the boundary layer is not always representative for the stratification in the layer above. In 57.5% of the observed cases, the stratification in the upper and the lower part correspond. During 37.3% of the cases the stratification deviates by only one stability class. But, for 5.1% of the cases the difference in stratification between both parts is larger than one stability class.

When discerning between the stability in the lower and in the upper level, variations of both stratifications influence the entire wind profile. The wind speed shows a strong response to changes in the lower layer stability. These impact the shape of the profile as well as the intensity of wind speed gradients. In unstable lower layer stability wind speed gradients are generally weak in lower levels and almost constant higher up. With increasing lower layer stability, wind speed gradients in all heights increase as well. Nevertheless, even changes in upper layer stability impact the wind profile in all measurement heights. This influence is strongest in higher levels. However, also in levels close to the ground, an influence is visible. If only lower layer stability is considered, the estimated wind speed can be about 30% less than expected in all heights.

In conclusion, atmospheric stratification is not always uniform throughout the entire measurement height. These deviations of stability result in deviations of wind speed as well. If upper layer stability is neglected, this can result in overestimation of wind speed. In this case, the wind speed can be around 30% less than expected.

How do varying surface roughness and atmospheric stratification influence the boundary layer wind profile?

Two main influencing factors on boundary layer wind profiles are surface roughness and atmospheric stratification. The impact of either varies with height.

Influence of different surface roughnesses is mainly seen in the lowest measurement height 10 m. Above the 10 m measurement level, no distinct dependency on surface roughness is visible. The wind speed in 10 m measuring height is smaller at higher surface roughnesses. This can be expected, since larger surface roughness provides higher friction which decelerates the wind. In the 10 m measurement level, the normalized wind speed $u/u_{250\,m}$ varies between 0.4 and 0.5 at different z_0 during neutral stratification. However, already at 50 m height is this effect not as noticeable. The surface roughness therefore mainly influences the wind speed close to the ground.

Influence of stratification on wind profile is more distinct with overall larger wind speed gradients in stable and weaker gradients in unstable stratification. When discerning between stratification in lower and upper layers, variation of stratification in the lower layer mainly causes wind profiles to change in lower levels, but also has an impact on the entire profile. On the other hand, variation of upper layer stability also results in changes of the wind profile, even at lower levels. In 110 m, the effect of varying stability is strongest if lower layer stability is neutral and upper layer stability is stable to very stable. If uniformly neutral stability throughout the entire height is assumed, this deviation of upper layer stability causes wind speed overestimations with wind speeds that are up to 34% smaller than assumed.

In 110 m, variation due to changes between stable stratification classes is already larger than those due to z_0. Normalized wind speed in 110 m $u_{110\,\mathrm{m}}/u_{250\,\mathrm{m}}$ ranges between approximately 0.6 and 1. On the other hand, at varying roughness lengths the normalized wind speed in 110 m is between 0.75 and 0.85. Which shows a smaller variability due to surface roughness than due to stability changes.

In summary, the impact of varying surface roughness and atmospheric stratification depends on height. In the lowest measurement level 10 m, the influence of roughness changes is largest. Nevertheless, even in this height, influence of varying stratification is dominant. In all other heights, the effect of variation of atmospheric stratification is considerably larger than that of changing surface roughness.

How well are mixing length models able to describe the wind profile in heterogeneous terrain in the surface layer and above?

Wind speed assessment is necessary in a number of applications. For wind energy purposes, expected wind speeds at a certain height are often estimated by extrapolation of wind speed utilizing the logarithmic wind profile. This is, strictly speaking, only valid within the surface layer. As the wind power generation evolves and wind turbines reach higher, an estimate for the conditions well above the surface layer is necessary. Both Gryning et al. (2007) and Peña et al. (2010) propose a model estimation of wind speeds in the surface layer and beyond which base upon the extension of the mixing length description for levels above the surface layer. Performance of these two models is systematically analyzed by comparison with long term measurements at a heterogeneous site.

Wind speed estimations by Gryning et al. (2007) and Peña et al. (2010) are sensitive to very small positive values of the Obukhov length L (extreme stability). This results in an overestimation of wind speed for those cases. Therefore, only profiles with stratification $|L| > 50$ m should be used for model estimations.

The model approaches of Gryning et al. (2007) and Peña et al. (2010) are validated with regard to surface roughness with measured wind profiles at neutral stratification. RMSE and bias are calculated. The RMSEs between models and observations range between 16 and 42% (errors of both models are

in the same order). In 110 m, the RMSE is still between 16 and 27% for both models. The errors are smallest for moderate roughness lengths and higher for more extreme values of z_0. The bias between models and observations demonstrates systematic over- or underestimation. Both models underestimate the wind speed at the Wettermast Hamburg by 5–25% in most cases. Only for small roughness lengths the estimated wind speed is overestimated by both models. In this case, both models overestimate wind speed by as much as 28% in 10 m and 5 to 10% in 110 m. At large z_0 values, the wind speed is underestimated by roughly 20% in all heights. This leads to the assumption that the value of z_0 in model calculations has too much impact on the results.

Additionally, both models are validated by evaluating the modeled and observed wind profiles at varying atmospheric stratification. The wind speed is best predicted from both models for unstable stratification when the top of the boundary layer lies presumably well above the mast height. During stable stratification, the error between the modeled and the measured wind speed is reasonably small in lower levels but increases distinctly with height. This could be explained by the fact that the top of the boundary layer in those cases often lies below the highest measuring height and therefore not all measurements are taken within the boundary layer.

In unstable stratification, both models produce small errors, especially at higher levels (110 m and above). Here, measurements are taken in a well developed surface layer and observation levels are far apart from surface and boundary layer top and their effects.

Overall, the average biases of the Peña et al. (2010) approach are closer to zero than those of the Gryning et al. (2007) approach. The wind speeds are underestimated in most stability categories (very unstable, unstable, neutral, and near stable) by both models. In near unstable and stable stratification however, the bias of the Peña et al. (2010) model is positive in some heights, which indicates an overestimation of wind speed. Although the error estimates of the Peña et al. (2010) model are smaller than those of the Gryning et al. (2007) approach, the model of Peña et al. (2010) still mostly underestimates the wind speed in all heights.

Because the height of the boundary layer is only estimated from the turbulent flux of momentum in the surface layer, it is only a rough approximation of reality. This is visible in particular in stable cases, when the top of the boundary layer can be below the highest measurement level at the Wettermast Hamburg. This results in height dependency of the model errors when comparing those with observations. To rectify this, observations of boundary layer height is needed.

At levels close to the ground (10 m at Wettermast Hamburg), varying z_0 results in larger RMSEs than variation in atmospheric stratification. However, in 110 m errors due to stability variation are larger than those due to z_0 variations. In general, RMSE values increase with height. However, errors of different stratification categories spread stronger at higher levels, whereas the spread of RMSE due to different surface roughnesses decreases at higher levels.

Mixing length models are able to predict wind speeds reasonably well. However, the quality of model results in lower levels ($< 110\,\mathrm{m}$) depends more on roughness length. At higher levels ($> 110\,\mathrm{m}$) the quality of model results depends more on stratification. In $110\,\mathrm{m}$, the error spread is of the same order for both.

This shows that for wind speeds estimations at levels close to ground, a correct representation of surface roughness is most important. The higher the level of predicted wind speed the more important the correct stability classification becomes. No considerable improvement of the Peña et al. (2010) model over the Gryning et al. (2007) model can be found when trying to estimate wind speeds at the Wettermast Hamburg.

How large are uncertainties of wind speed estimations at levels in the order of current and future wind turbine hub heights?

Observations at the Wettermast Hamburg can be used to estimate characteristics of the wind profile at the order of hub and rotor heights of wind turbines in heterogeneous terrain. Measurements at $110\,\mathrm{m}$ are approximately taken in the level of current large wind turbines. Since a further increase of hub heights is expected in future, conditions in this level are of great interest.

In $110\,\mathrm{m}$, variation of surface roughness in neutral stratification has a relatively small impact compared to the impact of varying atmospheric stratification. The wind speed in this height is sensitive to both variation of upper layer stability and lower layer stability. If upper layer stability deviates from lower layer stability and this is not considered in wind speed estimations, wind speed in $110\,\mathrm{m}$ is always overestimated. In some cases the true wind speed can be around 30% smaller than assumed.

Mixing length models by Gryning et al. (2007) and Peña et al. (2010) represent the wind speed in $110\,\mathrm{m}$ reasonably well. In fact, the errors between model results and observations are often smallest in this height. In unstable stratification, model results fit the observations best and the relative root mean square error (RMSE) between modeled and measured wind speed ranges between 16 and 21% for unstable categories. Wind speed estimation in stable stratification on the other hand, has the largest errors with relative RMSE of up to 33% in $110\,\mathrm{m}$.

To investigate wind speed gradients (wind shear) over the span of wind turbine rotors, the observations between heights $50\,\mathrm{m}$ and $175\,\mathrm{m}$ are analyzed closer. At current hub heights of 80 to $100\,\mathrm{m}$ and rotor diameters of around $100\,\mathrm{m}$ and up to $150\,\mathrm{m}$ measurements at these heights are a good representation of the conditions which wind turbine rotors are in.

As mentioned above, wind shear in this height range is mainly influenced by variation in atmospheric stratification. It can range between $0.2\,\mathrm{m\,s^{-1}}$ (at neutral stratification in upper levels) and up to $4.1\,\mathrm{m\,s^{-1}}$ (in stable stratification).

In summary, to estimate wind speed at hub heights and the height range of wind turbine rotors, it is necessary to assess atmospheric stratification as correctly as possible. Notably, not only the stratification in lower layers is important for this assessment, but with increasing observation height, the stratification in upper layers becomes more and more important as well.

Outlook

Several studies mention that at heterogeneous terrain, the roughness length is rather an integrated quantity over the whole upstream domain than a representation of one particular surface (Wieringa, 1986; Schmid and Oke, 1990; Verkaik and Holtslag, 2007). The derivation of roughness length z_0 from logarithmic wind profiles in this thesis has been adapted to take into account the particular conditions at this site. To this end, the wind profile description is extended with a linear term. It would be interesting to test this method of estimating z_0 also at other tall masts in heterogeneous terrain, to verify that this method remedies the challenges of heterogeneous surface conditions at tall masts. To accomplish this, observations from meteorological towers in Cabauw (van Ulden and Wieringa, 1996), Karlsruhe (Kalthoff and Vogel, 1992), or Boulder (Korrell et al., 1982) could be used.

The boundary layer during stable stratification can be rather shallow. This has been mentioned in the discussion of observed wind profiles and model results. To determine the location of measurement heights within the boundary layer, additional information about the height z_i of the boundary layer top is necessary. This could be derived from radio soundings, Sodar or Lidar measurements (Emeis et al., 2008; Beyrich and Leps, 2012). The closest operational radio soundings are released at 80 km distance from the site. Since the boundary layer is a feature of the atmosphere that is highly affected by local conditions, these would not result in a good representation of the boundary layer height at the Wettermast Hamburg site. Therefore, determination of boundary layer height from remote sensing measurements would be a possible solution to get continuous estimates of boundary layer height. Eresmaa et al. (2006) and Münkel et al. (2007) proposed a method to determine height of the convective boundary from ceilometer measurements. Haeffelin et al. (2012) outline different methods of determining boundary layer height from remote sensing also for stable boundary layers. In 2011 several remote sensing instruments were deployed at the Wettermast Hamburg site. Deriving boundary layer heights z_i from measurements of those instruments could expand the data set during that time. This would provide more insight about the structure of wind profiles with respect to the whole boundary layer. Corresponding analyses of observed and modeled wind profiles could be executed.

In this thesis some interesting effects are found that cannot be explained ultimately. The reason for the frequent occurrence of southeasterly winds during stable stratification remains unclear. To determine the horizontal and vertical extent of this phenomenon, additional temperature and wind measurements at several heights in the immediate vicinity and at greater distances would be helpful. Furthermore,

it remains unclear what ultimately causes the observed neutral wind profiles to deviate from the log-arithmic profile shape in some directions but not in others. It has been mentioned that changes of surface roughness could cause development of internal boundary layers. Floors et al. (2011b) investigate the influence of internal boundaries on the wind profile at a site at the west coast of Denmark. They mention that internal boundary layers impact the wind profile at this site considerably. Since internal boundary layers as a reason for the deviating shape cannot be ruled out, it might be worth-while to investigate those further. Additionally, in combination with the above mentioned derivation of boundary layer height, it could also be analyzed if a relation between those profiles and varying boundary layer heights exist.

The wind profile models by Gryning et al. (2007) and Peña et al. (2010) rely on empirically determined parameters. In case of the Gryning et al. (2007) model also a subset of the Wettermast Hamburg data, including Obukhov length from eddy covariance measurements, was used to derive these parameters. In the course of this thesis it has been determined that data from eddy covariance measurements are relatively uncertain. It might therefore be worthwhile to explore the derivation of these parameters with recalculated stability parameters.

Overall, this thesis gives deeper insight into the processes that shape the boundary layer wind profile. In future, this can help to improve wind speed predictions especially in levels above the surface layer, which are increasingly important for wind energy assessments. More knowledge about the relevant processes allows to assess possible sites and to predict yields more accurately. Therefore, power generation from wind energy can become more efficient and a larger fraction of human's energy demands can be covered by renewable energy sources.

A

Definitions and Formulas used

Some definitions and methods that are used throughout this thesis are summarized in this appendix for reference.

A.1 Statistical Measures

Statistical moments are used to characterize a distribution throughout this thesis (Steland, 2010). When measurements of a quantity x are taken, they commonly form a distribution of values. The central value of this distribution is described by the arithmetic mean $\bar{x}$. Variability within the distribution is characterized by standard deviation σ_x; the symmetry (or asymmetry) of a distribution is described by skewness s_x. The **arithmetic mean** $\bar{x}$ of a quantity x is calculated by:

$$\bar{x} = \frac{1}{n} \sum_{i=1}^{n} x_i \quad .$$

(A.1)

Here, n is the sample size and x_i are the individual measurements. The **standard deviation** σ_x as a measure of variability of x:

$$\sigma_x = \left(\frac{1}{n-1} \sum_{i=1}^{n} (x_i - \bar{x})^2 \right)^{1/2} \quad .$$

(A.2)

Larger values of standard deviation indicate larger variability of the quantity's distribution. Asymmetry of a distribution is described by **skewness** s_x:

$$s_x = \frac{1}{n} \frac{\sum_{i=1}^{n} (x_i - \bar{x})^3}{\sigma_x^3} \quad .$$

(A.3)

For values of $s_x > 0$ the distribution is right-tailed, indicating some extreme values to the right of the distribution, whereas $s_x < 0$ indicates a left-tailed distribution with some extreme values to the left.

A.2 Pearson's Correlation Coefficient

The correlation between two quantities x and y are determined using Pearson's correlation coefficient (Trauth, 2007):

$$r = \frac{\sum_{i=1}^{n} (x_i - \bar{x})(y_i - \bar{y})}{\sqrt{\sum_{i=1}^{n} (x_i - \bar{x})^2 \sum_{i=1}^{n} (y_i - \bar{y})^2}} \quad . \tag{A.4}$$

It is $r = 1$, if both variables are perfectly correlated (i.e. a linear relation between the two). If they are not linearly correlated at all, this results in $r = 0$.

A.3 Bootstrap Resampling

If statistical measures of a distribution are calculated, an uncertainty regarding the representativeness of this measure for the true distribution remains. The true distribution of measurements in environmental measurements is never known. Therefore, data resampling can provide a method to estimate the accuracy of calculated values.

In this thesis, bootstrap resampling (Efron, 1979) is used. To this end, sampling with replacement is conducted from all measurements and the statistical measure of interest (for example the average) of the resampled data is calculated. This is executed $100\,000$ times to minimize the effect of random resampling errors. From this data resampling a distribution of calculated values is obtained. To assess the variability of this distribution, measures of variation can be calculated. If the standard deviation is used, this gives an estimate of the range in which the true statistic measure (i.e. average) lies with 68.2% probability.

Good (2006) points out that for small sample sizes the resample data set may not represent the true data well. They recommend a minimum sample size of 100 for this method. This requirement is met in almost all stability categories in Section 5.4.2. Alone the (vs|vs) category consists of only 15 samples.

Bibliography

Arya, S. P., 2001: *Introduction to Micrometeorology*. Academic Press, London, 2. edition.

Barthlott, C. and F. Fiedler, 2003: Turbulence structure in the wake region of a meteorological tower. *Bound.-Layer Meteor.*, **108**, 175–190.

Bechtel, B., T. Langkamp, F. Ament, J. Böhner, C. Daneke, R. Günzkofer, B. Leitl, J. Ossenbrügge, and A. Ringeler, 2011: Towards an urban roughness parameterisation using interferometric SAR data taking the metropolitan region of Hamburg as an example. *Meteor. Z.*, **20**, 29–37.

Beyrich, F. and J.-P. Leps, 2012: An operational mixing height data set from routine radiosoundings at Lindenberg: Methodology. *Meteor. Z.*, **21**, 337–348.

Blackadar, A. K., 1962: The vertical distribution of wind and turbulent exchange in a neutral atmosphere. *J. Geophys. Res.*, **67**, 3095–3102.

— 1997: *Turbulence and Diffusion in the Atmosphere*. Springer, Berlin.

Blatt, A., 2010: *Roughness Length Analysis for Wind Energy Purposes*. Master thesis, Technical University of Denmark, DTU Wind Energy, Roskilde.

Borovenko, E. V., O. A. Volkovitskii, L. M. Zolotarev, and S. A. Isaeva, 1965: Estimation of the effect of the 300-meter meteorological mast structure on the wind-gauge readings. *Investigation of the Bottom 300-Meter Layer of the Atmosphere*, N. L. Byzova, ed., Israel Program for Scientific Translations, Jerusalem, 83–92.

Bradley, E. F., 1968: A micrometeorological study of velocity profiles and surface drag in the region modified by a change in surface roughness. *Quart. J. Roy. Meteor. Soc.*, **94**, 361–379.

Brümmer, B. and I. Lange, 2004: Die meteorologische Messanlage am NDR-Sendemast in Hamburg-Billwerder. *DMG-Mitteilungen*, **2**, 11–12.

Brümmer, B., I. Lange, and H. Konow, 2012: Atmospheric boundary layer measurements at the 280 m high Hamburg weather mast 1995–2011: Mean annual and diurnal cycles. *Meteor. Z.*, **21**, 319–335.

Bundesregierung, 2012: Energiewende – Schritt für Schritt. Booklet, Berlin, http://www.bundesregierung.de/Content/Infomaterial/BPA/Bestellservice/2012-07-19-energiewende-schritt-fuer-schritt.html.

Businger, J. A., J. C. Wyngaard, Y. Izumi, and E. F. Bradley, 1971: Flux-profile relationships in the atmospheric surface layer. *J. Atmos. Sci.*, **28**, 181–189.

Buzzi, M., M. W. Rotach, M. Holtslag, and A. A. Holtslag, 2011: Evaluation of the COSMO-SC turbulence scheme in a shear-driven stable boundary layer. *Meteor. Z.*, **20**, 335–350.

Cermak, J. E. and J. D. Horn, 1968: Tower shadow effect. *J. Geophys. Res.*, **73**, 1869–1876.

Christiansen, M. B. and C. B. Hasager, 2005: Wake effects of large offshore wind farms identified from satellite SAR. *Remote Sens. Environ.*, **98**, 251–268.

Dabberdt, W. F., 1968: Tower-induced errors in wind profile measurements. *J. Appl. Meteor.*, **7**, 359–366.

Devis, A., N. P. M. van Lipzig, and M. Demuzere, 2013: A new statistical approach to downscale wind speed distributions at a site in northern europe. *J. Geophys. Res.-Atm.*, **118**, 2272–2283.

Draxl, C., A. N. Hahmann, A. Peña, and G. Giebel, 2014: Evaluating winds and vertical wind shear from weather research and forecasting model forecasts using seven planetary boundary layer schemes. *Wind Energy*, **17**, 39–55.

Drechsel, S., G. J. Mayr, J. W. Messner, and R. Stauffer, 2012: Wind speeds at heights crucial for wind energy: Measurements and verification of forecasts. *J. Appl. Meteorol. Climatol.*, **51**, 1602–1617.

Dyer, A. J., 1974: A review of flux-profile relationships. *Bound.-Layer Meteor.*, **7**, 363–372.

Efron, B., 1979: Bootstrap methods: Another look at the jackknife. *Ann. Stat.*, **7**, 1–26.

Emeis, S., 2013: *Wind Energy Meteorology*. Springer, Berlin.

Emeis, S., K. Baumann-Stanzer, M. Piringer, M. Kallistratova, R. Kouznetsov, and V. Yushkov, 2007: Wind and turbulence in the urban boundary layer analysis from acoustic remote sensing data and fit to analytical relations. *Meteor. Z.*, **16**, 393–406.

Emeis, S., K. Schäfer, and C. Münkel, 2008: Surface-based remote sensing of the mixing-layer height: A review. *Meteor. Z.*, **17**, 621–630.

Eresmaa, N., A. Karppinen, S. M. Joffre, J. Räsänen, and H. Talvitie, 2006: Mixing height determination by ceilometer. *Atmos. Chem. Phys.*, **6**, 1485–1493.

Etling, D., 2008: *Theoretische Meteorologie*. Springer, Berlin, 3. edition.

Ferreres, E., M. Soler, and E. Terradellas, 2013: Analysis of turbulent exchange and coherent structures in the stable atmospheric boundary layer based on tower observations. *Dyn. Atmos. Oceans*, **64**, 62–78.

Fiedler, F. and H. A. Panofsky, 1972: The geostrophic drag coefficient and the 'effective' roughness length. *Quart. J. Roy. Meteor. Soc.*, **98**, 213–220.

Floors, R., E. Batchvarova, S.-E. Gryning, A. N. Hahmann, A. Peña, and T. Mikkelsen, 2011a: Atmospheric boundary layer wind profile at a flat coastal site – wind speed lidar measurements and mesoscale modeling results. *Adv. Sci. Res.*, **6**, 155–159.

Floors, R., S.-E. Gryning, A. Peña, and E. Batchvarova, 2011b: Analysis of diabatic flow modification in the internal boundary layer. *Meteor. Z.*, **20**, 649–659.

Foken, T., 2006a: 50 Years of the Monin–Obukhov Similarity Theory. *Bound.-Layer Meteor.*, **119**, 431–447.

— 2006b: *Angewandte Meteorologie*. Springer, Berlin, 2. edition.

Frank, H. P., E. L. Petersen, R. Hyvönen, and B. Tammelin, 1999: Calculations on the wind climate in northern Finland: the importance of inversions and roughness variations during the seasons. *Wind Energy*, **2**, 113–123.

Gill, G. C., L. E. Olsson, J. Sela, and M. Suda, 1967: Accuracy of wind measurements on towers or stacks. *Bull. Am. Meteorol. Soc.*, **48**, 665–674.

Golder, D., 1972: Relations among stability parameters in the surface layer. *Bound.-Layer Meteor.*, **3**, 47–58.

Good, P. I., 2006: *Resampling Methods, A Practical Guide to Data Analysis*. Birkhäuser, Boston.

Graf, A., A. van de Boer, A. Moene, and H. Vereecken, 2014: Intercomparison of methods for the simultaneous estimation of zero-plane displacement and aerodynamic roughness length from single-level eddy-covariance data. *Bound.-Layer Meteor.*, **151**, 373–387.

Grimmond, C., 1998: Aerodynamic roughness of urban areas derived from wind observations. *Bound.-Layer Meteor.*, **89**, 1–24.

Grimmond, C. S. B. and T. R. Oke, 1999: Aerodynamic properties of urban areas derived from analysis of surface form. *J. Appl. Meteor.*, **38**, 1262–1292.

Gryning, S.-E., E. Batchvarova, B. Brümmer, H. Jørgensen, and S. Larsen, 2007: On the extension of the wind profile over homogeneous terrain beyond the surface boundary layer. *Bound.-Layer Meteor.*, **124**, 251–268.

Gryning, S. E., E. Batchvarova, and R. Floors, 2013: A study on the effect of nudging on long-term boundary layer profiles of wind and weibull distribution parameters in a rural coastal area. *J. Appl. Meteorol. Climatol.*, **52**, 1201–1207.

Gryning, S.-E., E. Batchvarova, R. Floors, A. Peña, B. Brümmer, A. Hahmann, and T. Mikkelsen, 2014: Long-term profiles of wind and weibull distribution parameters up to 600 m in a rural coastal and an inland suburban area. *Bound.-Layer Meteor.*, **150**, 167–184.

Haeffelin, M., F. Angelini, Y. Morille, G. Martucci, S. Frey, G. Gobbi, S. Lolli, C. O'Dowd, L. Sauvage, I. Xueref-Rémy, B. Wastine, and D. Feist, 2012: Evaluation of mixing-height retrievals from automatic profiling Lidars and ceilometers in view of future integrated networks in Europe. *Bound.-Layer Meteor.*, **143**, 49–75.

Hasager, C., N. Nielsen, N. Jensen, E. Boegh, J. Christensen, E. Dellwik, and H. Soegaard, 2003: Effective roughness calculated from satellite-derived land cover maps and hedge-information used in a weather forecasting model. **109**, 227–254.

Hau, E., 2013: *Wind Turbines: Fundamentals, Technologies, Application, Economics*. Springer, Berlin.

He, Y., A. H. Monahan, and N. A. McFarlane, 2013: Diurnal variations of land surface wind speed probability distributions under clear-sky and low-cloud conditions. *Geophys. Res. Lett.*, **40**, 3308–3314.

Hein, C., 2012: *Vergleich von SODAR- und Sonic-Messungen für ein Jahr am Wettermast Hamburg.* Bachelor thesis, Universität Hamburg, Hamburg.

Heitmann, B., 2012: *Vergleich von vier Windmesssystemen am Hamburger Wettermast beim TallWind-Experiment vom 15. bis 20. Juni 2011.* Bachelor thesis, Universität Hamburg, Hamburg.

Hertwig, D., 2013: *On Aspects of Large-Eddy Simulation Validation for Near-Surface Atmospheric Flows.* Phd thesis, Universität Hamburg, Hamburg.

Hicks, B., 1981: An examination of turbulence statistics in the surface boundary layer. *Bound.-Layer Meteor.*, **21**, 389–402.

Hicks, B., I. Pendergrass, W.R., C. Vogel, J. Keener, R.N., and S. Leyton, 2014: On the micrometeorology of the southern great plains 1: Legacy relationships revisited. *Bound.-Layer Meteor.*, **151**, 389–405.

Holtslag, A. A. M., 1984: Estimates of diabatic wind speed profiles from near-surface weather observations. *Bound.-Layer Meteor.*, **29**, 225–250.

Holtslag, A. A. M., G. Svensson, P. Baas, S. Basu, B. Beare, A. C. M. Beljaars, F. C. Bosveld, J. Cuxart, J. Lindvall, G. J. Steeneveld, M. Tjernström, and B. J. H. Van De Wiel, 2013: Stable atmospheric boundary layers and diurnal cycles: Challenges for weather and climate models. *Bull. Amer. Meteor. Soc.*, **94**, 1691–1706.

Högström, U., 1988: Non-dimensional wind and temperature profiles in the atmospheric surface layer: A re-evaluation. *Bound.-Layer Meteor.*, **42**, 55–78.

— 1996: Review of some basic characteristics of the atmospheric surface layer. *Bound.-Layer Meteor.*, **78**, 215–246.

Irwin, J. S. and F. S. Binkowski, 1981: Estimation of the Monin-Obukhov scaling length using on-site instrumentation. *Atmos. Environ.*, **15**, 1091–1094.

Jacob, M., 2013: *Beeinflussung von Windmessungen an einem Rohrmast durch die Maststruktur.* Bachelor thesis, Universität Hamburg, Hamburg.

Kaimal, J. and J. Wyngaard, 1990: The Kansas and Minnesota experiments. *Bound.-Layer Meteor.*, **50**, 31–47.

Kalthoff, N. and B. Vogel, 1992: Counter-current and channelling effect under stable stratification in the area of Karlsruhe. *Theor. Appl. Climatol.*, **45**, 113–126.

Kelly, M., I. Troen, and H. Jørgensen, 2014: Weibull-k revisited: "tall" profiles and height variation of wind statistics. *Bound.-Layer Meteor.*, **152**, 107–124.

Korrell, A., H. Panosky, and R. Rossi, 1982: Wind profiles at the Boulder tower. *Bound.-Layer Meteor.*, **22**, 295–312.

Lange, I., 2001: *Eine Grenzschichtklimatologie für Hamburg aus Daten der meteorologischen Mess-anlage am NDR-Sendemast in Billwerder*. Diploma thesis, Universität Hamburg, Hamburg.

— 2010: Standardabweichung und Kovarianz über mehrere Mittelungsintervalle. Technical report, Universität Hamburg.

Leclerc, M. Y. and T. Foken, 2014: *Footprints in Micrometeorology and Ecology*. Springer, Berlin.

Lettau, H. H., 1962: Theoretical wind spirals in the boundary layer of a barotropic atmosphere. *Beitr. Phys. Atmos*, **35**, 195–212.

Liang, J., L. Zhang, Y. Wang, X. Cao, Q. Zhang, H. Wang, and B. Zhang, 2014: Turbulence regimes and the validity of similarity theory in the stable boundary layer over complex terrain of the Loess Plateau, China. *J. Geophys. Res.-Atm.*, **119**, 6009–6021.

Link, A., 1966: Messungen an Funktürmen zur Ermittlung der Ausbreitungsbedingungen, Teil II: Über den Einfluss eines Rohrmastes auf Windgeschwindigkeitsmessungen an demselben. Technical report, Institut für Meteorologie, Technische Hochschule Darmstadt.

Lumley, J. and H. Panofsky, 1964: *The Structure of Atmospheric Turbulence*. Wiley, New York.

Mauritsen, T., G. Svensson, S. S. Zilitinkevich, I. Esau, L. Enger, and B. Grisogono, 2007: A total turbulent energy closure model for neutrally and stably stratified atmospheric boundary layers. *J. Atmos. Sci.*, **64**, 4113–4126.

Mohan, M. and T. A. Siddiqui, 1998: Analysis of various schemes for the estimation of atmospheric stability classification. *Atmos. Environ.*, **32**, 3775–3781.

Monahan, A. H., 2010: The probability distribution of sea surface wind speeds: Effects of variable surface stratification and boundary layer thickness. *J. Climate*, **23**, 5151–5162.

Monahan, A. H., Y. He, N. McFarlane, and A. Dai, 2011: The probability distribution of land surface wind speeds. *J. Climate*, **24**, 3892–3909.

Münkel, C., N. Eresmaa, J. Räsänen, and A. Karppinen, 2007: Retrieval of mixing height and dust concentration with Lidar ceilometer. *Bound.-Layer Meteor.*, **124**, 117–128.

Panofsky, H. and J. Dutton, 1984: *Atmospheric Turbulence: Models and Methods for Engineering Applications*. Wiley, New York.

Panofsky, H., H. Tennekes, D. Lenschow, and J. Wyngaard, 1977: The characteristics of turbulent velocity components in the surface layer under convective conditions. *Bound.-Layer Meteor.*, **11**, 355–361.

Pedersen, J. G., 2013: *Large-eddy simulation of the atmospheric boundary layer: Influence of unsteady forcing, baroclinicity, inversion strength and stability on the wind profile*. Phd thesis, Technical University of Denmark, DTU Wind Energy, Roskilde.

Pelliccioni, A., P. Monti, C. Gariazzo, and G. Leuzzi, 2012: Some characteristics of the urban boundary layer above Rome, Italy, and applicability of Monin–Obukhov similarity. *Environ. Fluid Mech.*, **12**, 405–428.

Peña, A., S.-E. Gryning, and C. Hasager, 2010: Comparing mixing-length models of the diabatic wind profile over homogeneous terrain. *Theor. Appl. Climatol.*, **100**, 325–335.

Sathe, A., S.-E. Gryning, and A. Peña, 2011: Comparison of the atmospheric stability and wind profiles at two wind farm sites over a long marine fetch in the North Sea. *Wind Energy*, **14**, 767–780.

Sathe, A., J. Mann, T. Barlas, W. Bierbooms, and G. van Bussel, 2013: Influence of atmospheric stability on wind turbine loads. *Wind Energy*, **16**, 1013–1032.

Schmid, H. P. and T. R. Oke, 1990: A model to estimate the source area contributing to turbulent exchange in the surface layer over patchy terrain. *Quart. J. Roy. Meteor. Soc.*, **116**, 965–988.

Schmidt, J., 2012: *Untersuchung der turbulenten Vertikaltransporte an zwei scharfen Kaltfronten und einem markanten Schauer am Wettermast Hamburg*. Diploma thesis, Universität Hamburg, Hamburg.

Schwartz, M. and D. Elliott, 2005: Towards a wind energy climatology at advanced turbine hub-heights. *15th Conference on Applied Climatology, Savannah*, American Meteorological Society.

Sedefian, L., 1980: On the vertical extrapolation of mean wind power density. *J. Appl. Meteor.*, **19**, 488–493.

Sorbjan, Z., 1987: An examination of local similarity theory in the stably stratified boundary layer. *Bound.-Layer Meteor.*, **38**, 63–71.

Steland, A., 2010: *Basiswissen Statistik*. Springer, Berlin.

Stull, R. B., 1988: *An Introduction to Boundary Layer Meteorology*. Kluwer Academic Publishers.

Sudmeyer, F., 2012: *Vergleich von vier Windmesssystemen am Hamburger Wettermast beim "Tall Wind"-Experiment vom 4. bis 9. Oktober 2011*. Bachelor thesis, Universität Hamburg, Hamburg.

Suomi, I., T. Vihma, S. E. Gryning, and C. Fortelius, 2013: Wind-gust parametrizations at heights relevant for wind energy: A study based on mast observations. *Quart. J. Roy. Meteor. Soc.*, **139**, 1298–1310.

Trauth, M. H., 2007: *MATLAB® Recipes for Earth Sciences*. Springer, Berlin, 2. edition.

Troen, I. and E. L. Petersen, 1989: *European Wind Atlas*. Risø National Laboratory, Roskilde.

van de Wiel, B. J. H., A. F. Moene, H. J. J. Jonker, P. Baas, S. Basu, J. M. M. Donda, J. Sun, and A. A. M. Holtslag, 2012: The minimum wind speed for sustainable turbulence in the nocturnal boundary layer. *J. Atmos. Sci.*, **69**, 3116–3127.

van den Berg, G. P., 2008: Wind turbine power and sound in relation to atmospheric stability. *Wind Energy*, **11**, 151–169.

van Ulden, A. P. and J. Wieringa, 1996: Atmospheric boundary layer research at Cabauw. *Bound.-Layer Meteor.*, **78**, 39–69.

Verkaik, J. and A. Holtslag, 2007: Wind profiles, momentum fluxes and roughness lengths at Cabauw revisited. *Bound.-Layer Meteor.*, **122**, 701–719.

Wagner, R., I. Antoniou, S. M. Pedersen, M. S. Courtney, and H. E. Jørgensen, 2009: The influence of the wind speed profile on wind turbine performance measurements. *Wind Energy*, **12**, 348–362.

Wamser, C., 1976: *Über die Struktur der Turbulenz in der planetarischen Grenzschicht unter besonderer Berücksichtigung des Einflusses unterschiedlicher Bodenrauhigkeit*. Phd thesis, Universität Hamburg, Hamburg.

Wieringa, J., 1986: Roughness-dependent geographical interpolation of surface wind speed averages. *Quart. J. Roy. Meteor. Soc.*, **112**, 867–889.

— 1992: Updating the Davenport roughness classification. *J. Wind Eng. Ind. Aerodyn.*, **41**, 357–368.

— 1993: Representative roughness parameters for homogeneous terrain. *Bound.-Layer Meteor.*, **63**, 323–363.

Zilitinkevich, S. and A. Baklanov, 2002: Calculation of the height of the stable boundary layer in practical applications. *Bound.-Layer Meteor.*, **105**, 389–409.

Zilitinkevich, S. S. and I. N. Esau, 2005: Resistance and heat-transfer laws for stable and neutral planetary boundary layers: Old theory advanced and re-evaluated. *Quart. J. Roy. Meteor. Soc.*, **131**, 1863–1892.

Publication and Supervised Theses

Peer Reviewed Publication

Brümmer, B., I. Lange, and **H. Konow**, 2012: Atmospheric boundary layer measurements at the 280 m high Hamburg weather mast 1995–2011: Mean annual and diurnal cycles. *Meteor. Z.*, **21**, 319–335.

Supervised Theses

Heitmann, B., 2012: *Vergleich von vier Windmesssystemen am Hamburger Wettermast beim TallWind-Experiment vom 15. bis 20. Juni 2011*. Bachelor thesis, Universität Hamburg, Hamburg.

Sudmeyer, F., 2012: *Vergleich von vier Windmesssystemen am Hamburger Wettermast beim "Tall Wind"-Experiment vom 4. bis 9. Oktober 2011*. Bachelor thesis, Universität Hamburg, Hamburg.

Jacob, M., 2013: *Beeinflussung von Windmessungen an einem Rohrmast durch die Maststruktur*. Bachelor thesis, Universität Hamburg, Hamburg.

Acknowledgments

Hiermit erkläre ich an Eides statt, dass ich die vorliegende Dissertationsschrift selbst verfasst und keine anderen als die angegebenen Quellen und Hilfsmittel benutzt habe.

Hamburg, den

Heike Konow